VISMEDERI

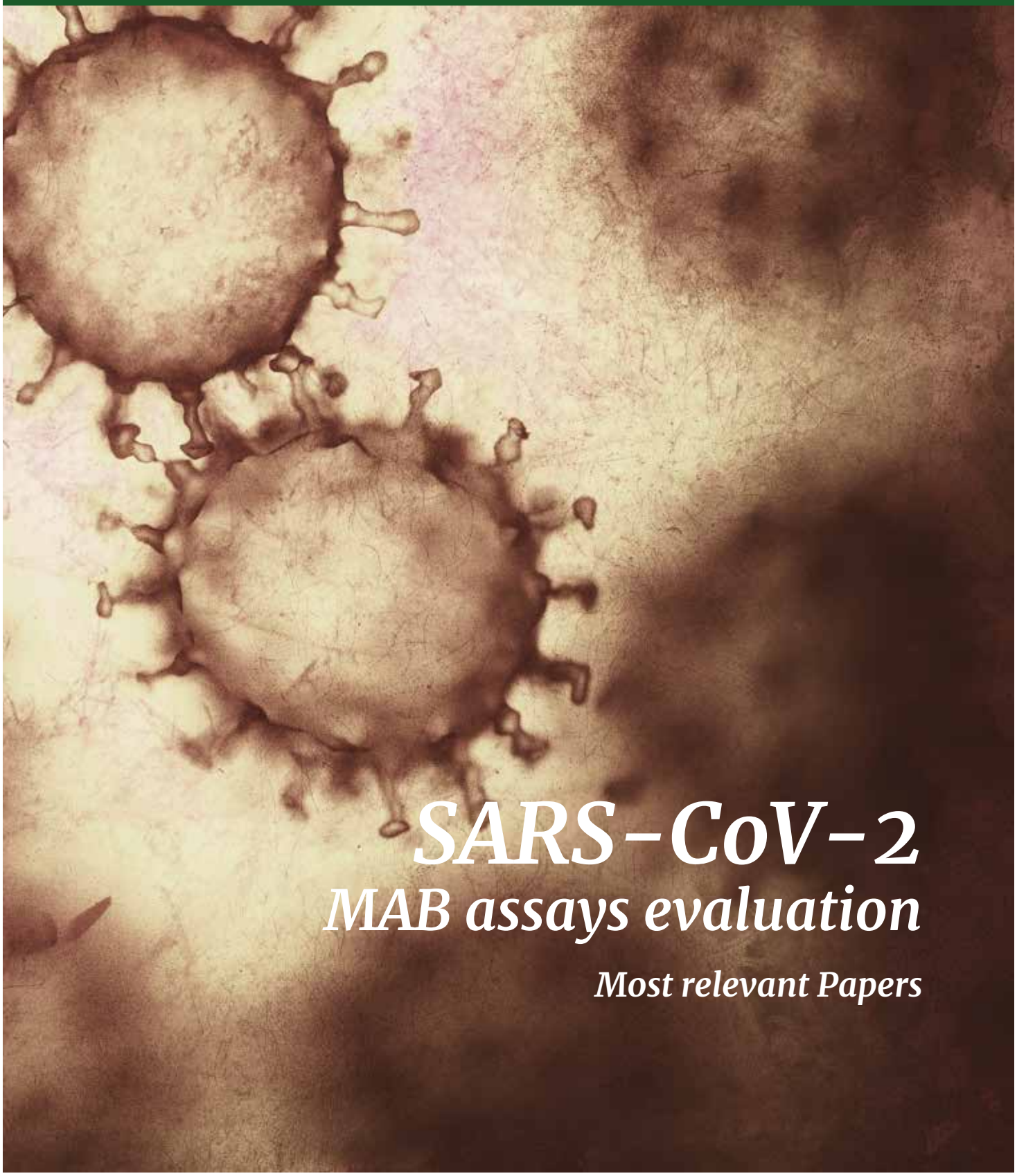

SARS-CoV-2

MAB assays evaluation

Most relevant Papers

www.vismederi.com / info@vismederi.com

INDEX

nature COMMUNICATIONS

ARTICLE

https://doi.org/10.1038/s41467-022-31115-8 OPEN

Anatomy of Omicron BA.1 and BA.2 neutralizing antibodies in COVID-19 mRNA vaccinees

Emanuele Andreano[1,9], Ida Paciello[1,9], Silvia Marchese[2], Lorena Donnici[3], Giulio Pierleoni[4,5], Giulia Piccini[4], Noemi Manganaro[1], Elisa Pantano[1], Valentina Abbiento[1], Piero Pileri[1], Linda Benincasa[5], Ginevra Giglioli[5], Margherita Leonardi[4,5], Piet Maes[6], Concetta De Santi[1], Claudia Sala[1], Emanuele Montomoli[4,5,7], Raffaele De Francesco[2,3] & Rino Rappuoli[1,8]✉

SARS-CoV-2 vaccines, administered to billions of people worldwide, mitigate the effects of the COVID-19 pandemic, however little is known about the molecular basis of antibody cross-protection to emerging variants, such as Omicron BA.1, its sublineage BA.2, and other coronaviruses. To answer this question, 276 neutralizing monoclonal antibodies (nAbs), previously isolated from seronegative and seropositive donors vaccinated with BNT162b2 mRNA vaccine, were tested for neutralization against the Omicron BA.1 and BA.2 variants, and SARS-CoV-1 virus. Only 14.2, 19.9 and 4.0% of tested antibodies neutralize BA.1, BA.2, and SARS-CoV-1 respectively. These nAbs recognize mainly the SARS-CoV-2 receptor binding domain (RBD) and target Class 3 and Class 4 epitope regions on the SARS-CoV-2 spike protein. Interestingly, around 50% of BA.2 nAbs did not neutralize BA.1 and among these, several targeted the NTD. Cross-protective antibodies derive from a variety of germlines, the most frequents of which were the IGHV1-58;IGHJ3-1, IGHV2-5;IGHJ4-1 and IGHV1-69;IGHV4-1. Only 15.6, 20.3 and 7.8% of predominant gene-derived nAbs elicited against the original Wuhan virus cross-neutralize Omicron BA.1, BA.2 and SARS-CoV-1 respectively. Our data provide evidence, at molecular level, of the presence of cross-neutralizing antibodies induced by vaccination and map conserved epitopes on the S protein that can inform vaccine design.

[1] Monoclonal Antibody Discovery (MAD) Lab, Fondazione Toscana Life Sciences, Siena, Italy. [2] Department of Pharmacological and Biomolecular Sciences DiSFeB, University of Milan, Milan, Italy. [3] INGM, Istituto Nazionale Genetica Molecolare "Romeo ed Enrica Invernizzi", Milan, Italy. [4] VisMederi S.r.l, Siena, Italy. [5] VisMederi Research S.r.l., Siena, Italy. [6] KU Leuven, Rega Institute, Department of Microbiology, Immunology and Transplantation, Laboratory of Clinical and Epidemiological Virology, Leuven, Belgium. [7] Department of Molecular and Developmental Medicine, University of Siena, Siena, Italy. [8] Department of Biotechnology, Chemistry and Pharmacy, University of Siena, Siena, Italy. [9] These authors contributed equally: Emanuele Andreano, Ida Paciello. ✉email: rino.r.rappuoli@gsk.com

Since its first appearance in December 2019, more than 495 million cases of SARS-CoV-2 infections were reported worldwide, with over 6.1 million deaths. Effective vaccines against the virus that first appeared in Wuhan, China, have been developed with unprecedented speed. However, their ability to contain the global pandemic has been compromised by the inability to timely deliver vaccines to low-income countries and by the appearance of several antigenic variants which escaped the natural and vaccine-induced immunity[1–3]. The main variants that emerged so far, and are listed as variants of concern (VoCs), are named B.1.1.7 (Alpha), B.1.351 (Beta), P.1 (Gamma), B.1.617.2 (Delta), and B.1.1.529.1 (Omicron; BA.1)[4,5]. The latter one showed to be the most efficient in spreading into partially immune populations and in a few months from its appearance has conquered most regions of the world[6,7]. Shortly after the appearance of the Omicron variant BA.1, the sublineage BA.2 (B.1.1.529.2) was identified, and it is now replacing the initial BA.1 variant worldwide[8,9]. Previous reports have shown that the unprecedented number of mutations carried on the Omicron BA.1 and BA.2 S protein drastically reduce the neutralizing efficacy of sera from infected and vaccinated people and that this VoC can escape more than 85% of nAbs described in literature, including several antibodies approved for clinical use by regulatory agencies[10–18]. Despite these observations, recent reports have shown different profiles of immune evasion between omicron BA.1 and BA.2[19–21]. While serum activity and neutralization efficacy of selected monoclonal antibodies against Omicron BA.1 and BA.2 have been reported, the functional and genetic anatomy of nAbs elicited in naïve (seronegative) and convalescent (seropositive) people immunized with two doses of the BNT162b2 mRNA vaccine remains to be explored. Taking advantage of our previous work[22], we tested 276 human monoclonal antibodies able to neutralize the original SARS-CoV-2 virus isolated in Wuhan, for their ability to neutralize the Omicron BA.1 and BA.2 variants, and the distantly related SARS-CoV-1 virus. Our work unravels the genetic signature of cross-protective antibodies and mapped conserved sites of pathogen vulnerability on the S protein that can be used to design the next generation of sarbecovirus vaccines.

Results

Distribution of BA.2 and BA.2 mutations on immunodominant sites. The SARS-CoV-2 B.1.1.529.1 (BA.1) and B.1.1.529.2 (BA.2) Omicron variants harbor 37 and 31 mutated residues in the spike (S) glycoprotein respectively (Supplementary Fig. 1a). The receptor binding domain (RBD) and N terminal domain (NTD) immunodominant sites are both highly mutated[14,19]. The NTDs of BA.1 and BA.2 carry 11 and 7 mutations respectively. BA.1 shows to be more remodeled compared to BA.2, presenting three substitutions (27%), A67V, T95I, and G142D, 5 deleted residues (46%), Δ69–70 and Δ143–145, and three inserted residues (27%), ins214EPE. On the other hand, BA.2 presents a NTD more similar to the original Wuhan virus carrying only four substitutions (57%), T19I, A27S, G142D, and V213G, and three deleted residues (43%), Δ24–26. The RBDs of BA.1 and BA.2 show a lower degree of plasticity compared to NTD, as only substituted residues are present in this domain. Within the RBD, which contains 15 and 16 mutations in total, the receptor binding motif (RBM), spanning from residues S438 to Y508[23], is the most mutated region. In fact, BA.1 RBM contains 10/15 (67%) mutated residues, while BA.2 carries 8/16 (50%) mutations. The eight mutated residues in the RBM of BA.2 are all shared with BA.1. Mutated residues in the RBM overlap with the epitopes of Class 1 and Class 2 neutralizing antibodies (nAbs), like J08[24,25], that target epitopes spanning from the left shoulder, through the neck and upper part of the right shoulder of the S protein (Supplementary Fig. 1b–d)[26,27]. Class 3 and 4 clusters of antibodies target the lower portion of the RBD, and their epitopes are located on the right and left flanks of this domain. Class 3 nAbs, like S309[28], target the right flank of the RBD where only 2/15 (13%) and 2/16 (12%) of all BA.1 and BA.2 mutations are found respectively (Supplementary Fig. 1d). Class 4 mAbs, like CR3022[29], are directed towards the left flank of the RBD which shows 3/15 (20%) and 6/16 (37%) mutations for BA.1 and BA.2 respectively (Supplementary Fig. 1b).

Omicron effects on vaccine-induced nAbs. To understand the impact of SARS-CoV-2 Omicron on the antibody response, we evaluated the neutralization activity of 276 nAbs previously isolated from seronegative ($n = 52$) and seropositive ($n = 224$) donors immunized with the BNT162b2 mRNA vaccine (Fig. 1)[22]. Data obtained from the neutralization analyses against Omicron BA.1 and BA.2 were compared with the neutralization data against the original Wuhan virus analyzed in our previous work[22]. While BA.1 cross-neutralizing nAbs were identified in all seropositives, these antibodies were found only in one out of five seronegatives (20%). Conversely, BA.2 cross-neutralizing nAbs were identified in all seropositives and in three out of five seronegatives (60%) (Supplementary Table 1). Only 1/52 (1.9%) and 4/52 (7.7%) nAbs from seronegatives neutralized Omicron BA.1 and BA.2 respectively, with a medium-low neutralization potency (Fig. 1a, c, d, f). As for seropositive vaccinees, 38/224 (17.0%) BA.1 and 51/224 (22.8%) BA.2 nAbs were identified (Fig. 1b, c, e, f). BA.1 nAbs showed a 3.16-fold decreased neutralization potency compared to the Wuhan virus, while BA.2 nAbs showed only a 1.76-fold decrease (Fig. 1b, c, e, f). Overall, 39 and 55 nAbs against BA.1 and BA.2 were identified respectively and none of these antibodies showed an extreme neutralization potency (IC_{100} below 10 ng ml^{-1}). To identify immunodominant sites of neutralization against BA.1 and BA.2, a flow cytometry-based competition assay was performed. In our previous study, we found that 215/276 (77.9%; 37 from seronegatives and 178 from seropositives) nAbs bound to the S protein RBD and the majority of these antibodies were competing with J08, which epitope spans between Class 1 and Class 2 regions, and S309, which target the Class 3 region[22]. In this work, all 215 RBD targeting-nAbs were additionally tested by competition assay against Class 4 targeting mAb CR3022. While Class 1/2, Class 3 and Not-competing nAbs were found in both seronegatives and seropositives, Class 4 competing nAbs were found exclusively in seropositives (Supplementary Fig. 2a; Supplementary Table 2). In both groups, Class 1/2 competing nAbs was the most abundant (70.3% in seronegatives and 64.0% in seropositives), followed by Not-competing (10.8%) and Class 3-competing nAbs (27.0%) for seronegatives and seropositives respectively. When tested for their neutralization activity against the BA.1 and BA.2 omicron variants, we observed that RBD-targeting Class 3 directed nAbs are the most abundant and potent class of nAbs against both BA.1 (29%) and BA.2 (52%) (Fig. 2b–d). In terms of overall neutralization potency, GM-IC_{100}, BA.1 nAbs showed a higher loss compared to BA.2 nAbs (Fig. 2d). Following, we evaluated the binding distribution of the 39 BA.1 and 55 BA.2 neutralizing antibodies and investigated the class of nAbs able to cross-neutralize both Omicron variants. Of the 39 BA.1 nAbs, the majority recognized the Class 1/2 region ($n = 20$; 51.3%), followed by Class 3 ($n = 15$; 38.5%), while nAbs targeting Class 4 region ($n = 1$; 2.6%), Not-competing ($n = 2$; 5.1%) and targeting the NTD ($n = 1$; 2.6%) were the least represented (Fig. 2e–g). As for the 55 BA.2 nAbs, the majority recognized the RBD Class 3 region ($n = 27$; 49.1%), followed by Class 1/2 (n = 18; 32.7%),

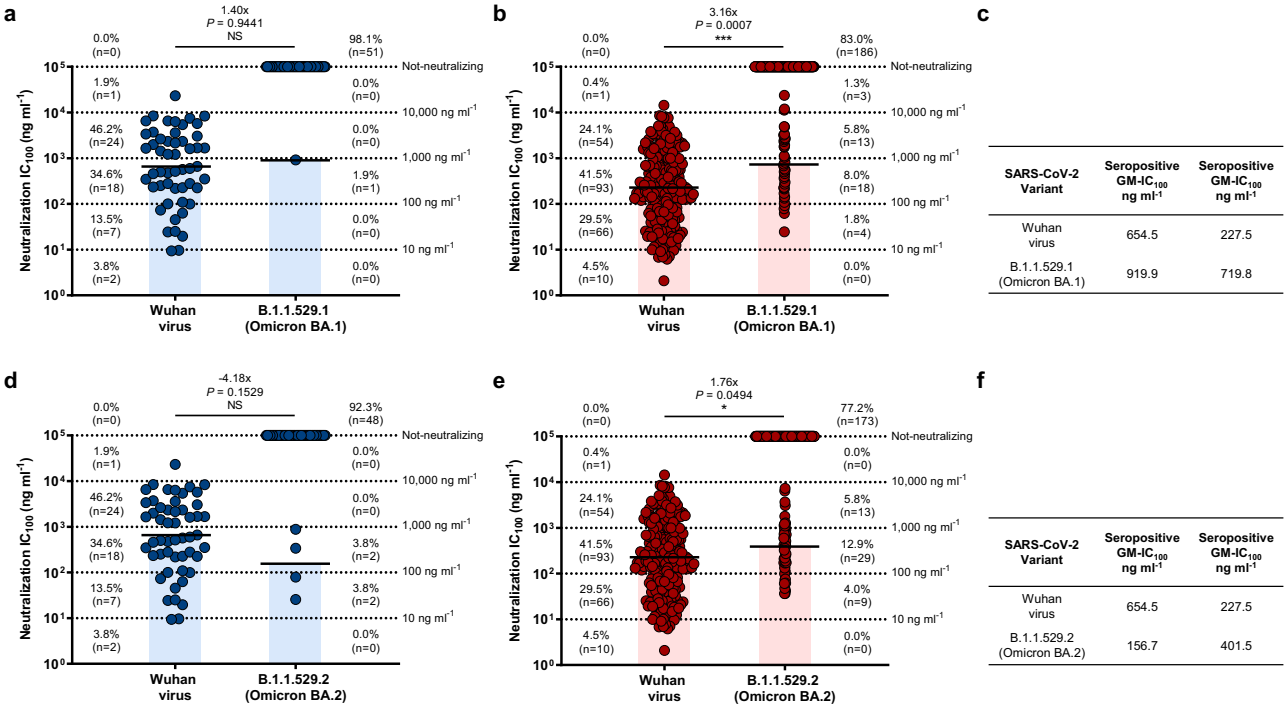

Fig. 1 Functional characterization of Omicron BA.1 and BA.2 nAbs. a–f Dot charts show the neutralization potency, reported as IC_{100} (ng ml^{-1}), of nAbs tested against the original SARS-CoV-2 virus first detected in Wuhan, the BA.1 and BA.2 Omicron VoC for seronegatives (**a**, **c**, **d**, **f**) and seropositives (**b**, **c**, **e**, **f**). The number and percentage of nAbs from individuals who were seronegative versus seropositive, fold change, neutralization IC_{100} geometric mean (black lines, blue and red bars) and statistical significance are denoted on each graph. Technical duplicates were performed for each experiment. A non-parametric Mann–Whitney *t*-test was used to evaluate statistical significances between groups. Two-tailed *P* value significances are shown as $^{*}P < 0.05$, $^{**}P < 0.01$, $^{***}P < 0.001$. NS, not significant. **c**, **f** Tables show the IC_{100} geometric mean (GM) of all nAbs pulled together from each group against Wuhan, BA.1 (**c**) and BA.2 (**f**) viruses.

NTD-targeting nAbs ($n = 9$; 16.4%), and Class 4 nAbs (1.8%) (Fig. 2e–g). Cross-Omicron variants nAbs were also characterized. While up to 74% ($n = 29/39$) of BA.1 nAbs were able to neutralize BA.2, only 53% ($n = 29/55$) of BA.2 nAbs showed cross-functional activity against BA.1. The majority of cross-Omicron nAbs were represented by Class 1/2 targeting nAbs ($n = 15$; 51.7%), followed by Class 3 ($n = 13$; 44.8%) and Class 4 ($n = 1$; 3.4%) targeting nAbs. None of the NTD-targeting nAbs were found to be cross-functional (Fig. 2e–g).

Antibody cross-protection to SARS-CoV-1. We investigated the ability of the BNT162b2 COVID-19 mRNA vaccine-elicited nAbs to neutralize the distantly related SARS-CoV-1 (SARS1) virus, using a lentiviral vector derived pseudoparticles, to identify immunodominant sites of cross-protection to different coronaviruses[30]. All 276 previously identified nAbs were tested for their ability to bind the SARS1 S protein (Supplementary Fig. 2b, c). Four out of five seropositives (80%) and one out of five seronegatives (20%) showed nAbs able to bind the SARS1 S protein (Supplementary Fig. 3a; Supplementary Table 1). Of the 52 nAbs isolated from seronegatives 3 (5.8%) recognized SARS1 S protein, while 16 out of 224 nAbs (7.1%) from seropositives were able to bind this antigen (Supplementary Fig. 3a; Supplementary Table 1). When nAbs were tested for their neutralization activity against SARS1, only 1 (1.9%) and 10 (4.5%) nAbs were found from seronegatives and seropositives respectively (Supplementary Fig. 3b; Supplementary Table 1). All SARS1 cross-neutralizing nAbs recognized the SARS-CoV-2 S protein RBD. Class 4 targeting nAbs able to cross-neutralize SARS1 were overall the most frequent, followed by Class 3 binding nAbs (Supplementary Fig. 3c; Supplementary Table 1). While Class 4 was the most frequent, Class 3 targeting nAbs showed the highest neutralization potency (Supplementary Fig. 3c, d; Supplementary Table 1). None of the 140 Class 1/2 regions targeting nAbs were able to cross-neutralize SARS1. Among the 11 SARS1 cross-neutralizing nAbs, the majority recognized the Class 3 region ($n = 6$; 54.5%), followed by Class 4 ($n = 4$; 36.4%) and Not-competing ($n = 1$; 9.1%) nAbs (Supplementary Fig. 3c, d).

Antibody repertoire to Omicron and SARS-CoV-1. To investigate the genetic basis of antibody cross-protection against BA.1, BA.2, and SARS1, we interrogated the functional antibody repertoire. In our previous work, we identified five predominant germlines shared among seronegatives and seropositives (IGHV1-2;IGHJ6-1, IGHV1–69;IGHJ4-1, IGHV3–30;IGHJ6-1, IGHV3–53;IGHJ6-1 and IGHV3–66;IGHJ4-1), and one rearrangement (IGHV2–5;IGHJ4-1), that encoded for potently neutralizing antibodies able to protect against all VoC from alpha (B.1.1.7) to delta (B.1.617.2), found exclusively in seropositives (Fig. 3a, top panel)[22]. Cross-protective nAbs against BA.1, BA.2, and SARS1 use a variety of genetic rearrangements (Fig. 3a, top, middle, and bottom heatmaps). The most frequent among BA.1 nAbs was the non-predominant gene rearrangement IGHV1–58;IGHJ3-1 (64.0%; 7/11) found in both seronegatives and seropositives, while predominant gene-derived nAbs only rarely were able to neutralize BA.1 (10/64; 15.6%) (Fig. 3a, top panel, and b-h). The most abundant germline among BA.2 nAbs is the predominant IGHV2–5;IGHJ4-1 gene family (6/7; 86%), while the remaining 57 predominant gene-derived nAbs poorly neutralized this variant (7/57; 12.3%) as observed for BA.1 (Fig. 3). Interestingly, we found that IGHV1–24;IGHJ6-1 gene-derived nAbs, known to encode for NTD-targeting antibodies[31], are abundantly used to protect from BA.2 but not from BA.1 or SARS1. As for SARS1 cross-

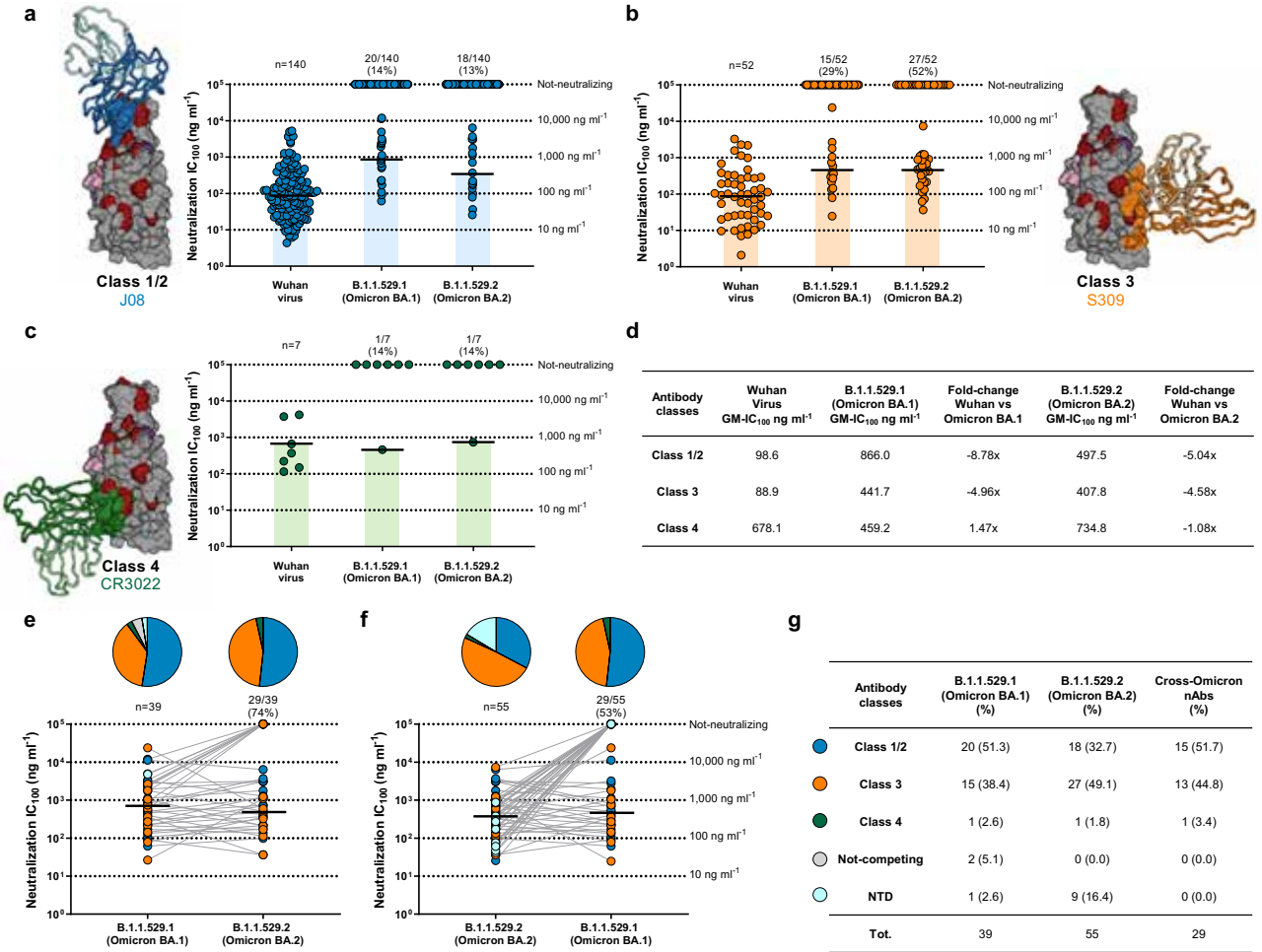

Antibody classes	Wuhan Virus GM-IC_{100} ng ml^{-1}	B.1.1.529.1 (Omicron BA.1) GM-IC_{100} ng ml^{-1}	Fold-change Wuhan vs Omicron BA.1	B.1.1.529.2 (Omicron BA.2) GM-IC_{100} ng ml^{-1}	Fold-change Wuhan vs Omicron BA.2
Class 1/2	98.6	866.0	-8.78x	497.5	-5.04x
Class 3	88.9	441.7	-4.96x	407.8	-4.58x
Class 4	678.1	459.2	1.47x	734.8	-1.08x

Antibody classes	B.1.1.529.1 (Omicron BA.1) (%)	B.1.1.529.2 (Omicron BA.2) (%)	Cross-Omicron nAbs (%)
Class 1/2	20 (51.3)	18 (32.7)	15 (51.7)
Class 3	15 (38.4)	27 (49.1)	13 (44.8)
Class 4	1 (2.6)	1 (1.8)	1 (3.4)
Not-competing	2 (5.1)	0 (0.0)	0 (0.0)
NTD	1 (2.6)	9 (16.4)	0 (0.0)
Tot.	39	55	29

Fig. 2 Distribution of Omicron BA.1 and BA.2 nAbs. a–c Dot charts show the distribution of Class 1/2 (**a**), Class 3 (**b**) and Class 4 (**c**) nAbs against the original SARS-CoV-2 virus first detected in Wuhan and the BA.1 and BA.2 Omicron VoCs. The number and percentage of nAbs and neutralization IC_{100} geometric mean (black lines, light blue, orange, and green bars) are denoted on each graph. **d** The table summarizes the IC_{100} geometric mean of nAbs against Wuhan, BA.1 and BA.2 VoCs and the GM-IC_{100} fold-change between the Omicron variants and the ancestral Wuhan virus. **e**, **f** Dot charts show the neutralization potency, reported as IC_{100} (ng ml^{-1}), of nAbs against Omicron BA.1 and their ability to cross-neutralize BA.2 (**e**) and of nAbs against Omicron BA.2 and their ability to cross-neutralize BA.1 (**f**). The number and percentage of nAbs and neutralization IC_{100} geometric mean (black lines) are denoted on each graph. Pie charts show the distribution of nAbs based on their ability to bind Class 1/2 (blue), Class 3 (orange), and Class 4 (dark green) regions on the RBD, as well as not-competing nAbs (gray) and NTD-targeting nAbs (cyan). **g** The table summarizes number and percentages of Class1/2 (blue), Class 3 (orange), Class 4 (dark green) not-competing (gray) and NTD-targeting nAbs (cyan) for BA.1, BA.2, and cross-Omicron nAbs.

neutralizing antibodies, only 7.8% (5/64) of the previously identified predominant germlines showed protection (Fig. 3i). Despite this observation, the most abundant germline used by these nAbs was the predominant IGHV1–69;IGHJ4-1 (4/; 22%) which was found in both seronegatives and seropositives and showed a medium-high 50% neutralization dose (ND_{50}) (Fig. 3a, top panel; Fig. 3i). None of the predominant gene-derived antibodies able to neutralize BA.1 and BA.2 cross-neutralized SARS1. We further analyzed the IGHV1–58;IGHJ3-1, IGHV2–5;IGHJ4-1 and IGHV1–69;IGHJ4-1 germlines which showed to be predominant in the functional response against BA.1, BA.2 and SARS1 and observed key differences among these rearrangements. All IGHV1–58;IGHJ3-1 nAbs bound the RBD and targeted Class 1/2 region (Supplementary Fig. 4a, d), and had heavy chain complementary determining region 3 (CDRH3) length of 16 amino acid (aa) with a median V gene mutation level of 3% (Fig. 3j). All IGHV2–5;IGHJ4-1 bound the RBD and targeted the Class 3 region on the RBD, carrying mainly a CDRH3 length of 10 aa and a median V gene mutation level of 3% (Fig. 3k; Supplementary Fig. 4b, d). IGHV1–58;IGHJ3-1 and IGHV2–5;IGHJ4-1 nAbs shows similar genetic characteristics independently from their ability to neutralize BA.1 and BA.2 respectively compared to the original Wuhan virus. IGHV1–69;IGHJ4-1 derived nAbs showed to be able to recognize both NTD and RBD, and to target Class 1/2 and Class 3 regions on this latter domain (Supplementary Fig. 4c, d). Conversely, IGHV1–69;IGHJ4-1 SARS1 nAbs, showed to bind only to the RBD and to target exclusively the Class 3 epitope region (Supplementary Fig. 4c, d). IGHV1–69;IGHJ4-1 nAbs showed to use a heterogenous CDRH3 length with SARS1 nAbs spanning from 11 to 12 amino acids and V gene mutation levels averaging 3.4% (Fig. 3l).

Discussion

In this work, we deeply characterized an extensive panel of BNT162b2 mRNA vaccine elicited-neutralizing human monoclonal antibodies against the heavily mutated Omicron variant BA.1, its sublineage BA.2, and the distantly related SARS-CoV-1. We found that only 14.2, 19.9. and 4.0% of our antibody panel was able to neutralize the Omicron BA.1, BA.2, and the SARS-CoV-1 virus respectively. Remarkably, from the group of seronegative people vaccinated with two doses of the BNT162b2 mRNA vaccine, we observed that only 5 of the 52 nAbs were able to

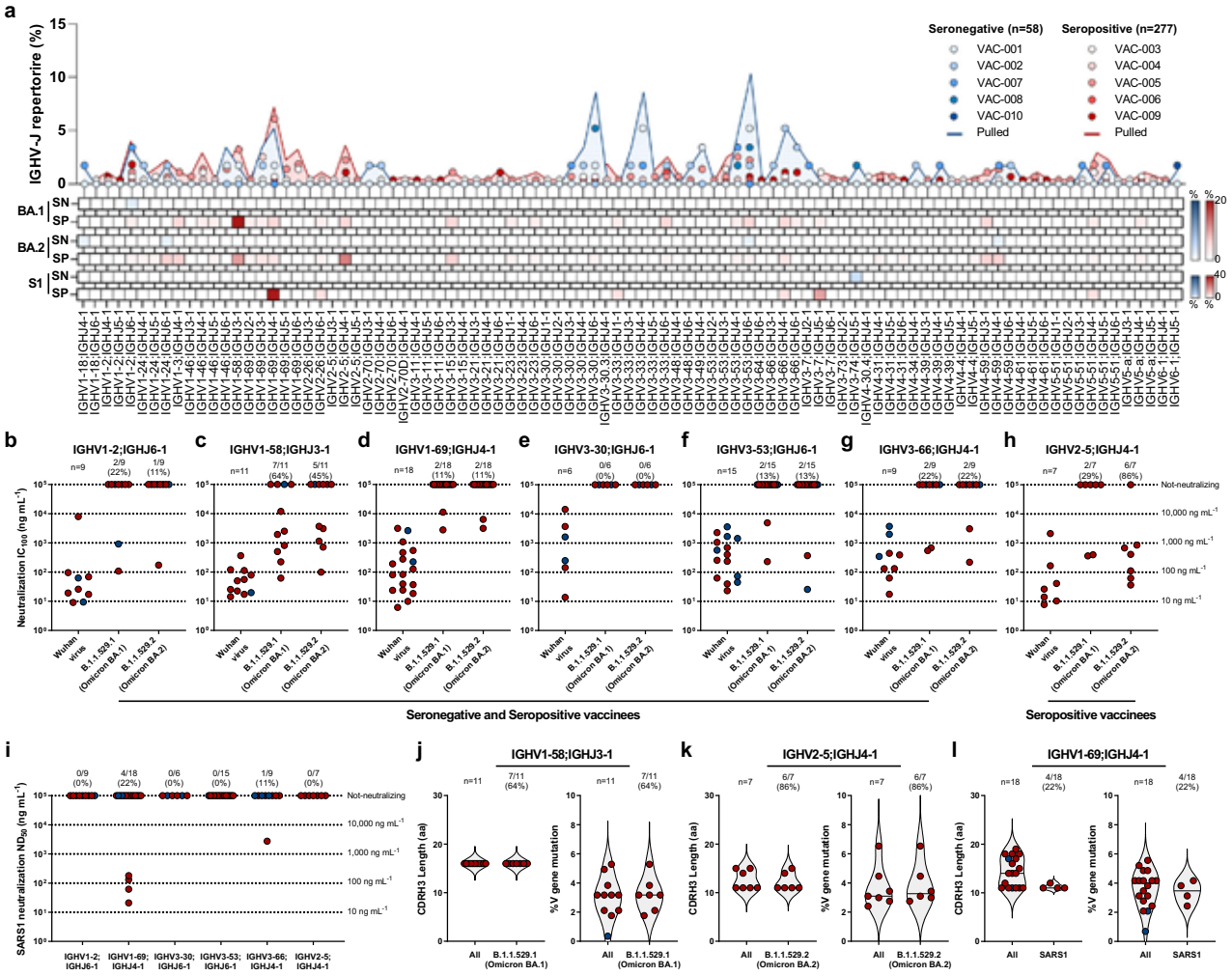

Fig. 3 Genetic characterization of BA.1, BA.2, and SARS1 nAbs. a The graph shows the IGHV-J rearrangement frequencies between vaccinees who were seronegative (SN) and seropositive (SP) (top), and the frequency within BA.1 (top heatmap), BA.2 (middle heatmap), and SARS1 (S1) (bottom heatmap) nAbs. **b**–**h** The graphs show the neutralization potency (IC_{100}) of IGHV1-2;IGHJ6-1 (**b**), IGHV1–58;IGHJ3-1 (**c**), IGHV1–69;IGHJ4-1 (**d**), IGHV3–30;IGHJ6-1 (**e**), IGHV3–53;IGHJ6-1 (**f**), IGHV3–66;IGHJ4-1 (**g**) and IGHV2–5;IGHJ4-1 (**h**) gene-derived nAbs, against the original SARS-CoV-2 virus first detected in Wuhan and the BA.1 and BA.2 VoCs. **i** The graph shows the neutralization potency (ND_{50}) of predominant germlines against SARS1. **j**–**l** Violin plots show differences in the aminoacidic (aa) CDRH3 length and percentage of V gene somatic mutations for all IGHV1–58;IGHJ3-1 (**j**) IGHV2–5;IGHJ4-1 (**k**) and IGHV1–69;IGHJ4-1 (**l**) antibodies compared to BA.1, BA.2, and SARS1 nAbs respectively.

neutralize BA.1 and BA.2, while none of their antibodies retained functionality against SARS-CoV-1. Cross-neutralizing antibodies were mainly isolated from vaccinees with previous infection, highlighting once again the broad cross-protection conferred by hybrid immunity[22,32]. Despite these results, we observed that antibody germlines mainly involved in BA.1 and SARS-CoV-1 cross-protection (IGHV1–58;IGHJ3-1 and IGHV1–69;IGHJ4-1) were used in both seronegative and seropositive vaccinees and differed from those initially identified against the original Wuhan virus and pre-omicron variants[33,34]. Interestingly, cross-protection to BA.2 was mainly driven by the Class 3 targeting germline IGHV2–5;IGHJ4-1, which was found to poorly neutralize BA.1. This scenario could partially be explained by the lack of the G446S mutation on the BA.2 spike protein, as mutations on this residue were previously shown to evade Class 3 targeting antibodies[35]. In addition to RBD-targeting antibodies, nAbs targeting the NTD "supersite" also showed to participate in the cross-protection to BA.2, as this sublineage shows a lower degree of mutations in this domain compared to BA.1. The re-acquired functionality of IGHV2–5;IGHJ4-1 Class 3 and NTD-targeting nAbs could partially explain, at the molecular level, the reason behind the higher nAbs neutralization potency to BA.2 observed in this study as well as the higher serum neutralization activity observed against BA.2 compared to BA.1 in vaccinated subjects[21]. Overall, this scenario suggests that a third booster dose in naïve people could enhance germline maturation and induce a more broad and persistent antibody response[36]. Firstly, a third booster dose could drive affinity maturation of poorly cross-reactive but predominant RBD-targeting B cell germlines elicited following SARS-CoV-2 Wuhan infection or vaccination, which were shown to persist for up to 6 months in the draining lymph nodes of vaccinated individuals[37]. Secondly, a third booster dose will also expand the population of NTD-targeting B cells, which were previously shown to be a prime target of COVID-19 mRNA vaccination[12,38], and could therefore play a pivotal role in the cross-protection against the fast-spreading BA.2 omicron variant. In addition, these data suggest that primary immunization with two doses of vaccine in naïve people is not sufficient to elicit a meaningful proportion of cross-neutralizing antibodies and that this requires a secondary immune response that can be obtained by vaccinating previously infected people or by providing a third booster dose[39]. Further studies will be necessary to understand whether a booster dose in

naïve people can elicit a hybrid immunity-like antibody response and to define the molecular basis of cross-protection in this population. In addition to previous observations on the activity of different classes of antibodies against SARS-CoV-2 and related sarbecoviruses[40–44], we herein comprehensively defined for the first time the anatomy of BA.1, BA.2, and SARS-CoV-1 neutralizing antibodies, highlighting epitope regions and predominant germlines responsible for cross-protection to these viruses. Our data can support the design of next-generation COVID-19 vaccines broadly protective against current and future coronavirus threats.

Methods

Enrollment of COVID-19 vaccinees and human sample collection. Human neutralizing antibodies tested in this work were isolated from COVID-19 vaccinated donors, of both sexes (six males and four females), who gave their written consent, thanks to a collaboration with the Azienda Ospedaliera Universitaria Senese, Siena (IT). The study was approved by the Comitato Etico di Area Vasta Sud Est (CEAVSE) ethics committees (Parere 17065 in Siena) and conducted according to good clinical practice in accordance with the declaration of Helsinki (European Council 2001, US Code of Federal Regulations, ICH 1997). This study was unblinded and not randomized. No statistical methods were used to predetermine sample size.

Transcriptionally active PCR expression of neutralizing antibodies. The transcriptionally active PCR (TAP) expression of neutralizing antibodies (nAbs) was performed as previously described[22,25]. Antibodies heavy and light chain vectors were initially digested using restriction enzymes AgeI, SalI, and Xho. PCR II products were ligated using the Gibson Assembly NEB into 25 ng of respective human Igγ1, Igκ, and Igλ expression vectors[45,46]. TAP reaction was performed using 5 µl of Q5 polymerase (NEB), 5 µl of GC Enhancer (NEB), 5 µl of 5X buffer, 10 mM of dNTPs, 0.125 µl of forward/reverse primers (forward: TTAGGCACCCCAGGCTTTAC; reverse: AGATGGTTCTTTCCGCCTCA) and 3 µl of ligation product, using the following cycles: 98 °C for 2 min, 35 cycles 98 °C for 10 s, 61 °C for 20 s, 72 °C for 1 min and 72 °C for 5 min. TAP products were purified, quantified using the Qubit Fluorometric Quantitation assay (Invitrogen), and used for transient transfection in Expi293F cell line (Thermo Fisher, Cat# A14527) following the manufacturer's instructions.

SARS-CoV-2 BA.1 and BA.2 authentic viruses neutralization assay. All SARS-CoV-2 authentic virus neutralization assays were performed in the biosafety level 3 (BSL3) laboratories at Toscana Life Sciences in Siena (Italy) and Vismederi Srl, Siena (Italy). BSL3 laboratories are approved by a Certified Biosafety Professional and are inspected every year by local authorities. To evaluate the neutralization activity of identified nAbs against SARS-CoV-2 and BA.1 and BA.2 Omciron VoCs a cytopathic effect-based microneutralization assay (CPE-MN) was performed[22,25]. Briefly, nAbs were co-incubated with a SARS-CoV-2 viral solution containing 100 median Tissue Culture Infectious Dose (100 $TCID_{50}$) of virus for 1 h at 37 °C, 5% CO_2. The mixture was then added to the wells of a 96-well plate containing a subconfluent Vero E6 cell monolayer (ATCC, Cat# CRL-1586). Plates were incubated for 3–4 days at 37 °C in a humidified environment with 5% CO_2, then examined for CPE by means of an inverted optical microscope by two independent operators. All nAbs were tested at a starting dilution of 1:10, diluted step 1:2, and the IC_{100} was evaluated based on their initial concentration. Technical duplicates for each experiment were performed. In each plate, positive and negative control were used as previously described[22,25].

SARS-CoV-2 virus variants CPE-MN neutralization assay. The SARS-CoV-2 Omicron BA.1 (B.1.1.529.1) and BA.2 (B.1.1.529.2) viruses used to perform the CPE-MN neutralization assay was supplied and sequenced by the NRC UZ/KU Leuven (Leuven, Belgium). Sequences were deposited on GISAID with the following ID: EPI_ISL_6794907 (BA.1) and EPI_ISL_10654979 (BA.2).

SARS-CoV-2 S protein competition assay. A competitive flow cytometry-based assay was performed to characterize nAbs binding profiles to SARS-CoV-2 S-protein as previously described[22]. Briefly, magnetic beads (Dynabeads His-Tag, Invitrogen) were covered with His-tagged S-proteins, following manufacturers' instructions. Then, 40 mg/mL of beads-bound-S-protein were incubated with unlabeled nAbs for 40 min at RT. Following incubation, samples were washed with PBS and incubated with fluorescently labeled Class 1/2 (J08-A647), Class 3 (S309-A488), or Class 4 (CR3022-A647) S-protein nAbs binders. Antibodies labeling was performed using Alexa Fluor NHS Ester kit (Thermo Scientific). Following 40 min of incubation at RT, the beads-antibodies mix was washed with PBS, resuspended in 150 µl of PBS-BSA 1%, and acquired using BD LSR II flow cytometer (Becton Dickinson). Results were analyzed using FlowJo™ Software (version 10). Beads with or without S-protein incubated with labeled antibodies were used as positive and negative controls respectively.

SARS-CoV-1 S protein binding assay. Expi293F cells (Thermo Fisher, Cat# A14527) were transiently transfected with SARS-CoV-1 S-protein expression vectors (pcDNA3.3_CoV1_D28) using Expifectamine Enhancer according to the manufacturer's protocol (Thermo Fisher). Two days later, to exclude dead cells from analysis, Expi293F were harvested, dispensed into a 96-well plate (3×10^5 cell/well), and stained for 30 min at room temperature (RT) with Live/Dead Fixable Aqua reagent (Invitrogen; Thermo Scientific) diluted 1:500. Following Live/Dead staining, cells were washed with PBS and incubated with nAbs candidates for 40 min at RT. Next, to identify the SARS-CoV-1 S protein mAbs binders, cells were washed and stained with the Alexa Fluor 488-labeled secondary antibody Goat anti-Human IgG (H + L) secondary antibody (Invitrogen) diluted 1:500. After 40 min of incubation, labeled cells were washed, resuspended in 150 µl of PBS, and analyzed using the BD LSR II flow cytometer (Becton Dickinson). Cells incubated with the SARS-CoV-1 nAb binder (S309) or incubated only with the secondary antibody were used as positive and negative controls respectively. Data were collected with the BD FACSDiva Software v9.0 (BD Biosciences) and analyzed with FlowJo™ Software (version 10).

HEK293TN-hACE2 cell line generation. HEK293TN-hACE2 cell line was generated by lentiviral transduction of HEK293TN (System Bioscience, Cat# LV900A-1) cells as described in Notarbartolo et al.[47]. Lentiviral vectors were produced following a standard procedure based on calcium phosphate co-transfection with 3rd generation helper and transfer plasmids. The transfer vector pLENTI_hACE2_HygR was obtained by cloning of hACE2 from pcDNA3.1-hACE2 (a gift from Fang Li, Addgene #145033) into pLenti-CMV-GFP-Hygro (a gift from Eric Campeau & Paul Kaufman, Addgene #17446). pLENTI_hACE2_HygR is now made available through Addgene (Addgene #155296). HEK293TN-hACE2 cells were maintained in DMEM, supplemented with 10% FBS, 1% glutamine, 1% penicillin/streptomycin, and 250 µg/ml Hygromycin (GIBCO).

Production of SARS-CoV-1 pseudoparticles. SARS-CoV1 lentiviral pseudotype particles were generated as described in Conforti et al. for SARS-CoV-2[30]. SARS-CoV1 SPIKE plasmid pcDNA3.3_CoV1_D28 is a gift from a gift from David Nemazee (Addgene plasmid # 170447).

SARS-CoV-1 neutralization assay. For neutralization assay, HEK293TN-hACE2 cells (System Bioscience, Cat# LV900A-1) were plated in white 96-well plates in a complete DMEM medium. 24 h later, cells were infected with 0.1 MOI of SARS-CoV-1 pseudoparticles that were previously incubated with serial dilution of purified or not purified (cell supernatant) mAb. In particular, a 7-point dose-response curve (plus PBS as untreated control), was obtained by diluting mAb or supernatant respectively five-fold and three-fold. Thereafter, nAbs of each dose-response curve point was added to the medium containing SARS-CoV-1 pseudoparticles adjusted to contain 0.1 MOI. After incubation for 1 h at 37 °C, 50 µl of mAb/SARS-CoV-1 pseudoparticles mixture was added to each well and plates were incubated for 24 h at 37 °C. Each point was assayed in technical triplicates. After 24 h of incubation cell infection was measured by luciferase assay using Bright-Glo™ Luciferase System (Promega) and Infinite F200 plate reader (Tecan) was used to read luminescence. Obtained relative light units (RLUs) were normalized to controls and dose-response curves were generated by nonlinear regression curve fitting with GraphPad Prism Version 8.0.2 (GraphPad Software, Inc., San Diego, CA) to calculate Neutralization Dose 50 (ND_{50}).

Functional repertoire analyses. nAbs VH and VL sequence reads were manually curated and retrieved using CLC sequence viewer (Qiagen). Aberrant sequences were removed from the data set. Analyzed reads were saved in FASTA format and the repertoire analyses were performed using Cloanalyst (http://www.bu.edu/computationalimmunology/research/software/)[48,49].

Statistical analysis. Statistical analysis was assessed with GraphPad Prism Version 8.0.2 (GraphPad Software, Inc., San Diego, CA). Nonparametric Mann–Whitney *t* test was used to evaluate statistical significance between the two groups analyzed in this study. Statistical significance was shown as * for values ≤0.05, ** for values ≤0.01, *** for values ≤0.001, and **** for values ≤0.0001.

Reporting summary. Further information on research design is available in the Nature Research Reporting Summary linked to this article.

Data availability

Source data are provided with this paper. All data supporting the findings in this study are available within the article or can be obtained from the corresponding author upon request. Source data are provided with this paper.

Received: 4 May 2022; Accepted: 5 June 2022;
Published online: 13 June 2022

References

1. Asundi, A., O'Leary, C. & Bhadelia, N. Global COVID-19 vaccine inequity: the scope, the impact, and the challenges. *Cell Host Microbe* **29**, 1036–1039 (2021).
2. Kavanagh, M. M., Gostin, L. O. & Sunder, M. Sharing technology and vaccine doses to address global vaccine inequity and end the COVID-19 pandemic. *JAMA* **326**, 219–220 (2021).
3. Andreano, E. & Rappuoli, R. SARS-CoV-2 escaped natural immunity, raising questions about vaccines and therapies. *Nat. Med.* **27**, 759–761 (2021).
4. Burki, T. The origin of SARS-CoV-2 variants of concern. *Lancet Infect. Dis.* **22**, 174–175 (2022).
5. Callaway, E. Beyond Omicron: what's next for COVID's viral evolution. *Nature* **600**, 204–207 (2021).
6. Karim, S. S. A. & Karim, Q. A. Omicron SARS-CoV-2 variant: a new chapter in the COVID-19 pandemic. *Lancet* **398**, 2126–2128 (2021).
7. Viana, R. et al. Rapid epidemic expansion of the SARS-CoV-2 Omicron variant in southern Africa. *Nature* **603**, 679–686 (2022).
8. Mykytyn, A. Z. et al. Omicron BA.1 and BA.2 are antigenically distinct SARS-CoV-2 variants. Preprint at *bioRxiv* https://doi.org/10.1101/2022.02.23.481644 (2022).
9. Chen, L.-L., Chu, A. W.-H., Zhang, R. R.-Q., Hung, I. F.-N. & To, K. K.-W. Serum neutralisation of the SARS-CoV-2 omicron sublineage BA.2. *Lancet Microbe* **3**, E404 (2022).
10. Cameroni, E. et al. Broadly neutralizing antibodies overcome SARS-CoV-2 Omicron antigenic shift. *Nature* **602**, 664–670 (2022).
11. Planas, D. et al. Considerable escape of SARS-CoV-2 Omicron to antibody neutralization. *Nature* **602**, 671–675 (2022).
12. Carreño, J. M. et al. Activity of convalescent and vaccine serum against SARS-CoV-2 Omicron. *Nature* **602**, 682–688 (2022).
13. Hoffmann, M. et al. The Omicron variant is highly resistant against antibody-mediated neutralization: Implications for control of the COVID-19 pandemic. *Cell* **189**, 447–456.e11 (2022).
14. McCallum, M. et al. Structural basis of SARS-CoV-2 Omicron immune evasion and receptor engagement. *Science* **0**, eabn8652 (2022).
15. Cao, Y. et al. Omicron escapes the majority of existing SARS-CoV-2 neutralizing antibodies. *Nature* **602**, 657–663 (2022).
16. VanBlargan, L. A. et al. An infectious SARS-CoV-2 B.1.1.529 Omicron virus escapes neutralization by therapeutic monoclonal antibodies. *Nat. Med.* **28**, 490–495 (2022).
17. Gruell, H. et al. mRNA booster immunization elicits potent neutralizing serum activity against the SARS-CoV-2 Omicron variant. *Nat. Med.* **28**, 477–480 (2022).
18. Dejnirattisai, W. et al. SARS-CoV-2 Omicron-B.1.1.529 leads to widespread escape from neutralizing antibody responses. *Cell* **185**, 467–484.e15 (2022).
19. Yu, J. et al. Neutralization of the SARS-CoV-2 Omicron BA.1 and BA.2 variants. *N. Engl. J. Med.* **386**, 1579–1580 (2022).
20. Bruel, T. et al. Serum neutralization of SARS-CoV-2 Omicron sublineages BA.1 and BA.2 in patients receiving monoclonal antibodies. *Nat. Med.* https://doi.org/10.1038/s41591-022-01792-5 (2022).
21. Bowen, J. E. et al. Omicron BA.1 and BA.2 neutralizing activity elicited by a comprehensive panel of human vaccines. Preprint at *bioRxiv* https://doi.org/10.1101/2022.03.15.484542 (2022).
22. Andreano, E. et al. Hybrid immunity improves B cells and antibodies against SARS-CoV-2 variants. *Nature* **600**, 530–535 (2021).
23. Yi, C. et al. Key residues of the receptor binding motif in the spike protein of SARS-CoV-2 that interact with ACE2 and neutralizing antibodies. *Cell. Mol. Immunol.* **17**, 621–630 (2020).
24. Torres, J. L. et al. Structural insights of a highly potent pan-neutralizing SARS-CoV-2 human monoclonal antibody. *Proc. Natl. Acad. Sci.* https://doi.org/10.1073/pnas.2120976119 (2022).
25. Andreano, E. et al. Extremely potent human monoclonal antibodies from COVID-19 convalescent patients. *Cell* **184**, 1821–1835.e1816 (2021).
26. Barnes, C. O. et al. SARS-CoV-2 neutralizing antibody structures inform therapeutic strategies. *Nature* **588**, 682–687 (2020).
27. Dejnirattisai, W. et al. The antigenic anatomy of SARS-CoV-2 receptor binding domain. *Cell* **184**, 2183–2200.e2122 (2021).
28. Pinto, D. et al. Cross-neutralization of SARS-CoV-2 by a human monoclonal SARS-CoV antibody. *Nature* **583**, 290–295 (2020).
29. Yuan, M. et al. A highly conserved cryptic epitope in the receptor binding domains of SARS-CoV-2 and SARS-CoV. *Science* **368**, 630–633 (2020).
30. Conforti, A. et al. COVID-eVax, an electroporated DNA vaccine candidate encoding the SARS-CoV-2 RBD, elicits protective responses in animal models. *Mol. Ther.: J. Am. Soc. Gene Ther.* **30**, 311–326 (2022).
31. Voss William, N. et al. Prevalent, protective, and convergent IgG recognition of SARS-CoV-2 non-RBD spike epitopes. *Science* **372**, 1108–1112 (2021).
32. Crotty, S. Hybrid immunity. *Science* **372**, 1392–1393 (2021).
33. Vanshylla, K. et al. Discovery of ultrapotent broadly neutralizing antibodies from SARS-CoV-2 elite neutralizers. *Cell host microbe* **30**, 69–82.e10 (2022).
34. Yuan, M. et al. Structural basis of a shared antibody response to SARS-CoV-2. *Science* **369**, 1119–1123 (2020).
35. Greaney, A. J. et al. Mapping mutations to the SARS-CoV-2 RBD that escape binding by different classes of antibodies. *Nat. Commun.* **12**, 4196 (2021).
36. Turner, J. S. et al. SARS-CoV-2 mRNA vaccines induce persistent human germinal centre responses. *Nature* **596**, 109–113 (2021).
37. Laidlaw, B. J. & Ellebedy, A. H. The germinal centre B cell response to SARS-CoV-2. *Nat. Rev. Immunol.* **22**, 7–18 (2022).
38. Amanat, F. et al. SARS-CoV-2 mRNA vaccination induces functionally diverse antibodies to NTD, RBD, and S2. *Cell* **184**, 3936–3948.e3910 (2021).
39. Pajon, R. et al. SARS-CoV-2 Omicron variant neutralization after mRNA-1273 booster vaccination. *N. Engl. J. Med.* **386**, 1088–1091 (2022).
40. Hastie Kathryn, M. et al. Defining variant-resistant epitopes targeted by SARS-CoV-2 antibodies: A global consortium study. *Science* **374**, 472–478 (2021).
41. Tan, C.-W. et al. Pan-Sarbecovirus Neutralizing Antibodies in BNT162b2-Immunized SARS-CoV-1 Survivors. *N. Engl. J. Med.* **385**, 1401–1406 (2021).
42. Martinez David, R. et al. A broadly cross-reactive antibody neutralizes and protects against sarbecovirus challenge in mice. *Sci. Transl. Med.* **14**, eabj7125 (2022).
43. Tortorici, M. A. et al. Broad sarbecovirus neutralization by a human monoclonal antibody. *Nature* **597**, 103–108 (2021).
44. Wang, Z. et al. Naturally enhanced neutralizing breadth against SARS-CoV-2 one year after infection. *Nature* **595**, 426–431 (2021).
45. Tiller, T. et al. Efficient generation of monoclonal antibodies from single human B cells by single cell RT-PCR and expression vector cloning. *J. Immunol. Methods* **329**, 112–124 (2008).
46. Wardemann, H. & Busse, C. E. Expression cloning of antibodies from single human B cells. *Methods Mol. Biol.* **1956**, 105–125 (2019).
47. Notarbartolo, S. et al. Integrated longitudinal immunophenotypic, transcriptional, and repertoire analyses delineate immune responses in patients with COVID-19. *Sci. Immunol.* **6**, eabg5021 (2021).
48. Kepler, T. B. Reconstructing a B-cell clonal lineage. I. Statistical inference of unobserved ancestors. *F1000Res* **2**, 103–103 (2013).
49. Kepler, T. B. et al. Reconstructing a B-cell clonal lineage. II. Mutation, selection, and affinity maturation. *Front. Immunol.* **5**, 170 (2014).

Acknowledgements

This work was funded by the European Research Council (ERC) advanced grant agreement number 787552 (vAMRes). This work was supported by a fundraising activity promoted by Unicoop Firenze, Coop Alleanza 3.0, Unicoop Tirreno, Coop Centro Italia, Coop Reno e Coop Amiatina. This publication was supported by the COVID-2020-12371817 project, which received funding from the Italian Ministry of Health. Piet Maes acknowledges support from the Research Foundation Flanders (COVID19 research grant G0H4420N) and Internal Funds KU Leuven (grant 3M170314). We would also like to acknowledge Dr. Jason McLellan, for kindly providing the SARS-CoV-2 and SARS1 S protein trimers, RBD, and NTD.

Author contributions

E.A. and R.R. conceived the study. I.P. performed binding and competition assays. N.M. expressed monoclonal antibodies. P.P. and E.A. performed repertoire analyses. E.P. and V.A. produced and purified SARS-CoV-2 constructs. E.A., I.P., G. Pierleoni, G. Piccini, L.B., and G.G. performed live SARS-CoV-2 neutralization assays. P.M. isolated SARS-CoV-2 BA.1 and BA.2 Omicron viruses. M.L. propagated SARS-CoV-2 viruses. S.M. and L.D. performed SARS1 pseudotype neutralization assays. C.D.S. supported day-to-day laboratory activities and management. E.A. and R.R. wrote the manuscript. E.A., I.P., L.D., S.M., G. Pierleoni, N.M., E.P., V.A., P.P., L.B., G.G., M.L., P.M., C.D.S., G. Piccini, C.S., R.D.F., E.M., and R.R. undertook the final revision of the manuscript. E.A., C.S., R.D.F., E.M., and R.R. coordinated the project.

Competing interests

R.R. is an employee of the GSK group of companies. E.A., I.P., N.M., P.P., E.P., V.A., C.D.S., C.S., and R.R. are listed as inventors of full-length human monoclonal antibodies described in Italian patent applications no. 102020000015754 filed on June 30th 2020, 102020000018955 filed on August 3rd 2020, and 102020000029969 filed on 4th of December 2020, and the international patent system number PCT/IB2021/055755 filed on the 28th of June 2021. All patents were submitted by Fondazione Toscana Life

Sciences, Siena, Italy. R.D.F. is a consultant for Moderna on activities not related to SARS-CoV-2. The remaining authors declare no competing interests.

Additional information

Supplementary information The online version contains supplementary material available at https://doi.org/10.1038/s41467-022-31115-8.

Correspondence and requests for materials should be addressed to Rino Rappuoli.

Peer review information *Nature Communications* thanks the anonymous reviewers for their contribution to the peer review of this work. Peer reviewer reports are available.

Reprints and permission information is available at http://www.nature.com/reprints

Publisher's note Springer Nature remains neutral with regard to jurisdictional claims in published maps and institutional affiliations.

PNAS RESEARCH ARTICLE | IMMUNOLOGY AND INFLAMMATION OPEN ACCESS

Structural insights of a highly potent pan-neutralizing SARS-CoV-2 human monoclonal antibody

Jonathan L. Torres[a,1], Gabriel Ozorowski[a,1], Emanuele Andreano[b], Hejun Liu[a], Jeffrey Copps[a], Giulia Piccini[c], Lorena Donnici[d], Matteo Conti[d], Cyril Planchais[e], Delphine Planas[f,g], Noemi Manganaro[b], Elisa Pantano[b], Ida Paciello[b], Piero Pileri[b], Timothée Bruel[f,g], Emanuele Montomoli[c,h,i], Hugo Mouquet[e], Olivier Schwartz[f,g], Claudia Sala[b], Raffaele De Francesco[d,j], Ian A. Wilson[a,k], Rino Rappuoli[b,l], and Andrew B. Ward[a,2]

Edited by Pamela Bjorkman, California Institute of Technology, Pasadena, CA; received November 18, 2021; accepted April 4, 2022

As the coronavirus disease 2019 (COVID-19) pandemic continues, there is a strong need for highly potent monoclonal antibodies (mAbs) that are resistant against severe acute respiratory syndrome coronavirus 2 (SARS-CoV-2) variants of concern (VoCs). Here, we evaluate the potency of the previously described mAb J08 against these variants using cell-based assays and delve into the molecular details of the binding interaction using cryoelectron microscopy (cryo-EM) and X-ray crystallography. We show that mAb J08 has low nanomolar affinity against most VoCs and binds high on the receptor binding domain (RBD) ridge, away from many VoC mutations. These findings further validate the phase II/III human clinical trial underway using mAb J08 as a monoclonal therapy.

SARS-CoV-2 | monoclonal therapy | neutralizing antibody | cryoelectron microscopy | variants of concern

Significance

Clinical candidate monoclonal antibody J08 binds the severe acute respiratory syndrome coronavirus 2 (SARS-CoV-2) S-protein independent of known escape mutations and is able to potently neutralize most variants of concern (VoCs). Here, we explore these properties using cell-based assays and structural studies. A relatively small epitope footprint high on the receptor binding domain (RBD) ridge and the ability to bind multiple conformational states of the S-protein contribute to strong neutralization across several variants.

To date, over 219 million cases and 4.5 million deaths worldwide have been caused by severe acute respiratory syndrome coronavirus 2 (SARS-CoV-2) (1), along with high levels of unemployment and far-reaching supply chain issues in the world's economy. While the situation is vastly improving with numerous vaccine rollouts and over 6.03 billion doses of vaccines administered worldwide, they have been heavily skewed toward developed nations (2). Hence, disadvantaged communities and low- and middle-income countries remain potential hotspots for the emergence of viral variants with increased infectivity and mortality. Designated variants of concern (VoCs) pose the greatest threat to progress made thus far because data have shown that they can reduce the effectiveness of the coronavirus disease 2019 (COVID-19) vaccines (3). These findings have led vaccine manufacturers to test booster shots (4–6) that will ultimately result in another logistical distribution and administration challenge.

COVID-19 vaccines, whether mRNA, protein, or viral vector based, aim to provide acquired immunity and protection against serious disease by presenting the SARS-CoV-2 spike protein (S-protein) to the immune system (7). The S-protein is a glycosylated, homotrimeric type I transmembrane fusion protein responsible for host cell attachment via its receptor binding domain (RBD) to human angiotensin-converting enzyme 2 (hACE2), a process that is enhanced by a coreceptor, cellular heparan sulfate (8). The S-protein is made up of the S1 domain (residues 1 to 685) containing the RBD and N-terminal domain (NTD) and the S2 domain (residues 686 to 1213) housing the fusion machinery. Both the RBD and NTD are immunodominant epitopes that are targeted by a majority of neutralizing antibodies (9).

Ending the pandemic is being challenged by the emergence of VoCs, uneven roll out of vaccines worldwide, vaccine hesitancy, uncertainty of whether COVID-19 vaccines can prevent transmission, breakthrough infections among vaccinated populations, and if vaccinated and naturally infected individuals will have long-lasting immunity against the virus. Therefore, having readily available, highly potent, and viral-variant-resistant monoclonal antibodies (mAbs) may serve to mitigate the propagation of troublesome variants worldwide and treat those that remain vulnerable after vaccination. Early efforts with monoclonal therapies have had mixed results. LY-CoV555 (bamlanivimab), developed by Eli Lilly and Company, was found to have no significant effect on viral load compared to a placebo in phase II trials and is easily susceptible to escape mutations present in common VOCs (10, 11). Monoclonal mixtures are one strategy to decrease the chance of viral escape, and a recent Emergency Use Authorization was given for Regeneron's casirivimab (REGN10933) and imdevimab (REGN10987) and for Eli Lilly and Company's bamlanivimab and etesevimab combinations (10, 12).

In this study, we characterized the neutralization breadth of a highly potent human mAb, J08, previously isolated from a convalescent COVID-19 patient (13), against the

Author contributions: J.L.T., G.O., E.A., R.R., and A.B.W. designed research; J.L.T., G.O., E.A., H.L., G.P., L.D., M.C., C.P., D.P., T.B., E.M., H.M., O.S., C.S., and R.D.F. performed research; H.L., J.C., L.D., M.C., N.M., E.P., I.P., P.P., and I.A.W. contributed new reagents/analytic tools; J.L.T., G.O., and E.A. analyzed data; and J.L.T., G.O., E.A., R.R., and A.B.W. wrote the paper.

Competing interest statement: The authors declare a competing interest. R.R. is an employee of the GlaxoSmithKline (GSK) group of companies. E.A., I.P., N.M., E.P., P.P., C.S., and R.R. are listed as inventors of full-length human monoclonal antibodies described in Italian patent applications n. 102020000015754 filed on June 30, 2020, 102020000018955 filed on August 3, 2020, and 102020000029969 filed on December 4, 2020, and the international patent system number PCT/IB2021/055755 filed on June 28, 2021. The other authors declare that they have no competing interests.

This article is a PNAS Direct Submission.

[1]J.L.T. and G.O. contributed equally to this work.

[2]To whom correspondence may be addressed. Email: andrew@scripps.edu.

This article contains supporting information online at http://www.pnas.org/lookup/suppl/doi:10.1073/pnas.2120976119/-/DCSupplemental.

Published May 12, 2022.

SARS-CoV-2 B.1.1.7 (Alpha), B.1.351 (Beta), P.1 (Gamma), B.1.617.2 (Delta), and recently emerged B.1.1.529 (Omicron) VoCs. Following functional characterization, we further investigated the structural details of J08 to define the epitope that retains neutralization activity against these VoCs.

Results

J08 Cross-Neutralizes All Current SARS-CoV-2 VoCs. To evaluate neutralization breadth, J08 was tested for binding, ACE2 blocking, and neutralization against the SARS-CoV-2 D614G virus and VoCs B.1.1.7 (isolated in the United Kingdom) (14), B.1.351 (isolated in South Africa) (15), P.1 (isolated in Brazil) (16), and B.1.617.2 (isolated in India) (17). These VoCs have been renamed by the World Health Organization as Alpha, Beta, Gamma, and Delta variants, respectively (18). We first tested antibody binding or ACE2 blocking in an enzyme-linked immunosorbent assay (ELISA) using the S-protein RBD from the original Wuhan strain and from the Alpha through Delta VoCs. J08 was able to bind and interfere with the RBD/ACE2 interaction with all tested variants (Fig. 1 *A* and *B*). We next evaluated the neutralization activity of J08 against authentic SARS-CoV-2 and VoC viruses using a cytopathic-effect-based microneutralization (CPE-MN) assay, an S-fuse neutralization assay, and a SARS-CoV-2 pseudovirus platform. The neutralization experiments were performed in three different and independent laboratories. The CPE-MN assay demonstrated that J08 was able to neutralize the SARS-CoV-2 D614G virus with a 100% inhibitory concentration (IC_{100}) of 3.9 ng/mL and maintain its extremely high neutralization activity against all tested VoCs with an IC_{100} of 3.9, 9.7, 4.9, and 6.2 ng/mL for the Alpha, Beta, Gamma, and Delta VoCs, respectively (Fig. 1 *C* and *F*). A similar scenario was observed with the S-fusion neutralization assay, where J08 was able to neutralize all VoCs tested. The S-fusion neutralization assay differs from the other methods as it uses cell lines (U2OS-ACE2 GFP1-10 or GFP 11) that emit fluorescence when they are productively infected by SARS-CoV-2. The antibody neutralization activity is evaluated as the ability of the mAb to block infection and therefore syncytial formation and fluorescence emission. Given the extremely high neutralization potency of J08, we were not able to define a 50% inhibitory concentration (IC_{50}) against the D614G, Alpha, and Delta variants, and therefore, we assigned it as <1 ng/mL. On the other hand, it was possible to define the neutralization potency of J08 against the Beta and Gamma variants that showed an IC_{50} of around 3.2 and 1.0 ng/mL, respectively (Fig. 1 *D* and *F*). Finally, we evaluated the neutralization activity of J08 using a lentiviral pseudovirus platform produced with a SARS-CoV-2 spike variant, which

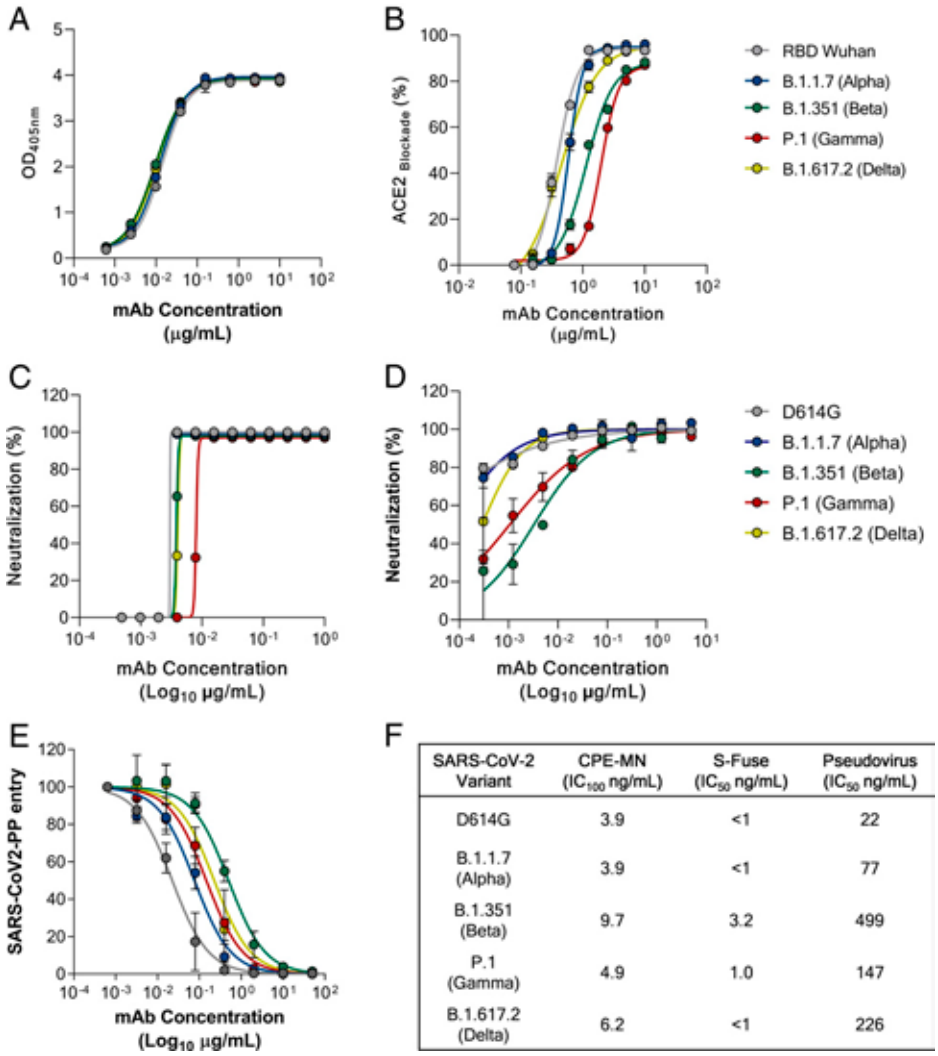

F

SARS-CoV-2 Variant	CPE-MN (IC_{100} ng/mL)	S-Fuse (IC_{50} ng/mL)	Pseudovirus (IC_{50} ng/mL)
D614G	3.9	<1	22
B.1.1.7 (Alpha)	3.9	<1	77
B.1.351 (Beta)	9.7	3.2	499
P.1 (Gamma)	4.9	1.0	147
B.1.617.2 (Delta)	6.2	<1	226

Fig. 1. J08 activity against SARS-CoV-2 and emerging variants. Graphs show the ability of mAb J08 to bind (*A*); block RBD/ACE2 interaction (*B*); and neutralize SARS-CoV-2 D614G, B.1.1.7, B.1.351, P.1, and B.1.617.2 using a CPE-MN (*C*), S-fuse (*D*), and pseudovirus platform (*E*). (*F*) Summary of the IC_{100} and IC_{50} results obtained for all neutralization assays. Errors bars display SEM for $N = 3$ measurements.

included a cytoplasmic tail deletion of 19 amino acids. Similar cytoplasmic tail deletions showed an enhanced spike incorporation into pseudovirions and increased viral entry into cells, compared to those with full-length S-protein (19). With our pseudovirus platform, we observed an overall lower neutralization IC_{50} by J08. The differences in measured inhibitory concentrations between assay types could arise from the pseudovirus platform used and its high incorporation of S-protein into pseudovirions, as well as the use of cell lines showing different levels of cell surface hACE2 presentation. In addition, the variations of neutralization potencies observed between authentic virus and pseudovirus might also be due to the diluted viral stocks used for these assays. Nonetheless, J08 showed an IC_{50} against the D614G, Alpha, Beta, Gamma, and Delta variants of 22, 77, 499, 147, and 226 ng/mL, respectively, further confirming its ability to neutralize all VoCs (Fig. 1 *E* and *F*). While we performed this work, the B.1.1.529 (Omicron) emerged and spread worldwide. Therefore, we evaluated the ability of J08 to neutralize this SARS-CoV-2 VoC. Despite that an important IC_{100} and IC_{50} reduction was observed in our CPE-MN and pseudovirus platform, J08 retained some neutralization activity against Omicron on the contrary of several mAbs recognizing a similar epitope region on the SARS-CoV-2 S-protein (20, 21) (*SI Appendix*, Fig. S1). Using biolayer interferometry, we detected appreciable affinity of J08 immunoglobulin G (IgG) to the Omicron-CoV-2-6P S-protein (dissociation constant [K_D], ∼98 nM), but compared to the SARS-CoV-2-6P D614G S-protein, against which we did not observe a measurable off-rate under similar assay conditions, J08 dissociates relatively rapidly from the Omicron-CoV-2-6P S-protein (*SI Appendix*, Fig. S1 *D* and *E*). The on-rate is also ∼sevenfold slower against Omicron, suggesting that altered binding kinetics are decreasing the neutralization potency of J08 against this variant (*SI Appendix*, Fig. S1).

Neutralization Activity of Competitor Antibodies against SARS-CoV-2 and Emerging Variants. To compare the neutralization potency and breadth of J08 to other SARS-CoV-2 neutralizing mAbs that have received emergency use authorization for COVID-19 treatment, we recombinantly expressed REGN10987 (12), REGN10933 (12), S309 (22), CoV2.2196 (23), and LY-CoV016 (10) as immunoglobulin G1 (IgG1). All mAbs were tested by the CPE-MN assay using authentic SARS-CoV-2 viruses and by our pseudovirus platform against the D614G, Alpha, Beta, Gamma, and Delta VoCs. REGN10987 showed a neutralization potency of 24.6, 19.5, 4.9, 3.1, and 19.7 ng/mL against D614G, Alpha, Beta, Gamma, and Delta VoCs, respectively (*SI Appendix*, Fig. S2 *A* and *K*). A similar trend for these variants was observed with our pseudovirus platform, although the Delta variant showed a 52-fold reduction (*SI Appendix*, Fig. S2 *F* and *K*). Antibody REGN10933, which recognizes the receptor binding motif of the S-protein, showed high neutralization potency against D614G, Alpha, and Delta VoCs but was heavily impacted by the Beta and Gamma VoCs, showing a 59- and 29.5-fold decrease, respectively (*SI Appendix*, Fig. S2 *B* and *K*). Our pseudovirus platform results were in accordance with the CPE-MN assay (*SI Appendix*, Fig. S2 *G* and *K*). We then evaluated antibody S309, which targets a region outside of the S-protein receptor binding motif (22). This antibody, when assessed by the CPE-MN assay, retained its neutralization potency against all SARS-CoV-2 variants showing an IC_{100} of 156, 248, 78, 25, and 79 ng/mL for the D614G, Alpha, Beta, Gamma, and Delta VoCs, respectively (*SI Appendix*, Fig. S2 *C* and *K*). In our pseudovirus platform, S309 was able to neutralize all SARS-CoV-2 variants but in the 4- to 41-μg/mL range (*SI Appendix*, Fig. S2 *H* and *K*). Antibody CoV2-2196 showed high neutralization potency against all variants in both the CPE-MN assay and pseudovirus platform ranging from 12.3 to 49.2 ng/mL and 45.0 to 425.0 ng/mL, respectively (*SI Appendix*, Fig. S2 *D*, *I*, and *K*). Despite CoV2-2196 being the only antibody that showed high neutralization potency against all variants, J08 remains the only antibody able to neutralize all VoCs with an IC_{100} below 10 ng/mL Finally, we evaluated antibody LY-CoV016 that was heavily impacted by the Alpha variant with a 12-fold decrease in neutralization and was unable to bind to the Beta and Gamma variants (*SI Appendix*, Fig. S2 *E* and *K*). LY-CoV016 lost activity to Alpha, Beta, and Gamma but was not impacted by the Delta VoC, showing an IC_{100} of 49.6 ng/mL (*SI Appendix*, Fig. S2 *E* and *K*). When LY-CoV016 was tested in our pseudovirus platform, it was able to neutralize the D614G and Delta variants with a similar potency of around 300 ng/mL (*SI Appendix*, Fig. S2 *J* and *K*). In addition to previous SARS-CoV-2 VoCs, REGN10987, REGN10933, S309, CoV2-2196, and LY-CoV016 were tested against the recently emerged Omicron in our CPE-MN and pseudovirus platform. REGN and LY-CoV016 antibodies did not show neutralization activity against this VoC. Conversely, S309 and CoV2-2196 retained activity, albeit showing up to 3.2- and 1,600-fold reduction, respectively, in our CPE-MN assay (*SI Appendix*, Fig. S1). These results are consistent with previously reported neutralization activity of each antibody (11, 21, 24–30).

J08 Can Bind Dynamic RBD Conformations. For structural studies, we generated the following two constructs based on SARS-CoV-2-6P (six proline): one with the RBDs restricted to the down configuration by introduction of an interprotomer disulfide bond at positions C383 and C985 (Mut2) (31) and a second with unrestricted RBD movement but higher stability, containing an interprotomer disulfide bond at C705 and C883 (Mut7). Single-particle cryoelectron microscopy (cryo-EM) analysis of two complexes, SARS-CoV-2-6P-Mut2 + fragment antigen binding (Fab) J08 and SARS-CoV-2-6P-Mut7 + Fab J08, resulted in four cryo-EM maps and associated models, as follows: SARS-CoV-2-6P-Mut2 trimer alone (3.2 Å), SARS-CoV-2-6P-Mut2 + Fab J08 conformation 1 (3.4 Å), SARS-CoV-2-6P-Mut2 + Fab J08 conformation 2 (3.4 Å), and SARS-CoV-2-6P-Mut7 + Fab J08 conformation 3 (4.0 Å) (Fig. 2*A* and *SI Appendix*, Fig. S3 and Table S1). Although Fab J08 has nanomolar affinity to the trimer, the short incubation time during sample preparation for cryo-EM enabled reconstruction of a trimer with no antibody bound, serving as a comparator for our analysis with J08-bound structures. Lastly, we determined a 2.53-Å crystal structure of recombinant RBD in complex with Fab J08 to address details in the antibody–antigen interface (*SI Appendix*, Table S2).

In the SARS-CoV-2-6P-Mut2 + Fab J08 complex, we captured two different poses of Fab J08 through three-dimensional (3D) classification, which we call conformation 1 and conformation 2. In conformation 1, the J08 Fabs are further apart with a more closed apex (RBD more down), while conformation 2 has the Fabs closer together and a more open apex (RBD slightly open) (Fig. 2*A*). Superimposition of the S-protein models revealed movement in the S1 subunit, in comparison to minimal movement in the S2 subunit (Fig. 2*B*). Both conformations consist of three Fab molecules bound to a single S-protein trimer. In the SARS-CoV-2-6P-Mut7 + Fab J08 complex (conformation 3), Fab J08 bound to one RBD-up while the two other RBDs were down. Unlike the Mut2 complexes, most particles had a stoichiometry of only one Fab per

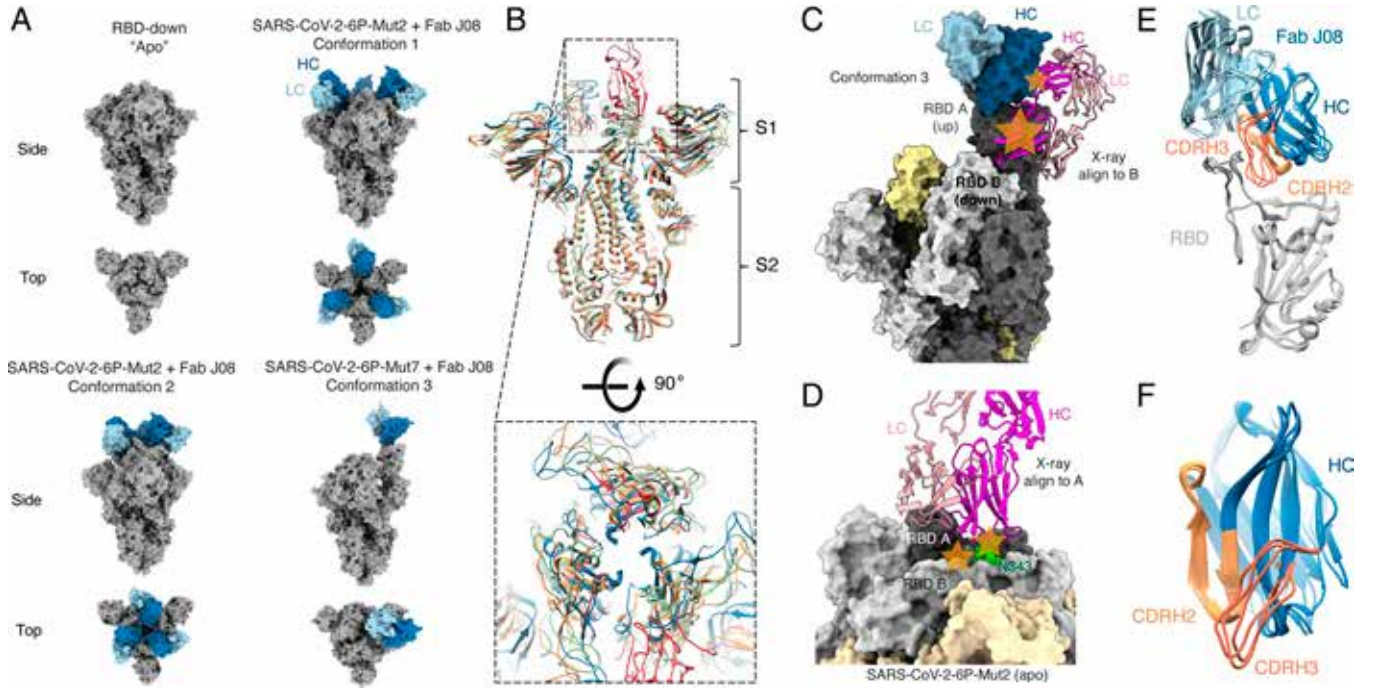

Fig. 2. Conformational states of the S-protein-Fab J08 complex observed by cryo-EM. (*A*) *Top* and *Side* view surface representations of SARS-CoV-2-6P + Mut2, SARS-CoV-2-6P-Mut2 + Fab J08 conformation 1, SARS-CoV-2-6P-Mut2 + Fab J08 conformation 2, and SARS-CoV-2-6P-Mut7 + Fab J08 conformation 3. S-protein is labeled in gray, HC in dark blue, and LC in light blue. (*B*) *Side* and *Top* views of superimposed models of SARS-CoV-2-6P-Mut 2 (blue), SARS-CoV-2-6P-Mut 2 + FabJ08 (conformations 1 and 2; orange and green, respectively), and SARS-CoV-2-6P-Mut 7 + Fab J08 (conformation 3; red) reveal flexibility at the S1 domain that affects the opening at the apex. (*C*) Alignment of RBD-J08 X-ray structure onto protomer B of cryo-EM conformation 3 reveals a clash between the neighboring up-RBD and antibody. Clash sites are displayed as orange stars. (*D*) Alignment of RBD-J08 X-ray structure onto the ligand-free SARS-CoV-2-6P-Mut2 model reveals a clash with a neighboring RBD and its N343 glycan. Clash sites are displayed as orange stars. (*E*) The structure of the RBD (gray) across conformations 1 to 3 does not change when Fab J08 is bound. (*F*) CDRH3 (salmon) of Fab J08 exhibits more movement to accommodate binding to the RBD-up or -down conformations. On the other hand, CDRH2 (light orange) shows less movement across the different models.

S-protein trimer (Fig. 2*A*), although there was a small minority of particles with two Fabs bound in the negative-stain electron microscopy and cryoEM two-dimensional (2D) classes (*SI Appendix*, Fig. S4*A*). Alignment of the RBD-J08 X-ray structure onto the first cryo-EM conformation 3 down RBD (clockwise from the antibody-bound up RBD as viewed toward the viral membrane) reveals that a direct clash would occur with the up RBD (Fig. 2*C*). When aligned to the second down RBD (counterclockwise from the antibody-bound up RBD), a clash occurs between J08 CDRH3 and the neighboring down RBD and is likely exacerbated by the neighboring N343 glycan (*SI Appendix*, Fig. S4*B*). Finally, we find that the alignment of the RBD-J08 X-ray structure onto the ligand-free SARS-CoV-2-6P-Mut2 model reveals the same clash with neighboring RBD and glycan N343 (Fig. 2*D*), and highlights that even in the down-RBD models there is some degree of structural rearrangement and opening at the apex.

Alignment of the RBD-antibody portion of each of the models revealed no major differences in the angle of the Fab relative to the RBD, and the epitope remained constant (Fig. 2*E*). However, more subtle differences were observed within the epitope–paratope interaction. The heavy chain complementarity-determining region 2 (CDRH2) loops were rigid, while the heavy chain CDRH3 loops were more variable, suggesting that CDRH2 was the anchoring interaction (Fig. 2*F*). These subtle differences might also be a result of differences in local resolution across the various datasets (*SI Appendix*, Fig. S3). Concomitant with these structural differences, we observed variable buried surface areas (BSAs) for Fab J08 bound to the three different conformations. Although J08 binds to the same epitope across the different conformations we observed that Fab J08 has the smallest footprint on the RBD in conformation 3 at 658 Å^2, followed by conformation 1 at 728 Å^2, and conformation 2 at 985 Å^2 (Fig. 3). When not under the constraints of an intact protomer or trimer, the BSA between J08 and RBD based on the X-ray structure is 676 Å^2, which is most similar to conformation 3.

J08 can accommodate the dynamic movement of the RBD with several key contacts (Fig. 3 *B*–*D* and *SI Appendix*, Table S3). CDRH2 appears to play an anchoring role and provides the most hydrogen bonds (including salt bridges) between antibody and RBD in conformations 1 and 2. In the up conformation 3, the antibody is tilted slightly, increasing the number of CDRH3 contacts, consistent with the X-ray structure of the RBD-Fab J08 complex (*SI Appendix*, Table S3). Accordingly, in conformations 1 and 3 and the X-ray structure, the heavy chain interface residues (defined as contributing greater than 5 Å^2 BSA) all reside in CDRH2 and CDRH3 (*SI Appendix*, Tables S3 and S4). A portion of the interprotomer Fab contacts in conformation 2 are provided by CDRH1 (*SI Appendix*, Tables S3 and S4). On the contrary, the antibody light chain makes fewer contacts with the RBD and around 25% of the total BSA (Fig. 3 and *SI Appendix*, Table S3). CDRL1 and CDRL3 are part of the RBD interface in all three conformations, with only CDRL1 contributing hydrogen bond/salt bridge interactions (*SI Appendix*, Tables S3 and S4). We hypothesize that the unique ability to bind both RBD down and up is a contributing factor to the high potency of Fab J08.

Molecular Description of the Epitope–Paratope Interface. A commonality across the three binding conformations of J08 is residue R56 on the side chain of CDRH2 projecting toward the RBD, in a region bound by E484 and Q493 on opposite

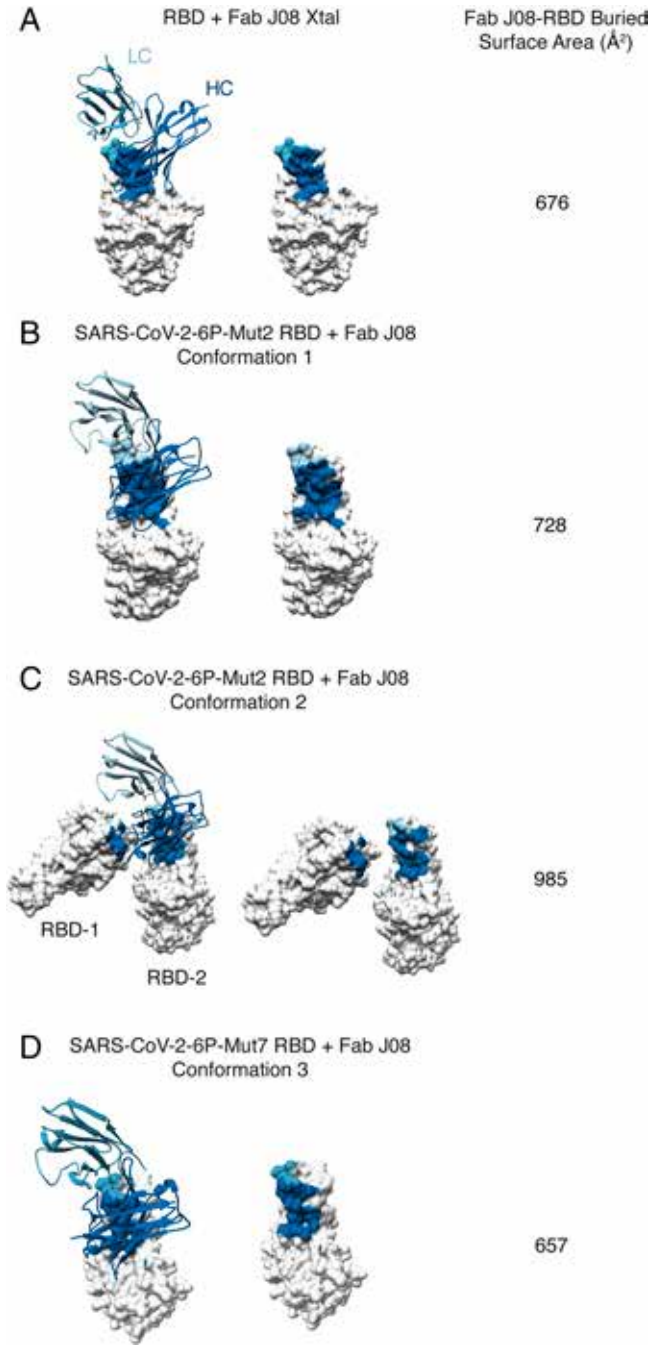

Fig. 3. BSA and epitope footprint of J08 in X-ray and cryo-EM structures. J08 epitope footprint and calculated buried surface area in X-ray structure (*A*), cryo-EM conformation 1 (*B*), cryo-EM conformation 2 (*C*), and cryo-EM conformation 3 (*D*). Shown are surface representation of the RBD (gray) and ribbon representation of Fab J08 (HC, dark blue; LC, light blue).

sides (Fig. 4*A*). In the X-ray structure of RBD-Fab J08, R56 is predicted to simultaneously form a salt bridge and hydrogen bond with the side chains of E484 and Q493, respectively (Fig. 4*A* and *SI Appendix*, Fig. S4*C*). Cryo-EM conformation 2 has the best-resolved map in this region and is predicted to also utilize a hydrogen bond with Q493, while swapping the E484 interaction with one to the F490 backbone carbonyl (Fig. 4*A* and *SI Appendix*, Fig. S4*D*). Antibody J08 is derived from IGHV1-69*02 and is hardly mutated relative to the germ line (96% amino acid sequence identity with only four mutations observed). Unexpectedly, all four mutations are in CDRH2 (corresponding to Kabat numbering 55 to 58) (*SI Appendix*, Fig. S4*E*). Relative to the germ line, the mutations include I56R, which is involved in key interactions as outlined above. The germ line I56 residue would not be capable of side-chain hydrogen bond interactions, suggesting this mutation was selected to increase affinity and/or specificity. Surprisingly, when we tested the R56I J08 IgG mutant using biolayer interferometry, we did not observe obvious changes in binding kinetics relative to wild-type J08 (*SI Appendix*, Fig. S1*F*). G55D and A57V do not directly interact with the RBD but appear to contribute to the overall stability and rigidity of CDRH2. D55 of CDRH2 forms a salt bridge with K73 of framework region 3 (FRH3), while V57, with its bulkier hydrophobic side chain relative to the germ line, points toward a region with several hydrophobic side chains, strengthening the interaction between beta strands of CDRH2 and FRH3 (*SI Appendix*, Fig. S4*F*). Based on the X-ray structure, N58M might also stabilize the local environment as it is part of a hydrophobic cluster that includes F486 (RBD), W47 (heavy chain [HC]), and L96 (light chain [LC]). All four of these mutations emphasize the importance of CDRH2 as the key anchoring point of J08 to the RBD. CDRH3, on the other hand, is predicted to form backbone hydrogen bonds with the side chains of RBD residues N487 and Y489, further strengthening the interaction of J08 to its relatively small epitope (*SI Appendix*, Fig. S4*H*). The light chain, derived from IGKV3-11, has two mutations relative to the germ line, one of which (L4M) might stabilize CDRL1, which is near the RBD ridge (*SI Appendix*, Fig. S4 *E* and *G*).

Fab J08 Does Not Interact with Most Mutations Found in VoCs. Since Fab J08 binds high on the RBD ridge, it is far less susceptible to the commonly mutated residues in the receptor binding site (RBS) in the emerging VoCs. As previously described (32), the RBS is subdivided into four epitopes, delineated as RBS-A, -B, -C, and -D. Fab J08 belongs to the RBS-B class, in comparison to other antibodies such as Fab C102 (RBS-A), Fab CV07-270 (RBS-C), and C110 (RBS-D) (Fig. 4*B*). Many of the commonly mutated residues exist in these epitopes, thus increasing the odds of viral escape (Fig. 4*B* and *SI Appendix*, Fig. S5). For example, K417 resides in RBS-A, E484 in RBS-B, L452 and E484 in RBS-C, and N501 in between RBS-A and RBS-D. Studies have shown that the binding potency and neutralization capacity of several previously isolated mAbs are severely reduced or abrogated in the presence of one of these point mutations (6).

N501Y, a mutation found in the Alpha, Beta, Gamma, and Omicron variants, is not part of the J08 interface, explaining why neutralization against the Alpha variant is unaffected. Common to the Beta, Gamma, and Omicron variants are mutations at position 417 (K417N in Beta and Omicron, K417T in Gamma). K417 is at the interface with J08 in conformations 1 and 3 and the X-ray structure, contributing a hydrogen bond via its side chain amine with CDRH3 in conformations 1 and 3 (*SI Appendix*, Fig. S4*D* and Tables S3 and S4). Since neutralization against Beta and Gamma variants is unaffected, we conjecture that this interaction is not critical and becomes redundant with additional CDRH3 residues involved in the RBD interaction. The E484K mutation is shared among the Alpha, Beta, and Gamma variants, while Omicron presents a shorter and hydrophobic E484A mutation at the same site. E484, as mentioned, is predicted to form a salt bridge with R56 of CDRH2 in some of the conformations (*SI Appendix*, Table S3), so introducing a basic residue in its place might affect binding. However, neutralization and a negative-stain

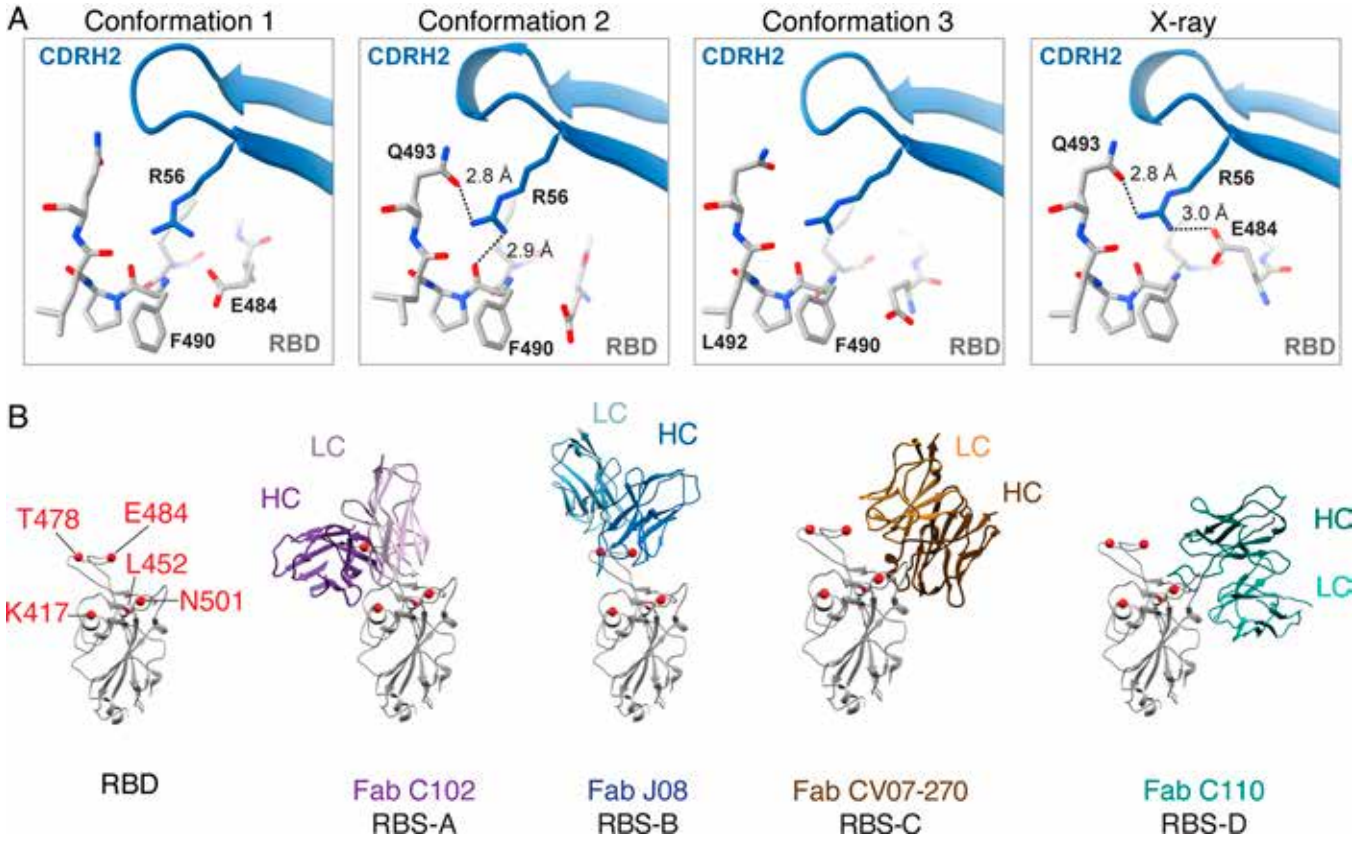

Fig. 4. Molecular contacts and RBD epitope classification of Fab J08. (*A*) The key molecular environment between J08 CDRH2 residue R56 and RBD are highlighted, and predicted hydrogen bonds are represented as dashed lines with distances labeled. (*B*) Fab J08 belongs to the RBS-B class of antibodies in comparison to Fab C102, Fab CV07-270, and Fab C110 that belong to RBS-A, RBS-C, and RBS-D, respectively.

EM complex of J08 and Gamma S-protein suggests otherwise (Fig. 1 and *SI Appendix*, Fig. S5*D*), perhaps due to the versatility of R56 finding alternate contacts (e.g., with RBD backbone carbonyls in conformation 3). Finally, the Delta variant has an L452R mutation, and shares an additional T478K mutation with Omicron, and while T478 appears at the LC interface, neither residue has a measured interaction with J08 in our structures (*SI Appendix*, Fig. S5 and Table S4).

The more recent Omicron VOC has over 35 mutations in the S-protein, with 15 residing in the RBD. As described above, specific point mutations shared with other VOCs do not appear to impede neutralization, but our assays reveal a sharp decrease in neutralization and high off-rate of J08 against Omicron itself. To address whether the overall epitope is altered on the Omicron surface, we generated a ~6-Å cryo-EM reconstruction of J08 in complex with the Omicron-CoV-2-6P S-protein (*SI Appendix*, Fig. S5 and Table S1). We observe one Fab bound to a subpopulation of S-protein, and a comparison to our SARS-CoV-2-6P D614G (Wuhan) S-protein-J08 complex (conformation 3) map suggests that the overall epitope footprint is not changed. However, Omicron contains a Q493R mutation not found in other VOCs. Our models of J08 in complex with the SARS-CoV-2 6P D614G (Wuhan) strain S-protein/RBD suggest an interdependence between E484 and Q493 of RBD with J08 CDRH2 R56, and we infer that a mutation of the 484 and 493 sites in Omicron is the primary factor leading to decreased sensitivity of J08 against this variant.

RBS-B antibodies that bind high on the RBD-ridge, which share a similar angle of approach as Fab J08 and sterically block binding of hACE2, include S2E12 (33), CV07-250 (34), A23-58.1 (35), and S2K146 (36) (Fig. 5*A*). In comparison to J08, S2E12, and A23-58.1, the HCs and LCs of CV07-250 and S2K146 are rotated ~90 degrees clockwise, thereby expanding the footprint on the RBD and using more LC contacts than just primarily HC contacts. In fact, this rotation and larger footprint are remarkably similar to hACE2 (Fig. 5*B*). In decreasing order, the RBD-antibody/receptor BSA is largest for S2K146 (980 Å^2), CV07-250 (943 Å^2), ACE2 (843 Å^2), S2E12 (753 Å^2), J08 (675 Å^2, based on the RBD-Fab J08 X-ray structure), and A23-58.1 (603 Å^2). S2E12 and A23-58.1 are most similar to J08 based on epitope, as the antibodies make most of their contacts with the RBD via the HC and can also neutralize variants containing the E484K/D614G and E484Q/D614G/Q779H mutations. A difference is that the CDRH3 of S2E12 and A23-58.1 are nestled more against the RBD ridge, in closer proximity to the 477/478 residues that are mutated in some VOCs. However, the CDRH2 of each antibody appears farther away from E484/Q493 than J08, perhaps making them less susceptible to mutations at those sites. Like J08, S2E12 and A23-58.1 would require a partially open Spike to avoid clashing with a neighboring RBD and glycan N343. While the Omicron variant has affected many mAbs targeting the RBD, including J08, it is noteworthy that 45% of RBD residues involved in the RBD-ACE2 interface are also part of the J08 interface, and these residues in turn account for 77% of the RBD-J08 interface (*SI Appendix*, Fig. S6), suggesting that escape mutations to J08 that do not also negatively impact viral fitness are rare.

Discussion

We used a combination of cell-based assays and structural biology to better understand the remarkable potency and resistance

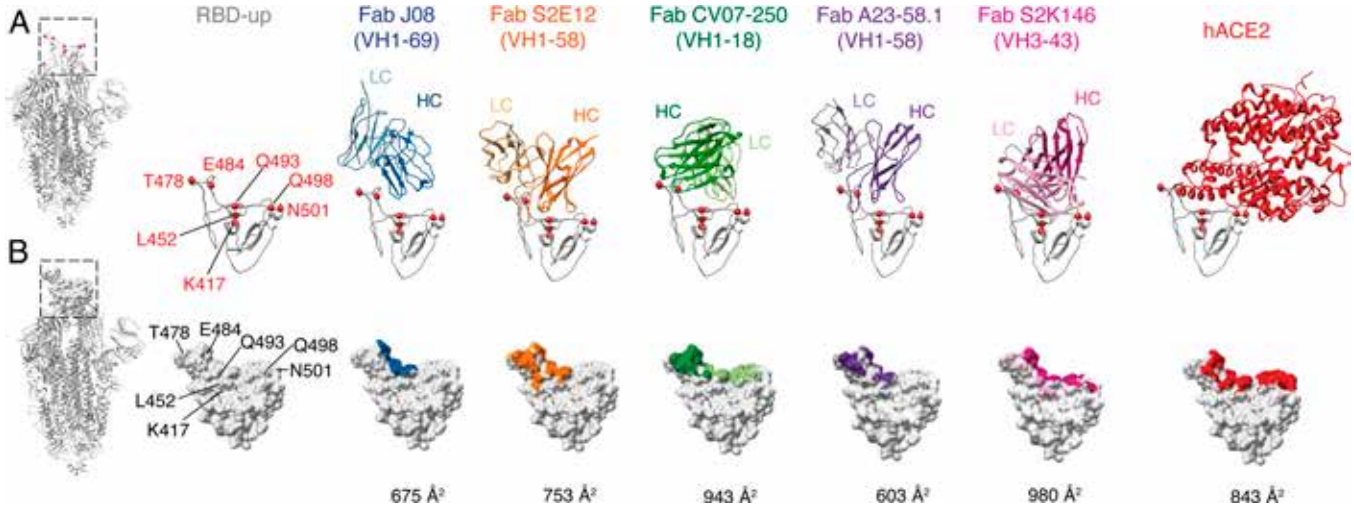

Fig. 5. Epitope footprint comparison of Fab J08 to similar antibodies and hACE2. (*A*) Fab J08 compared to antibodies S2E12, CV07-250, A23-58.1, and S2K146 that share similar angles of approach and bind high on the RBD ridge, thereby allosterically inhibiting hACE2 binding. Commonly mutated residues K417, L452, T478, E484, Q493, Q498, and N501 are shown as a point of reference and orientation of the RBD. (*B*) Surface representation of the RBD with antibody contacts colored on the surface and calculated BSA values (Å^2) reveal that Fab J08 has a small footprint and is therefore less susceptible to escape mutations.

to many VoCs by mAb J08. Neutralization assays using authentic virus and pseudovirus revealed that Fab J08 was able to neutralize VoCs at a low nanomolar affinity and outperform similar RBD-binding competitor antibodies, such as REGN10987/10933, S309, COV2.2196, and LY-COV016 in the low-nanomolar range. The Omicron variant presents a challenge to J08, but we still found the antibody capable of neutralization, again outperforming other monoclonals that are escaped by this VOC. Using cryo-EM and X-ray crystallography experiments, we showed that J08 can bind to multiple conformations of the S-protein with the RBD in either the up or partially down position and its smaller epitope footprint is distant from many of the common mutations found in the VOCs. E484, while on the edge of the epitope and a potential hydrogen bond or salt bridge partner, does not appear to be straddled by the antibody in a way that would create a clash in the E484K variant. Nonetheless, when coupled with a Q493H mutation, as the case in the Omicron VOC, both binding affinity and neutralization are negatively impacted. mAb J08 is currently being evaluated in clinical trials to test its utility as an important intervention therapeutic for moderate-to-severe COVID-19. The very high potency and ability to resist many escape mutations are critical properties for the next generation of SARS-CoV-2 mAb therapeutics.

Materials and Methods

ELISA. High-binding 96-well ELISA plates (Costar, Corning) were coated overnight with 250 ng/well of purified recombinant SARS-CoV-2 proteins. After being washed with 0.05% Tween 20–phosphate-buffered saline (PBST), plates were blocked for 2 h with 2% bovine serum albumin, 1 mM ethylenediaminetetraacetic acid (EDTA), and PBST (blocking buffer); washed; and incubated with purified monoclonal IgG antibodies at 10 μg/mL and 7 consecutive 1:4 dilutions in PBS. After the PBST washing, the plates were incubated with goat horseradish peroxidase (HRP)-conjugated anti-human IgG antibodies for 1 h (Jackson ImmunoReseach, 0.8 μg/mL final in blocking buffer) and analyzed by adding 100 μL of HRP chromogenic substrate (ABTS solution, Euromedex) after the washing steps. For competition experiments of RBD binding to ACE-2, ELISA plates were coated overnight with 250 ng/well of purified ACE-2 ectodomain. After the PBST wash step, plates were blocked for 2 h with blocking buffer, washed with PBST, and incubated with purified monoclonal IgG antibodies at 10 μg/mL and 7 consecutive 1:2 dilutions in PBS in the presence of biotinylated RBD proteins at 0.5 μg/mL After being washed, the plates were incubated for 30 min with HRP-conjugated streptavidin (BD Biosciences) and analyzed by adding 100 μL of the HRP chromogenic substrate (ABTS solution, Euromedex). Optical densities were measured at 405 nm (OD_{405nm}), and background values, assessed by incubation of PBS alone in coated wells, were subtracted. Experiments were performed using a HydroSpeed microplate washer and Sunrise microplate absorbance reader (Tecan Männedorf).

SARS-CoV-2 Authentic Virus Neutralization Assay. All SARS-CoV-2 authentic virus neutralization assays were performed in the biosafety level 3 (BSL3) laboratories at Toscana Life Sciences in Siena (Italy), Vismederi Srl, Siena (Italy), and Institute Pasteur, Paris (France). The BSL3 laboratories are approved by a Certified Biosafety Professional and inspected every year by local authorities. Two different approaches were used to evaluate the neutralization activity of J08 against SARS-CoV-2 and emerging variants and the neutralization breadth of tested antibodies. The first method is the cytopathic effect (CPE)-based neutralization assay described by Andreano and colleagues (13), while the second method is a S-fuse neutralization assay previously described by Planas et al. (26). Briefly, the CPE-based neutralization assay reports on the coincubation of mAbs with a SARS-CoV-2 solution containing 100 median tissue culture infectious dose ($TCID_{50}$) of virus and after 1 h incubation at 37 °C and 5% CO_2. The mixture was then added to the wells of a 96-well plate containing a subconfluent Vero E6 cell monolayer. Plates were incubated for 3 d at 37 °C in a humidified environment with 5% CO_2 and then examined for CPE by means of an inverted optical microscope. As for the S-fuse neutralization assay, U2OS-ACE2 GFP1-10 or GFP 11 cells, also termed S-Fuse cells, emit fluorescence when they are productively infected by SARS-CoV-2 (26, 37). Cells were tested negative for mycoplasma. Cells were mixed (1:1 ratio) and plated at 8×10^3 per well in a μClear 96-well plate (Greiner Bio-One). SARS-CoV-2s were incubated with mAbs for 15 min at room temperature and added to S-Fuse cells. After 18 h, cells were fixed with 2% paraformaldehyde, washed, and stained with Hoechst solution (1:1,000 dilution; Invitrogen). Images were acquired with an Opera Phenix high-content confocal microscope (PerkinElmer). The GFP area and the number of nuclei were quantified using the Harmony software (PerkinElmer). The percentage of neutralization was calculated using the number of syncytia as a value with the following formula: 100 × (1 – (value with mAb – value in "non-infected")/(value in "no mAb" – value in "non-infected")). We previously reported a correlation between neutralization titers obtained with the S-Fuse assay and a pseudovirus neutralization assay (38).

SARS-CoV-2 Variants for CPE-MN and S-fuse Neutralization Assays. The SARS-CoV-2s used to perform the CPE-MN neutralization assay were D614G(EVAg Cod: 008V-04005), B.1.1.7 (INMI GISAID accession number: EPI_ISL_736997), B.1.351 (EVAg Cod: 014V-04058), P.1 (EVAg CoD: 014V-04089),

B.1.617.2 (ID: EPI_ISL_2029113), and B.1.1.529 (ID: EPI_ISL_6794907). The SARS-CoV-2s used to perform the S-fuse neutralization assay were D614G, B.1.1.7, B.1.351, and B.1.617.2, and their sequences were deposited on GISAID, with the following identifiers: D614G: EPI_ISL_414631, B.1.1.7: EPI_ISL_735391, B.1.1.351: EPI_ISL_964916, and B.1.617.2: ID: EPI_ISL_2029113 (27).

HEK293TN-hACE2 Cell Line Generation. An HEK293TN-hACE2 cell line was generated by lentiviral transduction of HEK293TN cells as described in Notarbartolo S. et al. (39). Briefly, HEK293TN cells were obtained from System Bioscience. Lentiviral vectors were produced following a standard procedure based on calcium phosphate cotransfection with third generation helper and transfer plasmids. The following helper vectors were used (gifts from Didier Trono, School of Life Sciences, Ecole Polytechnique Fédérale de Lausanne (EPFL), Lausanne, Switzerland): pMD2.G/VSV-G (Addgene #12259), pRSV-Rev (Addgene #12253), and pMDLg/pRRE (Addgene #12251). The transfer vector pLENTI_hACE2_HygR was obtained by cloning hACE2 from pcDNA3.1-hACE2 (a gift from Fang Li, Department of Veterinary and Biomedical Sciences, University of Minnesota, Saint Paul, MN, Addgene #145033) into pLenti-CMV-GFP-Hygro (a gift from Eric Campeau & Paul Kaufman, Program in Gene Function and Expression, University of Massachusetts Medical School, Worcester, MA, Addgene #17446). hACE2 complementary DNA was amplified by PCR and inserted under the CMV promoter of the pLenti-CMV-GFP-Hygro after GFP excision with XbaI and SalI digestion. pLENTI_-hACE2_HygR is now available through Addgene (Addgene #155296). After transduction with the hACE2 lentiviral vector, cells were subjected to antibiotic selection with hygromycin at 250 μg/mL. The expression of hACE2 cells was confirmed by flow cytometry staining using an anti-hAce2 primary antibody (AF933; R&D system) and rabbit anti-goat IgG secondary antibody (Alexa Fluor 647). HEK293TN-hACE2 cells were maintained in Dulbecco's Modified Eagle Medium (DMEM) and supplemented with 10% FBS, 1% glutamine, 1% penicillin/streptomycin, and 250 μg/mL hygromicin (GIBCO), and the expression of hACE2 was found to be stable after multiple passages.

Production of SARS-CoV-2 Pseudoparticles Based on Lentiviral Vectors. To generate SARS-CoV-2 lentiviral pseudotype particles, 5×10^6 HEK-293TN cells were plated in a 15-cm dish in complete DMEM. The following day, 32 μg of reporter plasmid pLenti CMV-GFP-TAV2A-LUC Hygro, 12.5 mg of pMDLg/pRRE (Addgene #12251), 6.25 mg of pRSV-Rev (Addgene #12253), and 9 μg pcDNA3.1_ S-protein_del19 were cotransfected following a calcium phosphate transfection. pcDNA3.1_S-protein_del19 was generated by deletion of the last 19 amino acids of S-protein starting from pcDNA3.1-SARS2-S-protein (a gift from Fang Li, Addgene plasmid #145032) and is now available through Addgene (Addgene #155297). pLenti CMV-GFP-TAV2A-LUC Hygro was generated from pLenti CMV GFP Hygro (Addgene #17446) by addition of T2A-Luciferase by PCR cloning. At 12 h before transfection, the medium was replaced with complete Iscove medium. At 30 h after transfection, the supernatant was collected, clarified by filtration through 0.45-μm pore-size membranes, and concentrated by centrifugation for 2 h at 20,000 rpm using an SW32Ti rotor. Viral pseudoparticle suspensions were aliquoted and stored at −80 °C.

SARS-CoV-2 Pseudovirus Neutralization Assay. Pseudovirus neutralization assays were carried out as previously described (40). Briefly, HEK293TN-hACE2 cells were plated at 10^4 cells/well in white 96-well plates in complete DMEM. At 24 h later, cells were infected with a 0.1 multiplicity of infection (MOI) of SARS-CoV-2 pseudoparticles that were previously incubated with a serial dilution of mAb. In particular, mAbs under test were serially diluted fivefold in PBS in order to obtain a seven-point dose–response curve (plus PBS as an untreated control). Thereafter, 5 μL of each dose–response curve point was added to 45 μL of medium containing SARS-CoV-2 pseudoparticles adjusted to contain 0.1 MOI. After incubation for 1 h at 37 °C, 50 μL of a mAb/SARS-CoV-2 pseudoparticle mixture was added to each well and plates were incubated for 24 h at 37 °C. Each point was assayed in triplicate. After 24 h of incubation, cell infection was measured by a luciferase assay using the Bright-Glo luciferase system (Promega) and an Infinite F200 plate reader (Tecan) to read the luminescence. Obtained relative light units were normalized to controls, and dose–response curves were generated by nonlinear regression curve fitting with GraphPad Prism to calculate neutralization dose 50 (ND_{50}).

Expression and Purification of SARS-CoV-2 S-protein in the Prefusion Conformation. Mutagenesis was performed on the SARS-CoV-2-6P plasmid to include S383C and D985C for the SARS-CoV-2-6P-Mut2 construct and V705C and T883C for the SARS-CoV-2-6P-Mut7 construct. The Omicron SARS-CoV-2 plasmid contained only the 6P mutations (Omicron-CoV-2-6P). Expression of the SARS-CoV-2-6P-Mut2, SARS-CoV-2-6P-Mut7, or Omicron-CoV-2-6P S-protein was performed by incubating 0.5 mg of DNA with 1.5 mg of polyethylenimine for 20 min. The mixture was placed into 1 L of HEK293F cells (Thermo Fisher), incubated for 6 d at 37 °C with 8% CO_2 and shaken at 125 rpm. After cell harvest, the supernatant was passed over a StrepTactin XT 4FLOW column (IBA Lifesciences), washed with buffer W (100 mM Tris-Cl [pH 8], 150 mM NaCl, 1 mM EDTA), and eluted with buffer BXT (100 mM Tris-Cl [pH 8], 150 mM NaCl, 1 mM EDTA, 50 mM biotin). The eluant was then size exclusion purified over a Superose 6 Increase-16/600 pg, 120-mL column (Cytiva). Purified trimers were buffer exchanged back into buffer W using a 100-kDa concentrator (Amicon).

Sample Vitrification for Cryo-EM. SARS-CoV-2-6P-Mut2 was incubated with a threefold molar excess of Fab J08 at room temperature for 5 min. The final concentration of the complex was 3 mg/mL. To aid with sample dispersal on the grid, the complex was briefly incubated with n-dodecyl-B-D-maltoside (final concentration, 0.06 mM; Anatrace) and deposited on plasma-cleaned Quantifoil 1.2/1.3 4C grids. A Thermo Fisher Vitrobot Mark IV set to 4 °C, 100% humidity, 6-s wait time, and a 3-s blot time was used for the sample vitrification process. SARS-CoV-2-6P-Mut7 or Omicron-CoV-2-6P were incubated with a threefold molar excess of Fab J08 at room temperature for 30 min. The sample vitrification process was as described above except that the detergent for SARS-CoV-2-6P-Mut7 was fluorinated octyl maltoside (final concentration of 0.02%, wt/vol; Anatrace) and the grids were UltrAuFoil 1.2-1.3 3C. For Omicron-CoV-2-6P, the detergent used was lauryl maltose neopentyl glycol (final concentration of 0.005 mM; Anatrace) and the grids were Quantifoil 1.2/1.3 2C.

Cryo-EM Data Collection. Datasets for both SARS-CoV-2-6P-Mut2 and SARS-CoV-2-6P-Mut7 complexes were collected at 36,000× magnification on a Thermo Fisher Talos Arctica (200 keV, 1.15-Å pixel size) electron microscope with a 4k by 4k Gatan K2 Summit direct electron detector. Data collection was automated with the Leginon software (41), and raw micrographs were stored in the Appion database (42). For the Omicron-CoV-2-6P complex, data collection was performed on a Thermo Fisher Glacios (200 keV, 0.57-Å pixel size) using a Thermo Fisher Falcon 4 direct electron detector and Thermo Fisher EPU 2 software.

For the SARS-CoV-2-6P-Mut2 + Fab J08 complex, a total of 2,325 micrographs were collected with a total dose of 50 e-/Å^2 fractionated over 48 frames, with each frame receiving a dose rate of 5.5 electrons per pixel per second. A defocus range of −0.2 μm to −2.4 μm was used. For the SARS-CoV-2-6P-Mut7 + Fab J08 complex, 4,090 micrographs were collected with a total dose of 50 e-/Å^2 fractionated over 50 frames, with each frame receiving a dose rate of 5.2 electrons per pixel per second. In this case, a defocus range of −0.5 μm to −2.0 μm was used. For the Omicron-CoV-2-6P + Fab J08 complex, 4,146 micrographs were collected with a total dose of 49 e-/Å^2 fractionated over 40 frames, with each frame receiving a dose rate of 4.4 electrons per pixel per second. A defocus range of −0.7 μm to −1.4 μm was used.

Cryo-EM Data Processing, Model Building, and Refinement. The micrograph movie frames from the SARS-CoV-2-6P-Mut2 and SARS-CoV-2-6P-Mut7 datasets were aligned and dose weighted with MotionCorr2 (43). Aligned frames were imported into cryoSPARC v3.2 (44) where the contrast transfer function (CTF) was estimated using Patch CTF. For the Omicron-CoV-2-6P dataset, the Patch Motion Correction job of cryoSPARC Live was used for alignment and dose weighting of movies (44). Particles were picked using templates (created from an initial round of 2D classification after automated picking), extracted, and subjected to multiple rounds of 2D classification for cleaning. For the SARS-CoV-2-6P-Mut2 and SARS-CoV-2-6P-Mut7 datasets, an apo (unliganded) S-protein was imported for 3D classification (heterogeneous refinement) and the best classes were further refined. To further improve the resolution, the maps were subjected to global and local CTF refinements and 3D variability analyses. Final refinements were performed using the nonuniform refinement feature (45). The Omicron-CoV-2-6P dataset particles were exported to Relion 3.1 (46) and downscaled to 1.14 Å/pixel to reduce computational demands resulting from a large box

size. After an additional round of 2D classification and automated 3D refinement, the particles were subjected to C3 symmetry expansion. A 40-Å-diameter spherical mask was placed over the RBD/Fab of a single protomer and iterative rounds of 1) alignment-free 3D classification and 2) 3D refinement with restricted search angles using a mask over the trimer core and a single RBD+Fab were performed to isolate J08-bound particles. A summary of data collection and processing statistics can be found in *SI Appendix*, Table S1.

Initial models were generated by fitting Spike coordinates from Protein Data Bank (PDB) 6vsb and the RBD-J08 X-ray structure (see below) into the cryo-EM maps using University of California San Francisco Chimera (47). Several rounds of iterative manual and automated model building and relaxed refinement were performed using Coot 0.9.4 (48) and Rosetta (49). Models were validated using EMRinger (50) and MolProbity (51) as part of the Phenix software suite (52). Kabat numbering was applied to the antibody Fab variable LCs and HCs using the Abnum antibody numbering server (53). Final refinement statistics and PDB deposition codes for generated models can be found in *SI Appendix*, Table S1. Buried surface area calculations and distance measurements were performed using PDBePISA (54).

Crystallization and X-Ray Structure Determination. The J08 Fab complexed with SARS-CoV-2 RBD was formed by mixing each of the protein components in an equimolar ratio and incubating overnight at 4 °C. A total of 384 conditions of the JCSG Core Suite (Qiagen) were used for setting up trays for the complex (6 mg/mL) on the robotic CrystalMation system (Rigaku) at Scripps Research. Crystallization trials were set up by the vapor diffusion method in sitting drops containing 0.1 μL of protein complex and 0.1 μL of reservoir solution. Crystals appeared on day 3, were harvested on day 7, pre-equilibrated in cryoprotectant containing 10% ethylene glycol, and then flash cooled and stored in liquid nitrogen until data collection. Diffraction data were collected at cryogenic temperature (100 K) at beamline 12-1 of the Stanford Synchrotron Radiation Lightsource (SSRL) and processed with HKL2000 (55). Diffraction data were collected from crystals grown in drops containing 17% (wt/vol) polyethylene glycol 4000, 15% (vol/vol) glycerol, 8.5% (vol/vol) isopropanol, and 0.085 M sodium Hepes (pH 7.5). The X-ray structures were solved by molecular replacement (MR) using PHASER (56) with MR models for the RBD and Fab from PDB 7JMW (57). Iterative model building and refinement were carried out in COOT (48) and PHENIX (52), respectively. X-ray data collection and structural refinement statistics can be found in *SI Appendix*, Table S2.

Biolayer Interferometry. Anti-human IgG Fc Capture (AHC) biosensors (ForteBio) were used to assess the binding affinities of J08 IgG and J08 R56I IgG with SARS-2 CoV 6P D614G and Omicron 6P in kinetics buffer (PBS + 0.02% Tween-20 + 0.1% bovine serum albumin) on an Octet RED96 instrument (ForteBio). Initially, the biosensors were soaked in kinetics buffer prior to loading the IgGs to a threshold of 1.0 nm. The biosensors were dipped into kinetics buffer for a second baseline and then dipped into wells containing S-protein at twofold dilutions with seven different concentrations (31.3, 15.6, 7.3, 3.65, 1.82, 0.91, and 0.45 nM for SARS-CoV-2-6P D614G (Wuhan) and 1,000, 500, 250, 125, 62.5, 31.3, and 15.6 nM for Omicron-CoV-2-6P) to measure association. Biosensors were then dipped into wells containing kinetics buffer to measure dissociation. Data were reference subtracted based on a kinetics buffer baseline and aligned to each other using Octet Data Analysis software (ForteBio). Curve fitting was performed using a 1:1 binding model and data for the seven concentrations of S-protein, but only those that fit the raw data best were included, which are labeled with a red dashed line. On-rate, off-rate, and K_D values were determined with a global fit. Data were exported from the ForteBio Data Analysis software and plotted using GraphPad Prism.

Data Availability. The data needed to evaluate conclusions in this paper are present in both the paper itself and/or in *SI Appendix*. The cryo-EM maps have been deposited in the Electron Microscopy Data Bank (EMDB) with accession codes EMD-24876 (SARS-CoV-2-6P-Mut2), EMD-24877 (SARS-CoV-2-6P-Mut2 + Fab J08 conformation 1), EMD-24878 (SARS-CoV-2-6P-Mut2 + Fab J08 conformation 2), EMD-24879 (SARS-CoV-2-6P-Mut7 + Fab J08), and EMD-26389 (Omicron SARS-CoV-2-6P + Fab J08) and the atomic models deposited in the Protein Data Bank (PDB) with accession codes 7s6i (SARS-CoV-2-6P-Mut2), 7s6j (SARS-CoV-2-6P-Mut2 + Fab J08 conformation 1), 7s6k (SARS-CoV-2-6P-Mut2 + Fab J08 conformation 2), and 7s6l (SARS-CoV-2-6P-Mut7 + Fab J08). The coordinate and structure factor of the crystal structure of SARS-CoV-2 RBD in complex with Fab J08 has been deposited in the PDB with accession code 7sbu.

ACKNOWLEDGMENTS We thank B. Anderson and H. Turner for microscope assistance, C. Bowman for computational assistance, and G.K. Hedestam and M. Corcoran for scientific discussion regarding human antibody germline genes. We thank Dr. Piet Maes from NRC UZ/KU Leuven (Leuven, Belgium) for kindly providing the Omicron live. This work was funded by Toscana Life Sciences, through the European Research Council advanced Grant agreement number 787552 (vAMRes), the European Union's Horizon 2020 research and innovation program under Grant agreement no. 653316, and the Italian Ministry of Health COVID-2020-12371817 project, under collaborative agreements with The Scripps Research Institute. Work in the O.S. lab is funded by Institut Pasteur, Urgence COVID-19 Fundraising Campaign of Institut Pasteur, ANRS, the Vaccine Research Institute (ANR-10-LABX-77), Labex IBEID (ANR-10-LABX-62-IBEID), ANR/FRM Flash Covid PROTEO-SARS-CoV-2, and IDISCOVR. This work was also funded by the Bill & Melinda Gates Foundation (OPP1170236/INV-004923).

Author affiliations: [a]Department of Integrative Structural and Computational Biology, The Scripps Research Institute, La Jolla, CA 92037; [b]Monoclonal Antibody Discovery (MAD) Lab, Fondazione Toscana Life Sciences, 53100 Siena, Italy; [c]VisMederi S.r.l, 53100 Siena, Italy; [d]Istituto Nazionale Genetica Molecolare INGM "Romeo ed Enrica Invernizzi", 20122 Milan, Italy; [e]Laboratory of Humoral Immunology, Department of Immunology, Institut Pasteur, INSERM U1222, 75015 Paris, France; [f]Virus and Immunity Unit, Department of Virology, Institut Pasteur, CNRS UMR 3569, 75015 Paris, France; [g]Vaccine Research Institute, 94000 Creteil, France; [h]VisMederi Research S.r.l., 53100 Siena, Italy; [i]Department of Molecular and Developmental Medicine, University of Siena, 53100 Siena, Italy; [j]Department of Pharmacological and Biomolecular Sciences DiSFeB, University of Milan, 20122 Milan, Italy; [k]The Skaggs Institute for Chemical Biology, The Scripps Research Institute, La Jolla, CA 92037; and [l]Department of Biotechnology, Chemistry and Pharmacy, University of Siena, 53100 Siena, Italy

1. H. Ritchie *et al.*, Coronavirus pandemic (COVID-19). *OurWorldInData.org* (2020). https://ourworldindata.org/coronavirus.
2. E. Mathieu *et al.*, A global database of COVID-19 vaccinations. *Nat. Hum. Behav.* **5**, 947–953 (2021).
3. E. Hacisuleyman *et al.*, Vaccine breakthrough infections with SARS-CoV-2 variants. *N. Engl. J. Med.* **384**, 2212–2218 (2021).
4. J. Liu *et al.*, BNT162b2-elicited neutralization of B.1.617 and other SARS-CoV-2 variants. *Nature* **596**, 273–275 (2021).
5. K. Wu *et al.*, Variant SARS-CoV-2 mRNA vaccines confer broad neutralization as primary or booster series in mice. *bioRxiv* [Preprint] (2021). https://doi.org/10.1101/2021.04.13.439482 (Accessed 15 June 2021).
6. M. Yuan *et al.*, Structural and functional ramifications of antigenic drift in recent SARS-CoV-2 variants. *Science* **373**, 818–823 (2021).
7. F. Krammer, SARS-CoV-2 vaccines in development. *Nature* **586**, 516–527 (2020).
8. T. M. Clausen *et al.*, SARS-CoV-2 infection depends on cellular heparan sulfate and ACE2. *Cell* **183**, 1043–1057.e15 (2020).
9. L. Liu *et al.*, Potent neutralizing antibodies against multiple epitopes on SARS-CoV-2 spike. *Nature* **584**, 450–456 (2020).
10. R. L. Gottlieb *et al.*, Effect of bamlanivimab as monotherapy or in combination with etesevimab on viral load in patients with mild to moderate COVID-19: A randomized clinical trial. *JAMA* **325**, 632–644 (2021).
11. T. N. Starr, A. J. Greaney, A. S. Dingens, J. D. Bloom, Complete map of SARS-CoV-2 RBD mutations that escape the monoclonal antibody LY-CoV555 and its cocktail with LY-CoV016. *Cell Rep Med* **2**, 100255 (2021).
12. D. M. Weinreich *et al.*; Trial Investigators, REGN-COV2, a neutralizing antibody cocktail, in outpatients with Covid-19. *N. Engl. J. Med.* **384**, 238–251 (2021).
13. E. Andreano *et al.*, Extremely potent human monoclonal antibodies from COVID-19 convalescent patients. *Cell* **184**, 1821–1835.e16 (2021).
14. Variant Technical Group, "Investigation of novel SARS-CoV-2 variant: Technical briefing 35" (Public Health England, 2021).
15. H. Tegally *et al.*, Emergence and rapid spread of a new severe acute respiratory syndrome-related coronavirus 2 (SARS-CoV-2) lineage with multiple spike mutations in South Africa. *medRxiv* [Preprint] (2020). https://doi.org/10.1101/2020.12.21.20248640 (Accessed 15 June 2021).
16. N. R. Faria *et al.*, Genomics and epidemiology of the P.1 SARS-CoV-2 lineage in Manaus, Brazil. *Science* **372**, 815–821 (2021).
17. S. Cherian *et al.*, SARS-CoV-2 spike mutations, L452R, T478K, E484Q and P681R, in the second wave of COVID-19 in Maharashtra, India. *Microorganisms* **9**, 1542 (2021).
18. V. Parums, Editorial: Revised World Health Organization (WHO) terminology for variants of concern and variants of interest of SARS-CoV-2. *Med. Sci. Monit.* **27**, e933622 (2021).
19. J. Yu et al., Deletion of the SARS-CoV-2 spike cytoplasmic tail increases infectivity in pseudovirus neutralization assays. J. Virol. 95, e00044-21 (2021).
20. E. Cameroni *et al.*, Broadly neutralizing antibodies overcome SARS-CoV-2 Omicron antigenic shift. *Nature* **602**, 664–670 (2022).
21. L. Liu *et al.*, Striking antibody evasion manifested by the Omicron variant of SARS-CoV-2. *Nature* **602**, 676–681 (2022).
22. D. Pinto *et al.*, Cross-neutralization of SARS-CoV-2 by a human monoclonal SARS-CoV antibody. *Nature* **583**, 290–295 (2020).

23. S. J. Zost *et al.*, Potently neutralizing and protective human antibodies against SARS-CoV-2. *Nature* **584**, 443–449 (2020).
24. M. Hoffmann *et al.*, SARS-CoV-2 variants B.1.351 and P.1 escape from neutralizing antibodies. *Cell* **184**, 2384–2393.e12 (2021).
25. M. Hoffmann *et al.*, SARS-CoV-2 variant B.1.617 is resistant to bamlanivimab and evades antibodies induced by infection and vaccination. *Cell Rep.* **36**, 109415 (2021).
26. D. Planas *et al.*, Sensitivity of infectious SARS-CoV-2 B.1.1.7 and B.1.351 variants to neutralizing antibodies. *Nat. Med.* **27**, 917–924 (2021).
27. D. Planas *et al.*, Reduced sensitivity of SARS-CoV-2 variant Delta to antibody neutralization. *Nature* **596**, 276–280 (2021).
28. T. Tada *et al.*, The spike proteins of SARS-CoV-2 B.1.617 and B.1.618 variants identified in India provide partial resistance to vaccine-elicited and therapeutic monoclonal antibodies. *bioRxiv* [Preprint] (2021). https://doi.org/10.1101/2021.05.14.444076 (Accessed 15 June 2021).
29. P. Wang *et al.*, Antibody resistance of SARS-CoV-2 variants B.1.351 and B.1.1.7. *Nature* **593**, 130–135 (2021).
30. D. Planas *et al.*, Considerable escape of SARS-CoV-2 Omicron to antibody neutralization. *Nature* **602**, 671–675 (2022).
31. R. Henderson *et al.*, Controlling the SARS-CoV-2 spike glycoprotein conformation. *Nat. Struct. Mol. Biol.* **27**, 925–933 (2020).
32. M. Yuan, H. Liu, N. C. Wu, I. A. Wilson, Recognition of the SARS-CoV-2 receptor binding domain by neutralizing antibodies. *Biochem. Biophys. Res. Commun.* **538**, 192–203 (2021).
33. M. A. Tortorici *et al.*, Ultrapotent human antibodies protect against SARS-CoV-2 challenge via multiple mechanisms. *Science* **370**, 950–957 (2020).
34. J. Kreye *et al.*, A therapeutic non-self-reactive SARS-CoV-2 antibody protects from lung pathology in a COVID-19 hamster model. *Cell* **183**, 1058–1069.e19 (2020).
35. L. Wang *et al.*, Ultrapotent antibodies against diverse and highly transmissible SARS-CoV-2 variants. *Science* **373**, eabh1766 (2021).
36. Y.-J. Park *et al.*, Antibody-mediated broad sarbecovirus neutralization through ACE2 molecular mimicry. *Science* **375**, 449–454 (2022).
37. J. Buchrieser *et al.*, Syncytia formation by SARS-CoV-2-infected cells. *EMBO J.* **39**, e106267 (2020).
38. D. Sterlin *et al.*, IgA dominates the early neutralizing antibody response to SARS-CoV-2. *Sci. Transl. Med.* **13**, eabd2223 (2021).
39. S. Notarbartolo *et al.*, Integrated longitudinal immunophenotypic, transcriptional and repertoire analyses delineate immune responses in COVID-19 patients. *Sci. Immunol.* **6**, eabg5021 (2021).
40. A. Conforti *et al.*, COVID-eVax, an electroporated plasmid DNA vaccine candidate encoding the SARS-CoV-2 RBD, elicits protective immune responses in animal models. *Mol. Ther.* **30**, 311–326 (2021).
41. C. Suloway *et al.*, Automated molecular microscopy: The new Leginon system. *J. Struct. Biol.* **151**, 41–60 (2005).
42. G. C. Lander *et al.*, Appion: An integrated, database-driven pipeline to facilitate EM image processing. *J. Struct. Biol.* **166**, 95–102 (2009).
43. S. Q. Zheng *et al.*, MotionCor2: Anisotropic correction of beam-induced motion for improved cryo-electron microscopy. *Nat. Methods* **14**, 331–332 (2017).
44. A. Punjani, J. L. Rubinstein, D. J. Fleet, M. A. Brubaker, cryoSPARC: Algorithms for rapid unsupervised cryo-EM structure determination. *Nat. Methods* **14**, 290–296 (2017).
45. A. Punjani, H. Zhang, D. J. Fleet, Non-uniform refinement: Adaptive regularization improves single-particle cryo-EM reconstruction. *Nat. Methods* **17**, 1214–1221 (2020).
46. J. Zivanov, T. Nakane, S. H. W. Scheres, Estimation of high-order aberrations and anisotropic magnification from cryo-EM data sets in *RELION*-3.1. *IUCrJ* **7**, 253–267 (2020).
47. E. F. Pettersen *et al.*, UCSF Chimera–A visualization system for exploratory research and analysis. *J. Comput. Chem.* **25**, 1605–1612 (2004).
48. P. Emsley, B. Lohkamp, W. G. Scott, K. Cowtan, Features and development of Coot. *Acta Crystallogr. D Biol. Crystallogr.* **66**, 486–501 (2010).
49. P. Conway, M. D. Tyka, F. DiMaio, D. E. Konerding, D. Baker, Relaxation of backbone bond geometry improves protein energy landscape modeling. *Protein Sci.* **23**, 47–55 (2014).
50. B. A. Barad *et al.*, EMRinger: Side chain-directed model and map validation for 3D cryo-electron microscopy. *Nat. Methods* **12**, 943–946 (2015).
51. C. J. Williams *et al.*, MolProbity: More and better reference data for improved all-atom structure validation. *Protein Sci.* **27**, 293–315 (2018).
52. P. D. Adams *et al.*, PHENIX: A comprehensive Python-based system for macromolecular structure solution. *Acta Crystallogr. D Biol. Crystallogr.* **66**, 213–221 (2010).
53. K. R. Abhinandan, A. C. R. Martin, Analysis and improvements to Kabat and structurally correct numbering of antibody variable domains. *Mol. Immunol.* **45**, 3832–3839 (2008).
54. E. Krissinel, K. Henrick, Inference of macromolecular assemblies from crystalline state. *J. Mol. Biol.* **372**, 774–797 (2007).
55. Z. Otwinowski, W. Minor, Processing of X-ray diffraction data collected in oscillation mode. *Methods Enzymol.* **276**, 307–326 (1997).
56. A. J. McCoy *et al.*, Phaser crystallographic software. *J. Appl. Cryst.* **40**, 658–674 (2007).
57. H. Liu *et al.*, Cross-neutralization of a SARS-CoV-2 antibody to a functionally conserved site is mediated by avidity. *Immunity* **53**, 1272–1280.e5 (2020).

nature COMMUNICATIONS

ARTICLE

https://doi.org/10.1038/s41467-022-29909-x OPEN

Safety and serum distribution of anti-SARS-CoV-2 monoclonal antibody MAD0004J08 after intramuscular injection

Simone Lanini[1], Stefano Milleri[2], Emanuele Andreano[3], Sarah Nosari[4], Ida Paciello[3], Giulia Piccini[5], Alessandra Gentili[6], Adhuna Phogat[7], Inesa Hyseni[5,8], Margherita Leonardi[5,8], Alessandro Torelli[5], Emanuele Montomoli[5,8,9], Andrea Paolini[7,10], Andrea Frosini[7], Andrea Antinori[1], Emanuele Nicastri[1], Enrico Girardi[1], Maria Maddalena Plazzi[1], Giuseppe Ippolito[1], Francesco Vaia[1], Giovanni Della Cioppa[11] & Rino Rappuoli[3,12]✉

The emerging threat represented by SARS-CoV-2 variants, demands the development of therapies for better clinical management of COVID-19. MAD0004J08 is a potent Fc-engineered monoclonal antibody (mAb) able to neutralize in vitro all current SARS-CoV-2 variants of concern (VoCs) including the omicron variant even if with significantly reduced potency. Here we evaluated data obtained from the first 30 days of a phase 1 clinical study (EudraCT N.: 2020-005469-15 and ClinicalTrials.gov Identifier: NCT04932850). The primary endpoint evaluated the percentage of severe adverse events. Secondary endpoints evaluated pharmacokinetic and serum neutralization titers. A single dose administration of MAD0004J08 via intramuscular (*i.m.*) route is safe and well tolerated, resulting in rapid serum distribution and sera neutralizing titers higher than COVID-19 convalescent and vaccinated subjects. A single dose administration of MAD0004J08 is also sufficient to effectively neutralize major SARS-CoV-2 variants of concern (alpha, beta, gamma and delta). MAD0004J08 can be a major advancement in the prophylaxis and clinical management of COVID-19.

[1] Istituto Nazionale per le Malattie Infettive Lazzaro Spallanzani – IRCCS, Rome, Italy. [2] Centro Ricerche Cliniche di Verona, University and Hospital Trust of Verona, Verona, Italy. [3] Monoclonal Antibody Discovery (MAD) Lab, Fondazione Toscana Life Sciences, Siena, Italy. [4] AchilleS Vaccine, Siena, Italy. [5] VisMederi S.r.l, Siena, Italy. [6] CROss Research, Mendrisio, Switzerland. [7] Fondazione Toscana Life Sciences, Siena, Italy. [8] VisMederi Research S.r.l, Siena, Italy. [9] Department of Molecular and Developmental Medicine, University of Siena, Siena, Italy. [10] Toscana Life Sciences Sviluppo, Siena, Italy. [11] Clinical R&D Consultants, Rome, Italy. [12] Department of Biotechnology, Chemistry and Pharmacy, University of Siena, Siena, Italy. ✉email: rino.r.rappuoli@gsk.com

The COVID-19 pandemic highlighted the potential of human monoclonal antibodies (mAbs) to tackle pandemics as they demonstrated to be safe and effective therapeutic tools that can be brought from discovery to proof-of-concept trials in only 5–6 months[1]. Since the start of the pandemic, a dozen mAbs capable of neutralizing the SARS-CoV-2 virus have been identified and are under clinical development. Regulatory agencies have granted Emergency Use Authorization (EUA) to Eli Lilly's mAb bamlanivimab (LY-CoV555) and mAb combination bamlanivimab + etesevimab, to Regeneron's mAb combination casiribimab + imdevimab (REGN-COV2), to Celltrion regdanvimab, and GSK/VIR sotrovimab[2–5]. With the emergence of antibody-resistant SARS-CoV-2 variants of concern (VoCs) at the end of 2020, some mAbs lost their clinical efficacy and in April 2021 the FDA revoked EUA for bamlanivimab[6].

The Toscana Life Sciences Foundation has recently reported the isolation and characterization of the neutralizing mAb, MAD0004J08 from a convalescent COVID-19 patient[7]. MAD0004J08 appears to be one of the best candidates for clinical development as it displays the most desirable characteristics for the development of mAb-based prophylaxis and therapy: (1) unprecedented high neutralizing potency, implying low dose requirement, possibility to be administered intramuscularly (i.m.), and significant cost reduction of cost of goods; (2) breadth of neutralizing activity, in vitro vs. the original Wuhan virus and SARS-CoV-2 VoC; B.1.1.7 (alpha), B.1.351 (beta), P.1 (gamma) and B.1.617.2 (delta) with a potency below 10 ng/mL[7,8], implying broad clinical usefulness in countries with diverse SARS-CoV-2 epidemiology; (3) engineered immunoglobulin fragment crystallizable (Fc) region (M428L/N434S[9,10] and L234A/L235A/P329G[11]) to increase its serum half-life while silencing the Fc activity to abrogate binding to FcγRs and eliminate possible risks of antibody-dependent enhancement (ADE) of disease[7]. ADE mediated by the interaction of antibody and FcγRs was previously described for the closely related SARS-CoV virus following its outbreak in 2002 and therefore considered a high risk also for SARS-CoV-2 infection[12,13]. Due to these properties, MAD0004J08 is expected to accelerate clearance of the virus, not induce proinflammatory cytokine response, and thus prevent clinical deterioration of COVID-19 disease in patients.

This paper reports the results of the first 30 days of an ongoing phase 1, placebo-controlled, double-blind, randomized, single-dose, dose-escalation study to evaluate the safety, pharmacokinetics, and virus neutralization titers of the anti-SARS-CoV-2 monoclonal antibody MAD0004J08 in 30 healthy adults. The data generated thus far suggest MAD0004J08 has a strong potential as a global therapeutic tool against COVID-19.

Results

The trial was initiated by screening 50 healthy volunteers between March and May 2021. There was a total of 15 screen failures, 13 due to inclusion/exclusion criteria not met and two to withdrawal. Five screened volunteers were kept as reserves. Thirty subjects who tested negative for SARS-CoV-2 nucleocapsid (N) protein were enrolled and randomized. The serology ant-N test was introduced to exclude subjects presenting endogenous anti-SARS-CoV-2 antibodies induced by the previous infection. Baseline demographic characteristics of the participants in the safety population at enrolment were similar among the treatment groups in terms of sex, mean age, and race (Table 1). Three single ascending doses (48, 100, and 400 mg) and placebo were administered by *i.m.* injection to three study cohorts (cohort 1, cohort 2, and cohort 3 that received 48, 100, and 400 mg, respectively). Eight treated and two placebo subjects were enrolled in each group as described in Fig. 1.

Table 1 MAD0004J08 phase I clinical trial summary.

	Cohort 1 ($n = 10$)	Cohort 2 ($n = 10$)	Cohort 3 ($n = 10$)
Age, years	32.2	26.4	38.2
Min/Max	19–51	21–33	27–54
≥18–<30	4 (40%)	7 (70%)	3 (30%)
≥30–<40	3 (30%)	3 (30%)	2 (20%)
≥40	3 (30%)	0 (0%)	5 (50%)
Sex			
Male	5 (50%)	6 (60%)	6 (60%)
Female	5 (50%)	4 (40%)	4 (40%)
Ethnicity			
White	10 (100%)	10 (100%)	10 (100%)
Nucleocapsid (N) serology test			
Tested positive	0 (0%)	0 (0%)	0 (0%)
Tested negative	10 (100%)	10 (100%)	10 (100%)
Administered dosage			
48 mg	8 (80%)	0 (0%)	0 (0%)
100 mg	0 (0%)	8 (80%)	0 (0%)
400 mg	0 (0%)	0 (0%)	8 (80%)
Placebo	2 (20%)	2 (20%)	2 (20%)
Systemic adverse events			
Headache	4 (40%)	3 (30%)	3 (30%)
Fatigue	4 (40%)	1 (10%)	1 (10%)
New or worsen muscle pain	0 (0%)	0 (0%)	1 (10%)
New or worsen joint pain	0 (0%)	0 (0%)	0 (0%)
Nausea (mild)	2 (20%)	0 (0%)	0 (0%)
Asthenia	0 (0%)	1 (10%)	0 (0%)
Vomiting	0 (0%)	0 (0%)	0 (0%)
Diarrhea	0 (0%)	0 (0%)	0 (0%)
Chills	0 (0%)	0 (0%)	0 (0%)
Fever	0 (0%)	0 (0%)	0 (0%)
Local adverse events			
Pain at injection site	1 (10%)	0 (0%)	0 (0%)
Redness	1 (10%)	0 (0%)	0 (0%)
Swelling	0 (0%)	0 (0%)	0 (0%)
Severity of reported adverse events			
Mild	11 (91%)	5 (100%)	3 (60%)
Moderate	1 (9%)	0 (0%)	2 (40%)
Severe	0 (0%)	0 (0%)	0 (0%)
Pharmacokinetics ng/mL (95% CI)[a]			
Day 1 (0 h)	6.9	6.6	11.4
Day 1 (1 h)	22.6	36.3	43.1
Day 1 (2 h)	92.3	257.4	97.5
Day 1 (3 h)	203.1	434.7	835.3
Day 1 (4 h)	396.7	786.6	1740.8
Day 1 (6 h)	571.8	1259.1	3320.5
Day 1 (8 h)	691.8	1650	4922.1
Day 1 (12 h)	1017.3	2471.9	6695.5
Day 1 (24 h)	1543.4	3185.5	9900.2
Day 2	3119.7	6241.4	21,581.4
Day 8	5124.9	11,034.7	38,017.2
Day 15	5988.0	11,998.7	44,279.2
Day 22	6640.9	11,691.5	47,022.6
Day 30	6552.9	11,993.9	44,579.3
Day 60	6058.8	9856.5	31,624.6
GMT neutralization (95% CI)[a]			
Original Wuhan (48 h)	334.2	334.2	1173.8
Original Wuhan (day 8)	493.5	1076.3	2061.4
Original Wuhan (day 30)	397.4	562.0	1395.8
B.1.1.7 (alpha) (day 8)	306.4	794.8	4122.8
B.1.351 (beta) (day 8)	134.5	269.1	1291.4
P.1 (gamma) (day 8)	113.1	198.7	697.9
B.1.617.2 (delta) (day 8)	472.6	905.1	5120.0

Data are mean, *n*, *n* (%), GM ng/mL (95% CI), or GMT (95% CI). Adverse events severity is reported as mild, moderate, and severe.
[a]Data relative to placebo groups were not reported in the table as subjects tested negative for all the pharmacokinetics and serum neutralization analyses performed in this study.

Overall, the study population consisted of white healthy male and female participants with a mean age of 32.2 years (range 19–54 years); 56.6% were male and 43.4% were female (Table 1).

The study has now been unblinded and treated/placebo subjects allocated to their respective groups. Subjects from the placebo group tested negative for all tests performed in this study and therefore were not included in tables and figures.

No severe or serious treatment-emergent adverse event (TEAE) was reported through 7 days post dosing. Local and systemic solicited adverse events through day 7 occurred in a few subjects (Table 1), were all mild to moderate, lasted no more than 2 and 6 days for systemic and local TEAE respectively, and showed no

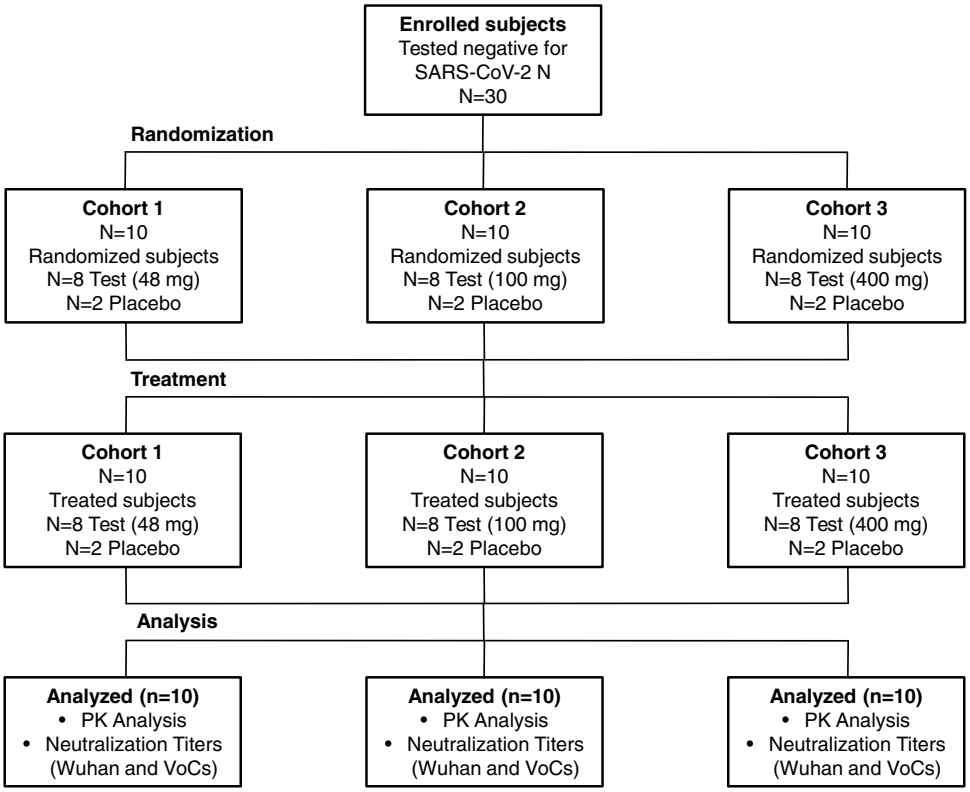

Fig. 1 CONSORT diagram phase 1 trial. The graph shows the enrollment of subjects and their allocation to treatment and analysis.

sign of dose-related increase of frequency or severity. Overall, systemic solicited adverse events ($n = 20$; 90.1%) were more frequent than local solicited adverse events ($n = 2$; 9.1%) (Table 1).

The baseline (pre-dose) geometric mean (GM) concentrations at day 1 (0 h) of anti-spike antibodies measured by ELISA were at background levels. Subjects in the placebo group had GM levels below the lower limit of quantification (LLOQ) at all timepoints. As for dosed subjects, detectable levels of antibodies were seen as quickly as two hours post-administration and increased constantly in a dose-dependent manner. On day 8, mean sera binding titers almost peaked showing a GM of 5124.9, 11,034.7, and 38,017.2 ng/mL for cohorts 1, 2, and 3, respectively. Sera binding titers continued to increase up to 30 days with a GM of 6552.9, 11,993.9, and 44,579.3 ng/mL for cohorts 1, 2, and 3, respectively, and maintained high titers up to 60 days with a GM of 6058.8, 9856.5, and 31,624.6 ng/mL for cohorts 1, 2, and 3, respectively (Fig. 2, Table 1, and Supplementary Table 1). Maximum serum concentration (Cmax) and Time of Maximum concentration observed (Tmax) were evaluated and reported as GM of all treated subjects ($n = 8$) per group. GM-Cmax were 7098.4, 13,472.8, and 52,907.9 ng/mL for cohort 1, 2, and 3, respectively, showing a dose-dependent response. GM-Tmax was 27.2, 17.2, and 18.1 days for cohorts 1, 2, and 3, respectively. While Cohort 2 and 3 show a very similar GM-Tmax, cohort 1 showed a 1.5-fold slower distribution.

The study assessed the neutralizing activity of sera from MAD0004J08 dosed subjects against SARS-CoV-2 original Wuhan virus. The results are represented as geometric mean neutralization titers (GMT) leading to 100% inhibitory dilution (ID_{100}). The GMT in MAD0004J08 administered subjects at baseline was below the lower limit of quantitation (LLOQ—<10). Placebo subjects had ID_{100} levels below the LLOQ at all study points. The GMT levels in cohort 1 (48 mg) on day 2 were 334.2, increased to 493.5 on day 8, and was 397.4 on day 30. The GMT in cohort 2 (100 mg) was 334.2 on day 2, improved further to 1076.3 on day 8, and was 562.0 on day 30. The GMT levels for cohort 3 (400 mg) were 1173.8, 2061.4, and 1395.8 on days 2, 8, and 30 respectively (Table 1 and Supplementary Table 2).

Additionally, we compared the neutralizing activity against the original Wuhan virus of sera from MAD0004J08 dosed subjects with COVID-19 convalescent patients ($n = 20$) and two groups of BNT162b2 mRNA vaccine (Comirnaty, Pfizer/BioNTech) recipients ($n = 5$/group) who were either seronegative or seropositive for SAR-CoV-2 before vaccination. The GMT for 20 COVID-19 convalescent patients had a wide range of 1–10,240, which can be explained by differences in clinical severity of COVID-19 disease as 15/20 (75%) were hospitalized and 10/15 (66.7%) of hospitalized patients were on oxygen therapy. Of the 15 hospitalized patients, 4/15 (26.7%) had a severe infection (with acute respiratory distress syndrome), 6/15 (40.0%) had a moderate infection (oxygen therapy), and the remaining 5/15 (33.3%) had a mild infection (paucisymptomatic). The average GMT for all 20 COVID-19 convalescent patients was 73.7, whereas the average GMT for seronegative and seropositive vaccinees was 27.0 and 269.3, respectively (Fig. 3 and Supplementary Table 3). Overall, the average neutralizing ability of sera from cohorts 1, 2, and 3 subjects on day 8 were 6.7-, 14.6-, and 27.9-fold significantly higher than COVID-19 convalescent sera and were 18.3-, 40.0-, 76.4-, and 1.83-, 4.0-, 7.6-fold higher compared to seronegative and seropositive vaccinees, respectively (Fig. 3, Table 1, and Supplementary Table 3).

Finally, we evaluated the sera neutralization activity on day 8 of all subjects that received MAD0004J08 against the SARS-CoV-2 variants of concern B.1.1.7 (alpha), B.1.351 (beta), P.1 (gamma), and B.1.617.2 (delta) (Fig. 4). Average GMT and 95% confidence interval (95% CI) are reported in Table 1 and Supplementary Table 2. Overall, a single i.m. injection of MAD0004J08 resulted in high neutralization titers against all tested SARS-CoV-2 variants in a dose-dependent fashion with average GMT levels for cohort 1 of 306.4, 134.5, 113.1, and 472.6, for cohort 2 of 794.8,

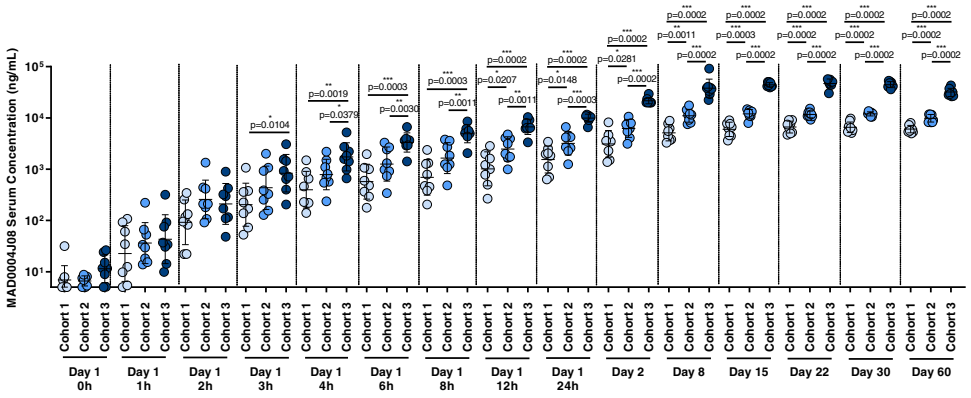

Fig. 2 MAD0004J08 pharmacokinetics. SARS-CoV-2 spike (S) protein IgG mean titers in (ng/mL) pre and post MAD0004J08 injection in three cohorts. Dots indicate the individual antibody titers for Cohort 1 (48mg-light blue; $n = 8$), Cohort 2 (100mg-blue; $n = 8$) and Cohort 3 (400mg-dark blue; $n = 8$). Only p values for statistically significant differences are shown in the figure. A nonparametric Mann–Whitney t test was used to evaluate statistical significance between groups. Two-tailed p value significances are shown as $^{*}p \le 0.05$, $^{**}p \le 0.01$, and $^{***}p \le 0.001$. Data are presented as geometric mean ± standard deviation. Subjects from the placebo group (2/group) were excluded from the analyses.

269.1, 198.7 and 905.1, and for cohort 3 of 4122.8, 1291.4, 697.9, and 5120.0 against the B.1.1.7, B.1.351, P.1 and B.1.617.2 respectively (Fig. 4a–d, Table 1, and Supplementary Table 2). Average GMT levels against the B.1.1.7 (alpha) and B.1.617.2 (delta) variants were comparable to the SARS-CoV-2 Wuhan virus for cohorts 1 and 2, while the GMT was 2- and 2.48-fold higher for cohort 3 against B.1.1.7 (alpha), and B.1.617.2 (delta), respectively (Fig. 4e–g). Average neutralization titers compared to the original Wuhan virus dropped by 3.67-, 4.00-, and 1.68-fold against B.1.351 (beta) and by 4.36-, 5.42-, and 2.95-fold against P.1 (gamma) for cohort 1, 2, and 3 respectively (Fig. 4e–g, Table 1, and Supplementary Table 2). However, despite reductions in neutralization titers were observed against the variants, GMT levels were either comparable, in case of cohort 1 (48 mg), or significantly higher, for cohorts 2 and 3 (100 and 400 mg), than those observed in convalescent patients and vaccinees against the Wuhan virus (Figs. 3 and 4).

Discussion

The results of this study show that, following a single i.m. administration, MAD0004J08 at 48, 100, and 400 mg is safe, well tolerated with minimal reactogenic adverse events, and rapidly distributes systemically. In addition, a single dose of MAD0004J08 resulted in extremely high serum neutralization titers which were 5–76-fold higher compared to COVID-19 convalescent donors and BNT162b2 mRNA vaccinees. With the emergence and worldwide spread of SARS-CoV-2 VOCs, it is imperative to develop mAbs able to neutralize circulating variants of concern (VoC), therefore maintaining their therapeutic efficacy. Some mAbs already in clinical application for the treatment of COVID-19, showed to fall short against emerging variants, and for one of them, due to lack of clinical efficacy, regulatory agencies revoked emergency use authorization[6]. In addition, with the emergence of the SARS-CoV-2 omicron variant and its sub-lineages, all antibodies except one lost their neutralization activity and consequent clinical effectiveness against this virus, and MAD0004J08 was also significantly impacted, but not completely evaded, by this variant[14]. In this study, we showed that sera from MAD0004J08 treated subjects retained high neutralization titers against major SARS-CoV-2 VoCs including the B.1.1.7 (alpha), B.1.351 (beta), P.1 (gamma), and B.1.617.2 (delta) variants highlighting the potential of this antibody to be used globally for the treatment of COVID-19. High antibody neutralization titers were previously shown to be predictive of immune protection from SARS-CoV-2 infection and long-term persistence of neutralizing antibodies was shown to estimate the duration of protection predicting disease severity and survival[15–18]. Although sera from 400 mg dose showed the highest neutralization titers against SARS-CoV-2 and variants of concern, the 100 mg dose, which was also found to have significantly higher neutralizing titers compared to convalescent patients and vaccinees, could be sufficient and strategically more suitable to develop. In fact, a single 100 mg dose of MAD0004J08 could increase the number of available doses to give to COVID-19 patients.

To complement the ability of MAD0004J08 to neutralize major SARS-CoV-2 VoC, the Fc modifications introduced to extend its serum half-life and to limit the risk of ADE in hospitalized COIVD-19 patients could further increase the clinical suitability of this antibody. Concerning the serum half-life extension, our data showed that sera neutralization titers were maintained at high levels up to the 60 days post-administration and follow-up is planned for up to 6 months. As for the silencing of the Fc-portion to minimize risks of ADE our strategy, compared to the use of unmodified or enhanced Fc-functions in antibodies already in the clinic, could result to be successful in hospitalized COVID-19 patients with and without high titers of serum antibodies against SARS-CoV-2. In fact, at the end of 2020, the Eli Lilly bamlanivimab (LY-CoV555) received emergency use authorization but the application was limited as the administration of this antibody may be associated with worse clinical outcomes when administered to hospitalized patients requiring high flow oxygen or mechanical ventilation with COVID-19[5]. In addition, a recent primary clinical trial under peer-review has shown that intravenous administration of REGEN-COV mAb cocktail, at a total dose of 8 g in hospitalized COVID-19 patients reduced 28-day mortality among patients who were seronegative at baseline, highlighting the important role of mAbs therapy even in hospitalized COVID-19 patients[19]. However, COVID-19 seropositive hospitalized patients did not benefit from REGEN-COV administration, suggesting that presence of high antibody titers induced by infection plus the infusion of the enormous quantity of mAbs for therapy may not be beneficial for these patients. A recent paper describing the longitudinal neutralizing antibodies in patients progressing to severe disease indicates ADE as one of the mechanisms of increased disease severity[20]. These previous reports indicate that removing Fc-functions could result to be a successful strategy for the treatment of hospitalized seronegative as well as seropositive COVID-19 patients.

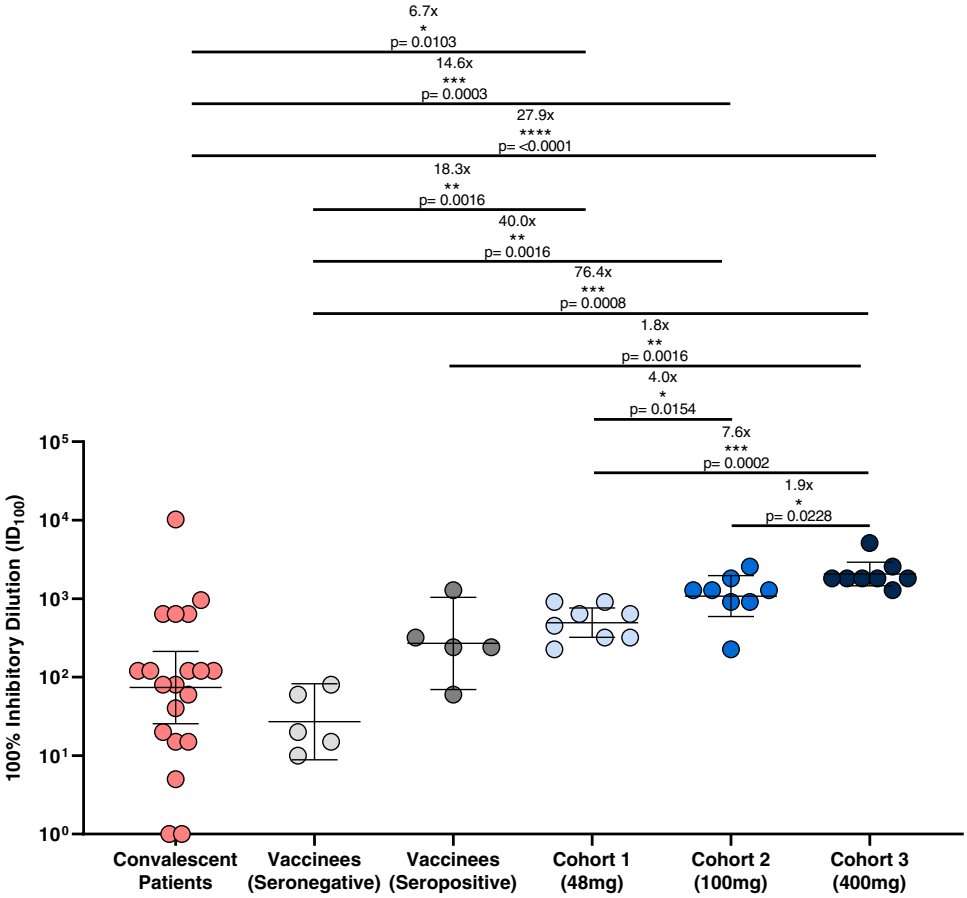

Fig. 3 Serum neutralization activity against SARS-CoV-2 Wuhan virus. The graph shows the neutralization reported as 100% inhibitory dilution (ID_{100}) of sera collected from COVID-19 convalescent patients ($n = 20$; red), average samples collection 10 days post-hospitalization, vaccinees not exposed (seronegative; $n = 5$; light gray), average samples collection 48 days post-vaccination, or previously exposed (seropositive; $n = 5$; dark gray), average samples collection 21 days post-vaccination, to SARS-CoV-2 and subjects that received MAD0004J08 at 48 ($n = 8$; light blue), 100 ($n = 8$; blue), and 400 mg ($n = 8$; dark blue) at day 8. Only p values for statistically significant differences are shown in the figure. A nonparametric Mann–Whitney t test was used to evaluate statistical significance between groups. Two-tailed p value significances are shown as $^{*}p \le 0.05$, $^{**}p \le 0.01$, $^{***}p \le 0.001$, and $^{****}p \le 0.0001$. Data are presented as geometric mean ± standard deviation.

The limitation of our study is that our first in human study was conducted in a healthy population of age 18–55 years without much diversity, whereas the risk for severity of COVID-19 disease is more in populations with comorbid conditions, older age groups, and in non-white populations. Our ongoing Phase 2–3 study will assess MAD0004J08 in mild/moderate diseased and stratified subjects groups to assess dose selection and efficacy.

To conclude, MAD0004J08 administration is safe, confers broad coverage against major SARS-CoV-2 variants of concern, and gives the low dosage needed and i.m. route of administration can be a globally available and affordable countermeasure to the COVID-19 pandemic[21].

Methods

Cohort of healthy adults treated with MAD0004J08. Our phase 1, first in human (FIH) trial is underway at two sites in Italy (Istituto Nazionale Malattie Infettive Lazzaro Spallanzani, Rome, and Centro Ricerche Cliniche di Verona s.r.l. (CRC), Verona). The final protocol and informed consent were approved by the institutional review boards of each of the participating investigational sites. The study was approved by the "Comitato Etico Unico dell'Istituto nazionale per le malattie infettive (INMI) Lazzaro Spallanzani", Rome (IT), ethic committee. This study is designed and conducted in accordance with the Declaration of Helsinki, the current revision of Good Clinical Practice (GCP), ICH topic E6 (R2), and the applicable local law requirements. The trial was registered with EudraCT N.: 2020-005469-15 on the 16th of November 2020 and ClinicalTrials.gov Identifier: NCT04932850. This is a dose-escalation study, open-label across doses and randomized, double blind within each dose level. A total of 30 healthy men and nonpregnant women, 18–55 years of age, meeting all inclusion/exclusion criteria were enrolled in three sequential cohorts of 10 subjects each. Within each cohort, subjects were randomized with 4:1 ratio to a single i.m. dose of MAD0004J08 (48 mg in Cohort 1, 100 mg in Cohort 2, and 400 mg in Cohort 3) or placebo using an interactive web response system (IWRS). Within each cohort, subjects were grouped into two groups of five: the five subjects of the first group, referred to as "sentinels" were randomized one at a time at 48-hour intervals, no safety concern was identified by the investigator; the five subjects of the second group were randomized and enrolled with no time restriction. An Independent Data Safety Monitoring Board (DSMB) recommended progress from Cohort 1 to Cohort 2 and from Cohort 2 to Cohort 3 based pre-defined criteria[22]. Each subject is to undergo 12 visits (V) over a 6-month period: V1-V2 for screening procedures, V1–V3 (Days 1–3) as inpatient in the study center, and V4-V12 as outpatient for follow-up. On day 1 (V3), a single 5 mL injection was administered in the right gluteus for cohorts 1 and 2 and two 5 mL injections, were administered one in the right and one left gluteus for cohort 3. Each subject was provided with two diaries to self-report and record solicited adverse events (AEs) from day 1 to day 7, and unsolicited AEs and concomitant medication throughout the study. The study is now unblinded and subjects were properly allocated to their respective treatment groups.

Eligibility criteria. A detailed list of inclusion/exclusion criteria can be found in the trial protocol. Key inclusion criteria were as follows: age 18-55, signed informed consent, willingness to use appropriate contraception, body mass index 18.5–30 kg/m^2; systolic blood pressure 90–139 mmHg, diastolic blood pressure 69–90 mmHg; heart rate 50–100 bpm; electrocardiogram (ECG) without clinically significant abnormalities; negative SARS-CoV-2 serology test (negative anti-S and anti-N) or negative SARS-CoV-2 qRT-PCR in the 72 h prior with the result before the treatment. Serology tests, performed to exclude the presence of endogenous anti-SARS-CoV-2 antibodies induced by the previous infection, were performed through an automated chemiluminescent immunoassay previously described by the Istituto Nazionale Malattie

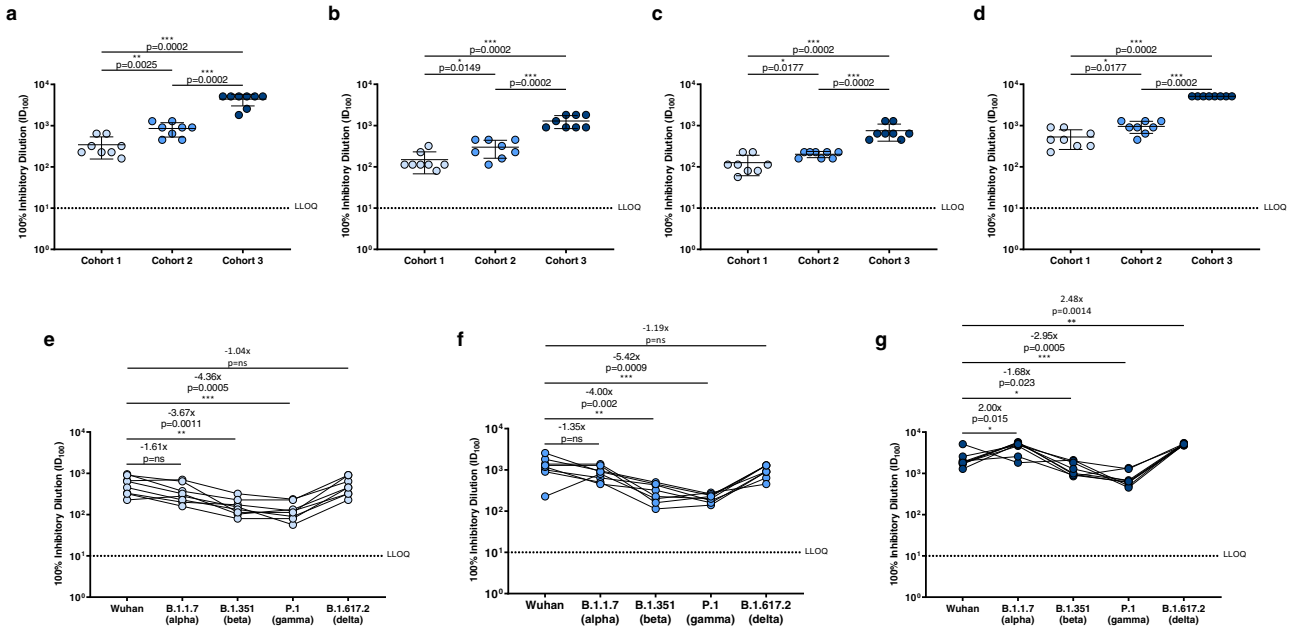

Fig. 4 Serum neutralization activity against SARS-CoV-2 variants of concern. a–d Graphs show the neutralization activity reported as 100% inhibitory dilution (ID_{100}) of sera collected from subjects who received MAD0004J08 at 48 (cohort 1; $n = 8$; light blue), 100 (cohort 2; $n = 8$; blue) and 400 (cohort 3; $n = 8$; dark blue) mg against SARS-CoV-2 B.1.1.7 (alpha), B.1.351 (beta), P.1 (gamma), and B.1.617.2 (delta) variants at day 8. Data are presented as geometric mean ± standard deviation. **e–g** Graphs show values of serum neutralization activity against the different SARS-CoV-2 VoCs tested in this study for Cohort 1 ($n = 8$), Cohort 2 ($n = 8$), and Cohort 3 ($n = 8$). Fold changes relative to Wuhan virus are reported for each VoCs. A nonparametric Mann–Whitney *t* test was used to evaluate statistical significances between groups and tested viruses. Two-tailed *p* value significances are shown as $^{*}p \leq 0.05$, $^{**}p \leq 0.01$, and $^{***}p \leq 0.001$. Data are presented as geometric mean ± standard deviation. Data are presented as geometric mean.

Infettive Lazzaro Spallanzani, Rome, and through a commercially available kit (Anti-SARS-CoV-2 NCP ELISA (IgG), cat. number EI 2606-9601/9620-2 G) following the manufacturer's instructions by the Centro Ricerche Cliniche di Verona s.r.l. (CRC), Verona[23]. Key exclusion criteria were as follows: prior intake of investigational or licensed vaccine for the prevention of SARS-CoV-2; history of infection with SARS or MERS; positive or missing pregnancy test at screening or day 1 or lactating women; history of allergic reactions likely to be exacerbated by any component of the investigational product; previous intake of a mAb within 6 months; history of malignancy in the past 5–7 years; Immunodeficiency due to illness, any course of glucocorticoid therapy exceeding 2 weeks; acute illnesses—history of renal, hepatic, gastrointestinal, cardiovascular, respiratory, dermatologic, hematological, endocrine, psychiatric or neurological diseases that may interfere with the aim of the study or increase subjects risks in investigator's opinion. A statement was included in the study protocol that if during the study, a subject is included in a vaccination list according to the national guidelines, the best option for the subject will be pursued. However, such a situation did not arise during the study.

Investigational medicinal product (IMP). MAD0004J08, human monoclonal antibody 100 mg/2.5 mL solution for injection was manufactured by Menarini Biotech, and was characterized and filled, at Istituto Biochimico Italiano (IBI) Lorenzini. The placebo was prepared as a 2.5 mL of a 0.9% w/v sterile solution of sodium chloride (NaCl) in water for injections (WFI) by IBI. The investigational products were stored at 2–8 °C in a dry locked place.

End points. In this report, results from the following study end points are presented. The full set of endpoints (see protocol) in the complete sample will be presented upon completion of the study. Primary end point: Proportion of subjects with severe and/or serious treatment-emergent adverse events (TEAEs), including clinically relevant laboratory abnormalities, vital signs, and adverse reactions at the injection site) in the 7 days post-treatment. A TEAE is defined as any AE with onset after administration of the study drug ($N = 30$).

Secondary end points: Proportion of subjects with solicited local AEs (pain, redness, and swelling at the injection site) and systemic AEs (headache, fatigue, muscle pain, joint pain, vomiting, diarrhea, chills, fever) from day 1 to day 7 ($N = 30$); MAD0004J08 sera concentrations on day 1 (0, 1, 2, 3, 4, 6, 8, 12, and 24 h), days 2, 8, 15, 22, 30 and 60 (N = 24; placebo subjects were excluded from the analyses); MAD0004J08 sera neutralizing ability at baseline, and on days 2, 8, and 30 ($N = 24$; placebo subjects were excluded from the analyses).

ELISA for PK analyses. The method for detection of MAD0004J08 in human serum is a quantitative sandwich ELISA. Briefly, a 96-wells plate is coated with SARS-CoV-2 Spike protein; after blocking of the plate with PBS + 1% BSA, samples containing MAD0004J08 are pipetted into the wells, followed by a wash with PBS + 0.05% Tween-20 to remove all unbound matrix components; alkaline phosphatase labeled anti-Human IgG (γ chain specific) diluted 1:2000 is added to bind to the immobilized MAD0004J08; the complex is detected by pNPP substrate; after a wash to remove unbound reagents, the enzyme is revealed by its action on the pNPP substrate; after stopping the reaction with a strong base, the intensity of the color (read at 405 nm) is directly proportional to the amount of MAD0004J08 present in the sample. Data were collected by using the BioTek Gen5 Data Analysis Software v3.0.

SARS-CoV-2 viruses. The SARS-CoV-2 viruses used to perform the CPE-MN neutralization assay were the original Wuhan SARS-CoV-2 virus (SARS-CoV-2/INMI1-Isolate/2020/Italy: MT066156), SARS-CoV-2 B.1.1.7 (INMI GISAID accession number: EPI_ISL_736997), SARS-CoV-2 B.1.351 (EVAg Cod: 014V-04058), P.1 (EVAg CoD: 014V-04089), and SARS-CoV-2 B.1.617.2 (GISAID ID: EPI_ISL_2029113).

SARS-CoV-2 neutralization assay. SARS-CoV-2 neutralization assay was performed as previously described[7]. Briefly, plasma samples were tested at a starting dilution of 1:10 and then diluted in steps of 1:2 for twelve points. All samples were mixed with a SARS-CoV-2 wild type, SARS-CoV-2 B.1.17 (alpha), B.1.351 (beta), P.1 (gamma), and B.1.617.2 (delta) viral solution containing 100 $TCID_{50}$ of the virus. After 1 h incubation at 37 °C, 5% CO_2, virus–mAb mixture was added to the wells of a 96-well plate containing a sub-confluent Vero E6 cell monolayer. Plates were incubated for 3–4 days at 37 °C in a humidified environment with 5% CO_2, then examined for CPE by means of an inverted optical microscope. Technical duplicates were performed for each experiment. Neutralizing activities are represented as geometric mean neutralization titers (GMT) leading to 100% viral neutralization/inhibition (ID_{100}). In the original protocol, only GMT against the wild-type (WT) Wuhan strain was envisaged. As post hoc analyses, in light of the evolving epidemiology GMTs vs. alpha, beta, gamma, and delta variants of concern were also assessed. In addition, as post hoc analyses, GMTs following administration of MAD0004J08 were compared to matching GMTs obtained from pools of convalescent and vaccinated sera.

Plasma specimens from COVID-19 convalescent and vaccinated subjects. Plasma specimens from COVID-19 convalescent subjects and SARS-COV-2

vaccinated subjects used as comparators in the present paper were previously collected from a separate study conducted in collaboration with the National Institute for Infectious Diseases, IRCCS – Lazzaro Spallanzani Rome (IT) and Azienda Ospedaliera Universitaria Senese, Siena (IT). The study was approved by local ethics committees and conducted according to good clinical practice Plasma neutralization titers of COVID-19 convalescent subjects and vaccinated donors were previously reported[24,25].

Statistical analysis. To assess the pharmacokinetics of MAD0004J08 in the three different cohorts, a non-parametric Mann–Whitney *T* test was performed among groups at all different time points. For the analyses of sera or plasma neutralization antibody titers against SARS-CoV-2 and VoCs, the 100% inhibitory dilution (ID_{100}) was calculated as the geometric mean of two technical duplicates, and the statistical significance of the differences among groups was determined by non-parametric Mann–Whitney *T* test using the GraphPad Prism software (version 8.0.2). Two-tailed *p* value significances are shown as $*p \le 0.05$, $**p \le 0.01$, $***p \le 0.001$, and $****p \le 0.0001$.

Reporting summary. Further information on research design is available in the Nature Research Reporting Summary linked to this article.

Data availability

All data supporting the findings in this study are available within the article, Supplementary Information, or can be obtained from the corresponding author upon request. SARS-CoV-2 sequences are accessible within the global initiative on sharing all influenza data (GISAID) database. Source data are provided with this paper.

Received: 27 January 2022; Accepted: 7 April 2022;
Published online: 27 April 2022

References

1. Kelley, B. Developing therapeutic monoclonal antibodies at pandemic pace. *Nat. Biotechnol.* **38**, 540–545 (2020).
2. EMA. EMA issues advice on use of regdanvimab for treating COVID-19. (2021). https://www.ema.europa.eu/en/news/ema-issues-advice-use-regdanvimab-treating-covid-19.
3. EMA. EMA issues advice on use of sotrovimab (VIR-7831) for treating COVID-19. (2021). https://www.ema.europa.eu/en/news/ema-issues-advice-use-sotrovimab-vir-7831-treating-covid-19.
4. FDA. Coronavirus (COVID-19) update: FDA authorizes monoclonal antibodies for treatment of COVID-19. (2020). https://www.fda.gov/news-events/press-announcements/coronavirus-covid-19-update-fda-authorizes-new-monoclonal-antibody-treatment-covid-19-retains.
5. Lilly. Lilly's neutralizing antibody bamlanivimab (LY-CoV555) receives FDA emergency use authorization for the treatment of recently diagnosed COVID-19. (2020). https://investor.lilly.com/news-releases/news-release-details/lillys-neutralizing-antibody-bamlanivimab-ly-cov555-receives-fda.
6. FDA. Coronavirus (COVID-19) update: FDA revokes emergency use authorization for monoclonal antibody bamlanivimab. (2021). https://www.fda.gov/news-events/press-announcements/coronavirus-covid-19-update-fda-revokes-emergency-use-authorization-monoclonal-antibody-bamlanivimab.
7. Andreano, E. et al. Extremely potent human monoclonal antibodies from COVID-19 convalescent patients. *Cell* **184**, 1821.e6–1835.e6 (2021).
8. Torres, J. L. et al. Structural insights of a highly potent pan-neutralizing SARS-CoV-2 human monoclonal antibody. Preprint at *bioRxiv* https://doi.org/10.1101/2021.09.28.462234 (2021).
9. Zalevsky, J. et al. Enhanced antibody half-life improves in vivo activity. *Nat. Biotechnol.* **28**, 157–159 (2010).
10. Gaudinski, M. R. et al. Safety and pharmacokinetics of the Fc-modified HIV-1 human monoclonal antibody VRC01LS: a phase 1 open-label clinical trial in healthy adults. *PLoS Med.* **15**, e1002493 (2018).
11. Schlothauer, T. et al. Novel human IgG1 and IgG4 Fc-engineered antibodies with completely abolished immune effector functions. *Protein Eng. Des. Sel.* **29**, 457–466 (2016).
12. Lee, W. S., Wheatley, A. K., Kent, S. J. & DeKosky, B. J. Antibody-dependent enhancement and SARS-CoV-2 vaccines and therapies. *Nat. Microbiol.* **5**, 1185–1191 (2020).
13. Iwasaki, A. & Yang, Y. The potential danger of suboptimal antibody responses in COVID-19. *Nat. Rev. Immunol.* **20**, 339–341 (2020).
14. Iketani, S. et al. Antibody evasion properties of SARS-CoV-2 Omicron sublineages. *Nature* https://doi.org/10.1038/s41586-022-04594-4 (2022).
15. Khoury, D. S. et al. Neutralizing antibody levels are highly predictive of immune protection from symptomatic SARS-CoV-2 infection. *Nat. Med.* **27**, 1205–1211 (2021).
16. Dispinseri, S. et al. Neutralizing antibody responses to SARS-CoV-2 in symptomatic COVID-19 is persistent and critical for survival. *Nat. Commun.* **12**, 2670 (2021).
17. Lau, E. H. Y. et al. Long-term persistence of SARS-CoV-2 neutralizing antibody responses after infection and estimates of the duration of protection. *EClinicalMedicine* **41**, 101174 (2021).
18. Garcia-Beltran, W. F. et al. COVID-19-neutralizing antibodies predict disease severity and survival. *Cell* **184**, 476.e1–488.e1 (2021).
19. Group, R. C. et al. Casirivimab and imdevimab in patients admitted to hospital with COVID-19 (RECOVERY): a randomised, controlled, open-label, platform trial. *Lancet* **399**, 665–676 (2021).
20. Lucas, C. et al. Delayed production of neutralizing antibodies correlates with fatal COVID-19. *Nat. Med.* **27**, 1178–1186 (2021).
21. Wellcome. Expanding access to monoclonal antibody-based products: a global call to action. (2020). https://wellcome.org/reports/expanding-access-monoclonal-antibodies.
22. EMA. Guideline on strategies to identify and mitigate risks for first-in-human and early clinical trial with investigational medicinal products. (2021). https://www.ema.europa.eu/en/strategies-identify-mitigate-risks-first-human-early-clinical-trials-investigational-medicinal.
23. Meschi, S. et al. Predicting the protective humoral response to a SARS-CoV-2 mRNA vaccine *J. Clin. Chem. Lab. Med.* **59**, 2010–2018 (2021).
24. Andreano, E. et al. Hybrid immunity improves B cells and antibodies against SARS-CoV-2 variants. *Nature* **600**, 530–535 (2021).
25. Andreano, E. et al. SARS-CoV-2 escape from a highly neutralizing COVID-19 convalescent plasma. *Proc. Natl Acad. Sci. USA* **118**, e2103154118 (2021).

Acknowledgements

The authors would like to thank the donors, physicians, and staff participating in this phase I clinical trial aimed to evaluate the safety and tolerability of MAD0004J08. We would also like to thank CROss Allience, Mendrisio, Svizzera, Ardena Bioanalyses, Assen, Netherlands, ExcellGene, Monthey, Switzerland, Menarini Biotech S.r.l., Pomezia, Italy and Istituto Biochimico Italiano (IBI) Lorenzini, Aprilia, Italy, for their support to this study. The authors would also like to acknowledge Concetta Castelletti (laboratory), clinical team: Ilaria Mastrorosa, Alessandra Vergori, Sandrine Ottou, Serena Vita, Laura Scorzolini, Alessandra D'Abramo. This study was supported by the EU Malaria Fund, inaugurated on the 3rd of June 2020 and initiated by the kENUP Foundation. This publication was supported by the COVID-2020-12371817 project, which has received funding from the Italian Ministry of Health (Ministero della Salute), from the Italian Ministry of Economic (Ministero dello Sviluppo Economico) through the "Contratti di Sviluppo" funding program, and from Regione Toscana. This work was funded by the European Research Council (ERC) advanced grant agreement number 787552 (vAMRes). This publication was supported by the European Virus Archive goes Global (EVAg) project, which has received funding from the European Union's Horizon 2020 research and innovation program under grant agreement No 653316.

Author contributions

Conceived the study: S.L., G.D.C., G.I., and R.R.; contributed to acquisition of data: S.L., S.M., A.A., E.N., E.G., M.M.P., E.A., I.P., G.P., A.G., I.H., and M.L.; contributed to data analysis and interpretation: E.A., A. Phogat, A.G., S.N., and R.R.; acquired funding for the study: A. Paolini, A.F., and R.R.; contributed to the logistic of the study: S.N., A.T., G.P., E.M., G.I., F.V., and R.R.; manuscript writing: E.A., A. Phogat, and R.R.; final revision of the manuscript: S.L., S.M., E.A., S.N., I.P., G.P., A.G., A. Phogat, I.H., M.L., A.T., E.M., A. Paolini, A.F., A.A., E.N., E.G., M.M.P., G.I., F.V., G.D.C., and R.R.

Competing interests

R.R. is an employee of the GSK group of companies. E.A., I.P., and R.R. are listed as inventors of full-length human monoclonal antibodies described in Italian patent application nos. 102020000015754 filed on 30 June 2020, 102020000018955 filed on 3 August 2020, and 102020000029969 filed on 4 December 2020 and the international patent system number PCT/IB2021/055755 filed on 28 June 2021. All patents were submitted by Fondazione Toscana Life Sciences, Siena, Italy. The remaining authors have no competing interests to declare.

Additional information

Supplementary information The online version contains supplementary material available at https://doi.org/10.1038/s41467-022-29909-x.

Correspondence and requests for materials should be addressed to Rino Rappuoli.

Peer review information *Nature Communications* thanks the anonymous reviewers for their contribution to the peer review of this work. Peer reviewer reports are available.

Reprints and permission information is available at http://www.nature.com/reprints

Publisher's note Springer Nature remains neutral with regard to jurisdictional claims in published maps and institutional affiliations.

SARS-CoV-2 escape from a highly neutralizing COVID-19 convalescent plasma

Emanuele Andreano[a], Giulia Piccini[b], Danilo Licastro[c], Lorenzo Casalino[d], Nicole V. Johnson[e], Ida Paciello[a], Simeone Dal Monego[c], Elisa Pantano[a], Noemi Manganaro[a], Alessandro Manenti[b,f], Rachele Manna[b], Elisa Casa[b,f], Inesa Hyseni[b,f], Linda Benincasa[f], Emanuele Montomoli[b,f,g], Rommie E. Amaro[d], Jason S. McLellan[e], and Rino Rappuoli[a,h,1]

[a]Monoclonal Antibody Discovery Lab, Fondazione Toscana Life Sciences, 53100 Siena, Italy; [b]VisMederi S.r.l., 53100 Siena, Italy; [c]ARGO Open Lab Platform for Genome Sequencing, 34149 Trieste, Italy; [d]Department of Chemistry and Biochemistry, University of California San Diego, La Jolla, CA 92093; [e]Department of Molecular Biosciences, The University of Texas at Austin, Austin, TX 78712; [f]VisMederi Research S.r.l., 53100 Siena, Italy; [g]Department of Molecular and Developmental Medicine, University of Siena, 53100 Siena, Italy; and [h]Faculty of Medicine, Imperial College, SW7 2DD London, United Kingdom

Contributed by Rino Rappuoli, June 7, 2021 (sent for review February 16, 2021; reviewed by Rafi Ahmed and Shane Crotty)

To investigate the evolution of severe acute respiratory syndrome coronavirus 2 (SARS-CoV-2) in the immune population, we coincupi bated the authentic virus with a highly neutralizing plasma from a COVID-19 convalescent patient. The plasma fully neutralized the virus for seven passages, but, after 45 d, the deletion of F140 in the spike N-terminal domain (NTD) N3 loop led to partial breakthrough. At day 73, an E484K substitution in the receptor-binding domain (RBD) occurred, followed, at day 80, by an insertion in the NTD N5 loop containing a new glycan sequon, which generated a variant completely resistant to plasma neutralization. Computational modeling predicts that the deletion and insertion in loops N3 and N5 prevent binding of neutralizing antibodies. The recent emergence in the United Kingdom, South Africa, Brazil, and Japan of natural variants with similar changes suggests that SARS-CoV-2 has the potential to escape an effective immune response and that vaccines and antibodies able to control emerging variants should be developed.

SARS-CoV-2 | COVID-19 | emerging variants | immune evasion | antibody response

Severe acute respiratory syndrome coronavirus 2 (SARS-CoV-2), causative agent of COVID-19, accounts for over 105 million cases of infections and more than 2.3 million deaths worldwide. Thanks to an incredible scientific and financial effort, several prophylactic and therapeutic tools, such as vaccines and monoclonal antibodies (mAbs), have been developed in less than 1 y to combat this pandemic (1–4). The main target of vaccines and mAbs is the SARS-CoV-2 spike protein (S protein), a large class I trimeric fusion protein which plays a key role in viral pathogenesis (3, 5, 6). The SARS-CoV-2 S protein is composed of two subunits: S1, which contains the receptor-binding domain (RBD) responsible for the interaction with receptors on the host cells, and S2, which mediates membrane fusion and viral entry (7, 8). The S1 subunit presents two highly immunogenic domains, the N-terminal domain (NTD) and the RBD, which are the major targets of polyclonal and monoclonal neutralizing antibodies (4, 9, 10). The continued spread in immune-competent populations has led to adaptations of the virus to the host and generation of new SARS-CoV-2 variants. Indeed, S-protein variants have been recently described in the United Kingdom, South Africa, Brazil, and Japan (11–13), and the Global Initiative on Sharing All Influenza Data (GISAID) database reports more than 1,100 amino acid changes in the S protein (14, 15).

An important question for vaccine development is whether the authentic virus, under the selective pressure of the polyclonal immune response in convalescent or vaccinated people, can evolve to fully escape immunity and antibody treatment. To address this question, we incubated the authentic SARS-CoV-2 wild-type (WT) virus for more than 90 d in the presence of a potent neutralizing plasma.

Results

Characterization of COVID-19 Convalescent Donor Plasma Samples. Plasma samples from 20 convalescent patients with confirmed COVID-19 infection were collected for this study. All plasmas were collected between March and May 2020 where only the original Wuhan virus and D614G variants were circulating. All plasmas, tested by enzyme-linked immunosorbent assay (ELISA), were found to bind the SARS-CoV-2 S-protein trimer, and most of them also bound the S1 and S2 subunits, and the RBD. However, a broad range of reactivity profiles were noticed, ranging from weak binders with titers of 1/10 to strong binders with titers of 1/10,240 (Table 1 and *SI Appendix*, Fig. S1*A*). PT008, PT009, PT015, PT122, and PT188 showed the strongest binding toward the S trimer, and, among them, PT188 had also the highest binding to the S1–S2 subunits and among the highest binding titers against the RBD (1/1,280). All but one plasma sample (PT103) were able to bind the S-protein S1 subunit, while three plasma samples (PT103, PT200, and PT276) were negative for binding to

Significance

This work shows that, under strong immune pressure, SARS-CoV-2 can use mutations in both the N-terminal domain and the receptor-binding domain to escape potent polyclonal neutralizing responses. Indeed, after a long period under immune selective pressure, SARS-CoV-2 evolved to evade the immunity of a potent polyclonal serum from a COVID-19 convalescent donor. Only three mutations were sufficient to generate this escape variant. The new virus was resistant to 70% of the neutralizing antibodies tested and had a decreased susceptibility to all convalescent sera. Our data predict that, as the immunity in the population increases, following infection and vaccination, new variants will emerge, and therefore vaccines and monoclonal antibodies need to be developed to address them.

Author contributions: E.A. and R.R. designed research; E.A., G.P., D.L., L.C., N.V.J., I.P., S.D.M., E.P., N.M., A.M., R.M., E.C., I.H., L.B., and R.E.A. performed research; E.A., D.L., L.C., N.V.J., E.M., R.E.A., J.S.M. and R.R. analyzed data; and E.A. and R.R. wrote the paper.

Reviewers: R.A., Emory University; and S.C., La Jolla Institute for Allergy & Immunology.

Competing interest statement: R.R. is an employee of the GSK group of companies. E.A., I.P., E.P., N.M., and R.R. are listed as inventors of full-length human monoclonal antibodies described in Italian patent applications 102020000015754 filed on June 30, 2020 and 102020000018955 filed on August 3, 2020.

This article is a PNAS Direct Submission.

[1]To whom correspondence may be addressed. Email: rino.r.rappuoli@gsk.com.

This article contains supporting information online at https://www.pnas.org/lookup/suppl/doi:10.1073/pnas.2103154118/-/DCSupplemental.

Published August 20, 2021.

Table 1. Summary of COVID-19 convalescent plasma characteristics

Sample ID	S-protein trimer-binding titer	RBD-binding titer	S1-binding titer	S2-binding titer	Neutralization titer WT	Neutralization titer D614G	Neutralization titer PT188-EM
PT003	1/320	1/10	1/80	1/320	1/15	Not neutralizing	Not neutralizing
PT004	1/2,560	1/80	1/320	1/2,560	1/120	1/60	1/20
PT005	1/320	1/80	1/160	1/1,280	1/80	1/30	1/10
PT006	1/640	1/160	1/1,280	1/640	1/120	1/20	1/10
PT008	1/10,240	1/80	1/640	1/640	1/120	1/80	1/40
PT009	1/10,240	1/2,560	1/1,280	1/2,560	1/640	1/320	1/120
PT010	1/320	1/80	1/80	1/2,560	1/15	1/10	1/10
PT012	1/1,280	1/160	1/320	1/320	1/120	1/80	1/15
PT014	1/1,280	1/80	1/160	1/1,280	1/120	1/40	1/20
PT015	1/10,240	1/10,240	1/2,560	1/5,120	1/640	1/320	1/160
PT041	1/640	1/40	1/160	1/80	1/40	1/10	1/10
PT042	1/5,120	1/320	1/1,280	1/5,120	1/960	1/320	1/60
PT100	1/1,280	1/80	1/160	1/1,280	1/80	1/30	1/40
PT101	1/640	1/40	1/160	1/320	1/20	1/10	1/10
PT102	1/160	1/20	1/80	1/640	1/10	Not neutralizing	Not neutralizing
PT103	1/160	Not binder	Not binder	1/160	Not neutralizing	Not neutralizing	Not neutralizing
PT122	1/10,240	1/1,280	1/1,280	1/2,560	1/640	1/480	1/320
PT188	1/10,240	1/1,280	1/5,120	1/5,120	1/10,240	1/10,240	1/40
PT200	1/1,280	Not binder	1/160	1/10,240	1/60	1/30	Not neutralizing
PT276	1/80	Not binder	1/80	1/320	Not neutralizing	Not neutralizing	Not neutralizing

The table shows the binding profile and neutralization activities of 20 COVID-19 convalescent plasma samples.

the RBD. Neutralization activity tested against the SARS-CoV-2 WT and D614G variant also showed variable titers. Most of the plasma samples neutralized the viruses with titers ranging from 1/20 to 1/320. Four samples had extremely low titers (1/10), whereas sample PT188 showed extremely high titers (1/10,240). Four plasma samples did not show neutralization activity against the SARS-CoV-2 WT and SARS-CoV-2 D614G variant. Plasma from subject PT188, which had the highest neutralizing titer and ELISA binding reactivity (Table 1 and *SI Appendix*, Fig. S1 *B–D*), was selected to test whether SARS-CoV-2 can evolve to escape a potent humoral immunity.

Evolution of SARS-CoV-2 Convalescent Plasma Escape Mutant. Twofold dilutions of plasma PT188 ranging from 1/10 to 1/20,480 were coincubated with 10^5 median tissue culture infectious dose ($TCID_{50}$) of the WT virus in a 24-well plate. This viral titer was approximately 3 logs more than what is conventionally used in microneutralization assays (16–20). The plasma/virus mixture was coincubated for 5 d to 8 d. Then, the first well showing cytopathic effect (CPE) was diluted 1:100 and incubated again with serial dilutions of plasma PT188 (Fig. 1*A* and *SI Appendix*, Table S1). For six passages and 38 d, PT188 plasma neutralized the virus with a titer of 1/640 and did not show any sign of escape. However, after seven passages and 45 d, the neutralizing titer decreased to 1/320. Sequence analyses revealed a deletion of the phenylalanine in position 140 (F140) on the S-protein NTD N3 loop in 36% of the virions (Fig. 1 *B* and *C* and *SI Appendix*, Table S1). In the subsequent passage (P8), this mutation was observed in 100% of the sequenced virions, and an additional twofold decrease in neutralization activity was observed, reaching an overall neutralization titer of 1/160. Following this initial breakthrough, a second mutation occurred after 12 passages and 80 d of plasma/virus coincubation (P12). This time, the glutamic acid in position 484 of the RBD was substituted with a lysine (E484K). This mutation occurred in 100% of sequenced virions and led to a fourfold decrease in neutralization activity which reached a titer of 1/40 (Fig. 1 *B* and *C* and *SI Appendix*, Table S1). The E484K substitution was rapidly followed by a third and final change comprising an 11-amino acid insertion between Y248 and L249 in the NTD N5 loop ($_{248a}$KTRNKSTSRRE$_{248k}$). The insertion contained an N-linked glycan sequon ($_{248d}$NKS$_{248f}$), and this viral variant resulted in complete abrogation of neutralization activity by the PT188 plasma sample. Initially, this insertion was observed in only 49% of the virions, but, when the virus was kept in culture for another passage (P14), the insertion was fully acquired by the virus (Fig. 1 *B* and *C* and *SI Appendix*, Table S1).

Reduced Susceptibility to Convalescent Plasma and Monoclonal Antibodies. To evaluate the ability of the SARS-CoV-2 PT188 escape mutant (PT188-EM) to evade the polyclonal antibody response, all 20 plasma samples from COVID-19 convalescent patients were tested in a traditional CPE-based neutralization assay against this viral variant using the virus at 100 $TCID_{50}$. All samples showed at least a twofold decrease in neutralization activity against SARS-CoV-2 PT188-EM (Fig. 2*A*, Table 1, and *SI Appendix*, Fig. S1 *B–D*). As expected, the plasma used to select the escape mutant showed the biggest neutralization decrease against this escape mutant with a 256-fold decrease compared to WT SARS-CoV-2. Plasma PT042, PT006, PT005, PT012, and PT041 also showed a substantial drop in neutralization efficacy (Table 1). In addition, we observed that a higher response toward the S-protein S1 subunit correlates with loss of neutralization activity against SARS-CoV-2 PT188-EM (see *SI Appendix*, Fig. S2*A*), whereas a high response toward the S-protein S2 subunit did not show correlation (see *SI Appendix*, Fig. S2*B*).

We also tested a previously identified panel of 13 neutralizing mAbs (nAbs) by CPE-based neutralization assay to assess their neutralization efficacy against SARS-CoV-2 PT188-EM. These antibodies were classified into three groups based on their binding profiles to the S protein. Group I nAbs were able to bind the S1-RBD, group II targeted the S1 subunit but not the RBD, and group III nAbs were specific for the S-protein trimer (Table 2). These antibodies also showed a variable neutralization potency against the SARS-CoV-2 WT and D614G viruses ranging from 3.9 ng/mL to 500.0 ng/mL (Fig. 2*B*, Table 2, and *SI Appendix*, Fig. S1 *E–G*). The three mutations selected by SARS-CoV-2 PT188-EM to escape the highly neutralizing plasma completely abrogated the neutralization activity of two of the six tested RBD-directed antibodies (F05 and G12) (Fig. 2*B*, Table 2, and *SI Appendix*, Fig. S1 *E–G*), suggesting that their epitopes include E484. In contrast, the extremely potent neutralizing antibody J08 was the most potently

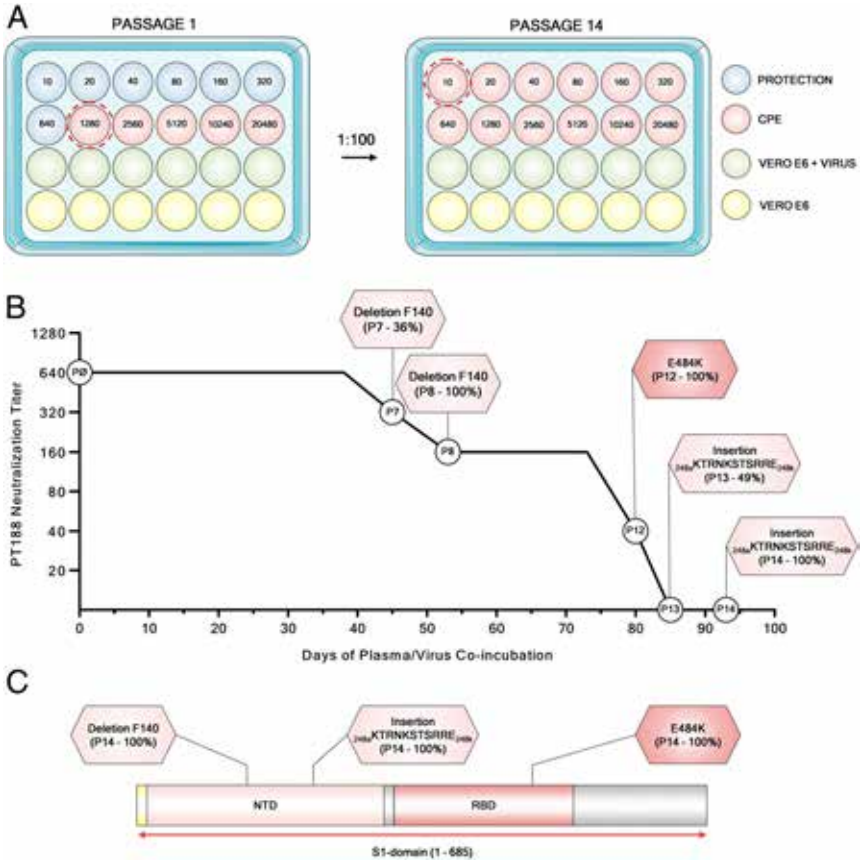

Fig. 1. Evolution of an authentic SARS-CoV-2 escape mutant. (*A*) Schematic representation of the 24-well plate format used to select the authentic SARS-CoV-2 escape mutant. Blue, red, green, and yellow wells show feeder cells protect from PT188 neutralization, CPE, authentic virus on Vero E6 cells, and Vero E6 alone, respectively. (*B*) The graph shows the PT188 neutralization titer after each mutation acquired by the authentic virus. Specific mutations, fold decrease, and days on which the mutations occur are reported in the figure. (*C*) SARS-CoV-2 S-protein gene showing type, position of mutations, and frequency of mutations.

neutralizing antibody against this escape mutant, with an IC_{100} of 22.1 ng/mL. Interestingly, the S1-RBD–directed antibody C14 showed a twofold increase in neutralization activity compared to the SARS-CoV-2 WT virus, whereas I14 and B07 showed a 16-fold and twofold decrease, respectively. All tested antibodies derived from group II (S1-specific not RBD) and group III (S-protein trimer specific) completely lost their neutralization ability against SARS-CoV-2 PT188-EM (Fig. 2*B*, Table 2, and *SI Appendix*, Fig. S1 *E*–*G*). To better understand the abrogation of activity of some of the tested antibodies, J13, I21, and H20 were cocomplexed with SARS-CoV-2 WT S protein and structurally evaluated by negative-stain EM. Two-dimensional (2D) class averages of the three tested antibodies showed that they all bind to the NTD of the S protein (Fig. 2*C*). A 3D reconstruction for the J13 Fab complex provided further evidence that this antibody binds to the NTD (Fig. 2*D*).

Putative Structural Effects Enabling Viral Escape. Computational modeling and simulation of the WT and PT188-EM spikes provides a putative structural basis for understanding antibody escape. The highly antigenic NTD is more extensively mutated, containing the F140 deletion as well as the 11-amino acid insertion in loop N5 that introduces a novel N-glycan sequon at position N248d (Fig. 3 *A*–*C*). In contrast, the single mutation in the RBD (E484K) swaps the charge of the sidechain, which would significantly alter the electrostatic complementarity of antibody binding to this region (Fig. 3*D*). Upon inspection of molecular dynamics (MD) simulations of the NTD escape mutant model, we hypothesize that the F140 deletion alters the packing of the N1, N3, and N5 loops (see *SI Appendix*, Fig. S3), where the loss of the bulky aromatic sidechain would overall reduce the stability of this region (Table 1). Subsequently, the extensive insertion within the N5 loop appears to remodel this critical antigenic region, predicting substantial steric occlusion with antibodies targeting this epitope, such as antibody 4A8 (Fig. 3*B*) (21). Furthermore, introduction of a new N-glycan at position N248d (mutant numbering scheme) would effectively eliminate neutralization by such antibodies (Fig. 3*B* and *SI Appendix*, Fig. S4).

Escape Mutant Shows Similar Viral Fitness Compared to the WT Virus. To determine the extent to which the escape mutations were detrimental to the infectivity of SARS-CoV-2 PT188-EM, the viral fitness was evaluated. Four different measures were assessed: visible CPE, viral titer, RNA-dependent RNA polymerase (RdRp), and nucleocapsid (N) RNA detection by RT-PCR (see *SI Appendix*, Fig. S5). Initially, the SARS-CoV-2 WT virus and the PT188-EM variant were inoculated at a multiplicity of infection of 0.001 on Vero E6 cells. Every day, for four consecutive days, a titration plate was prepared and optically assessed after 72 h of incubation to evaluate the CPE effect on Vero E6 cells and viral titer. Furthermore, the RNA was extracted to assess RdRp and N-gene levels in the supernatant. We collected pictures at 72 h postinfection to evaluate the morphological status of noninfected Vero E6 cells and the CPE on infected feeder cells. Vero E6 cells were confluent at 72 h, and no sign of CPE was optically detectable (see *SI Appendix*, Fig. S5*A*). Conversely, SARS-CoV-2 WT and PT188-EM showed significant and comparable amounts of CPE (see *SI Appendix*, Fig.

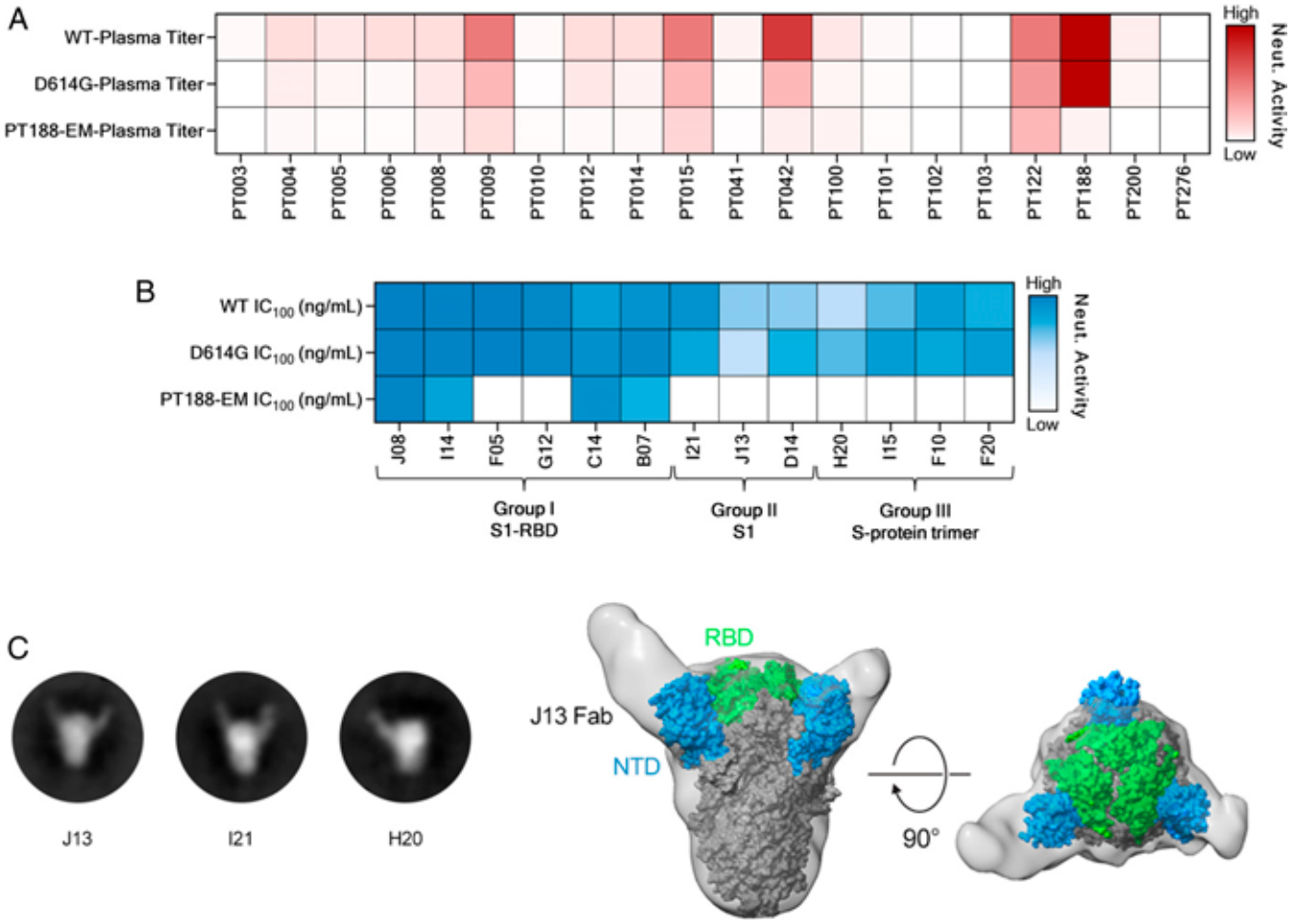

Fig. 2. Neutralization (Neut.) efficacy of plasma and 13 mAbs against SARS-CoV-2 PT188-EM. (*A*) Heat map showing the neutralization activity of tested plasma samples to the SARS-CoV-2 WT and D614G and PT188-EM variants. (*B*) Heat maps showing neutralization profiles of tested mAbs. (*C*) Negative stain EM 2D class averages showing J13, I21, and H20 Fabs bound to the SARS-CoV-2 S protein. (*D*) A 3D reconstruction of J13 bound to the NTD domain of the S protein viewed looking along (*Left*) or toward (*Right*) the viral membrane.

S5*A*). Viral titers were evaluated for both SARS-CoV-2 WT and PT188-EM, and no significant differences were observed, as the viruses showed almost identical growth curves (see *SI Appendix*, Fig. S5*B*). A similar trend was observed when RdRp and N-gene levels in the supernatant were detected, even if slightly higher levels of RdRp and N gene were detectable for SARS-CoV-2 PT188-EM

Table 2. Features of 13 SARS-CoV-2 neutralizing antibodies

mAb ID	Binding specificity*	Neutralization WT IC_{100} (ng:mL)*	Neutralization D614G IC_{100} (ng:mL)*	Neutralization PT188-EM IC_{100} (ng:mL)
J08	S1-RBD	3.9	7.8	22.1
I14	S1-RBD	11.0	19.7	176.8
F05	S1-RBD	3.9	4.9	Not neutralizing
G12	S1-RBD	39.4	39.4	Not neutralizing
C14	S1-RBD	157.5	78.7	88.4
B07	S1-RBD	99.2	49.6	250.0
I21	S1	99.2	198.4	Not neutralizing
J13	S1	396.8	500.0	Not neutralizing
D14	S1	396.8	250.0	Not neutralizing
H20	S protein	492.2	310.0	Not neutralizing
I15	S protein	310.0	155.0	Not neutralizing
F10	S protein	155.0	195.3	Not neutralizing
F20	S protein	246.1	155.0	Not neutralizing

The table shows the binding and neutralization profile of 13 previously identified SARS-CoV-2 nAbs.
*Column refers to previously published data (1).

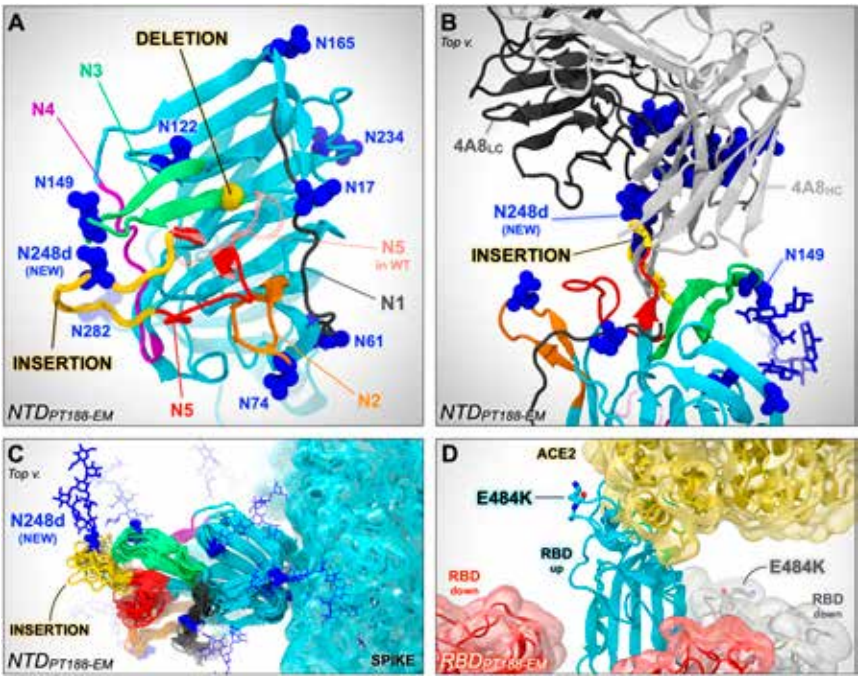

Fig. 3. In silico modeling of the PT188-EM spike NTD and RBD. (*A*) In silico model of the NTD of the SARS-CoV-2 PT188-EM spike protein based on PDB ID code 7JJI. This model accounts for the 11-amino acid insertion (yellow ribbon) and F140 deletion (highlighted with a yellow bead). N5 loop as in the WT cryo-EM structure (PDB ID code 7JJI) is shown as a transparent red ribbon. (*B*) Close-up of the PT188-EM spike NTD model in complex with antibody 4A8. Both heavy chain (HC, light gray) and light chain (LC, dark gray) of 4A8 are shown. The 11-amino acid insertion (yellow ribbon) within N5 loop introduces a new N-linked glycan (N248d) that sterically clashes with 4A8, therefore disrupting the binding interface. The N-glycan at position N149 is, however, compatible with 4A8 binding. (*C*) Conformational dynamics of the PT188-EM spike NTD model resulting from 100 ns of MD simulation is shown by overlaying multiple frames along the generated trajectory. (*D*) In silico model of the PT188-EM spike RBD based on PDB ID code 6M17, where the E484K mutation is shown with licorice representation.

at day 0 and day 1 (see *SI Appendix*, Fig. S5*C*). Finally, strong correlations between viral titers and RdRp/N-gene levels were observed for both SARS-CoV-2 WT and PT188-EM (see *SI Appendix*, Fig. S5 *D* and *E*).

Discussion

We have shown that the authentic SARS-CoV-2, if constantly pressured, has the ability to escape even a potent polyclonal serum targeting multiple neutralizing epitopes. These results are remarkable because SARS-CoV-2 shows a very low estimated evolutionary rate of mutation, as this virus encodes a proofreading exoribonuclease machinery, and, therefore, while escape mutants can be easily isolated when viruses are incubated with single mAbs, it is usually believed that a combination of two mAbs is sufficient to eliminate the evolution of escape variants (22–25). The recent isolation of SARS-CoV-2 variants in the United Kingdom, South Africa, Brazil, and Japan with deletions in or near the NTD loops shows that what we describe here can occur in the real world. The ability of the virus to adapt to the host immune system was also observed in clinical settings where an immunocompromised COVID-19 patient, after 154 d of infection, presented different variants of the virus, including the E484K substitution (26). Therefore, we should be prepared to deal with virus variants that may be selected by the immunity acquired from infection or vaccination. This can be achieved by developing second-generation vaccines and mAbs, possibly targeting universal epitopes and able to neutralize emerging variants of the virus.

A limitation of this study is that viral evolution of SARS-CoV-2 was evaluated only for one plasma sample, limiting the observation of possible spike protein mutations only to a specific polyclonal response. In fact, PT188-EM impacted our plasma samples differently, where PT188, used to pressure the virus in vitro, was the most impacted sample (256-fold decrease), while the remaining 15 neutralizing plasmas showed a median neutralization titer reduction of ∼sevenfold.

Our data also confirm that the SARS-CoV-2 neutralizing antibodies acquired during infection target almost entirely the NTD and the RBD. In the RBD, the possibility to escape is limited, and the mutation E484K that we found is one of the most frequent mutations to escape mAbs (22) and among the most common RBD mutations described in experimental settings (27). Remarkably, the evolution of the E484K substitution observed in our experimental setting was replicated a few months later in the real world by the emergence of E484K variants in South Africa, Brazil, and Japan (14). This is likely due to residue E484 being targeted by antibodies derived from IGHV3-53 and closely related IGHV3-66 genes, which are the most common germlines for antibodies directed against the RBD (28). Recently, this mutation has also been shown to reduce considerably the neutralizing potency of vaccine-induced immunity and to escape mAbs already approved for emergency use by the Food and Drug Administration (29–31).

On the other hand, the NTD loops can accommodate many different changes, such as insertions, deletions, and amino acid alterations. Interestingly, in our case, the final mutation contained an insertion carrying an N-glycosylation site which has the potential to hide or obstruct the binding to neutralizing epitopes. The introduction of a glycan is a well-known immunogenic escape strategy described in influenza (32), HIV-1, and other viruses (33–35), although this finding presents a patient-derived escape mutant utilizing this mechanism for SARS-CoV-2. Surprisingly, only three mutations, which led to complete rearrangement of NTD N3 and N5 loops and substitution to a key residue on the RBD, were sufficient to eliminate the neutralization ability of a

potent polyclonal serum. Fortunately, not all plasma and mAbs tested were equally affected by the three mutations, suggesting that natural immunity to infection can target additional epitopes that can still neutralize the PT188-EM variant. Vaccine-induced immunity, which is more robust than natural immunity, is likely to be less susceptible to emerging variants. Indeed, so far, the virus has not mutated sufficiently to completely avoid the antibody response raised by current vaccines (36, 37).

Going forward, it will be important to continue to closely monitor which epitopes on the S protein are targeted by the vaccines against SARS-CoV-2 that are being deployed in hundreds of millions of people around the world.

Materials and Methods

Enrollment of SARS-CoV-2 Convalescent Donors and Human Sample Collection. COVID-19 convalescent plasma samples were provided by the National Institute for Infectious Diseases, Institute for Scientific Based Recovery and Cure—Lazzaro Spallanzani Rome (Italy) and Azienda Ospedaliera Universitaria Senese, Siena (Italy). Samples were collected from convalescent donors who gave their written consent. The study was approved by local ethics committees (Parere 18_2020 in Rome and Parere 17065 in Siena) and conducted according to good clinical practice in accordance with the Declaration of Helsinki (European Council 2001, US Code of Federal Regulations, International Conference on Harmonization 1997). This study was unblinded and not randomized.

SARS-CoV-2 Authentic Virus Neutralization Assay. The mAbs and plasma neutralization activity was evaluated using a CPE-based assay as previously described (17, 20). Further details are available in *SI Appendix, Materials and Methods*.

Viral Escape Assay Using Authentic SARS-CoV-2. All SARS-CoV-2 authentic virus procedures were performed in the biosafety level 3 (BSL3) laboratories at Toscana Life Sciences in Siena (Italy) and Vismederi S.r.l., Siena (Italy). BSL3 laboratories are approved by a certified biosafety professional and are inspected every year by local authorities. To detect neutralization-resistant SARS-CoV-2 escape variants, a standard concentration of the virus was sequentially passaged in cell cultures in the presence of serially diluted samples containing SARS-CoV-2-specific antibodies. Briefly, 12 serial twofold dilutions of PT188 plasma prepared in complete Dulbecco's modified Eagle's medium 2% fetal bovine serum (starting dilution 1:10) were added to the wells of one 24-well plate. Virus solution containing 10^5 $TCID_{50}$ of authentic SARS-CoV-2 was dispensed in each antibody-containing well, and the plates were incubated for 1 h at 37 °C, 5% CO_2. The mixture was then added to the wells of a 24-well plate containing a subconfluent Vero E6 cell monolayer. Plates were incubated for 5 d to 7 d at 37 °C, 5% CO_2 and examined for the presence of CPE using an inverted optical microscope. A virus-only control and a cell-only control were included in each plate to assist in distinguishing absence or presence of CPE. At each virus passage, the content of the well corresponding to the lowest sample dilution that showed complete CPE was diluted 1:100 and transferred to the antibody-containing wells of the predilution 24-well plate prepared for the subsequent virus passage. At each passage, both the virus pressured with PT188 and the virus-only control were harvested, propagated in 25-cm^2 flasks, and aliquoted at −80 °C to be used for RNA extraction, RT-PCR, and sequencing.

Negative Stain Electron Microscopy. SARS-CoV-2 S protein was expressed and purified as previously described (38). Purified spike was combined with individual Fabs at final concentrations of 0.04 mg/mL and 0.16 mg/mL, respectively. Following a 30-min incubation on ice, each complex was deposited on plasma cleaned CF-400 grids (EMS) and stained using methylamine tungstate (Nanoprobes). Grids were imaged at 92,000× magnification in a Talos F200C transmission electron microscope (TEM) equipped with a Ceta 16M detector (Thermo Fisher Scientific). Contrast transfer function estimation and particle picking were performed using cisTEM (39), and particle stacks were exported to cryoSPARC v2 (40) for 2D classification, ab initio 3D reconstruction, and heterogeneous refinement.

Computational Methods. The PT188-EM spike escape mutant was modeled using in silico approaches. As the mutations are localized in two different domains of the spike, namely the NTD and the RBD, separate models were generated for each domain. In detail, two models of the PT188-EM spike NTD (residues 13 to 308) were built starting from two different cryoelectron microscopy (cryo-EM) structures of the WT S protein as templates: 1) one bearing a completely resolved NTD [Protein Data Bank (PDB) ID code 7JJI (41)], which includes all the loops from N1 to N5, and 2) one bound to the antibody 4A8 [PDB ID code 7C2L (21)], which presents only one small gap within the N5 loop. The model of the PT188-EM spike RBD was based on the cryo-EM structure of the spike's RBD in complex with ACE2 [PDB ID code 6M17 (42)]. The generated models were subsequently refined using explicitly solvated all-atom MD simulations. The systems and the simulations were visually inspected with visual molecular dynamics, which was also used for image rendering (43). Further details on the computational method analyses are reported in *SI Appendix, Materials and Methods*.

Data Availability. All study data are included in the article and *SI Appendix*.

ACKNOWLEDGMENTS. This work was funded by European Research Council Advanced Grant Agreement 787552 (vaccines as a remedy for antimicrobial resistant bacterial infections [vAMRes]). This publication was supported by funds from the "Centro Regionale Medicina di Precisione" and by all the people who answered the call to fight with us the battle against SARS-CoV-2 with their kind donations on the platform ForFunding (https://www.forfunding.intesasanpaolo.com/DonationPlatform-ISP/nav/progetto/id/3380). This publication was supported by the European Virus Archive Goes Global project, which has received funding from the European Union's Horizon 2020 Research and Innovation Programme under Grant Agreement 653316. This publication was supported by the COVID-2020-12371817 project, which has received funding from the Italian Ministry of Health. This work was supported by NIH Grant GM132826, NSF Grants for Rapid Response Research Grant MCB-2032054, an award from the Research Corporation for Science Advancement, and a University of California San Diego Moore's Cancer Center 2020 SARS-CoV-2 seed grant to R.E.A and National Institute of Allergy and Infectious Diseases Grant R01-AI127521 awarded to J.S.M. We are grateful for the efforts of the Texas Advanced Computing Center Frontera team and for the compute time made available through a Director's Discretionary Allocation (made possible by NSF Award OAC-1818253). We also thank Dr. Fiona Kearns for assistance with the NTD glycan modeling.

1. S. Jiang, C. Hillyer, L. Du, Neutralizing antibodies against SARS-CoV-2 and other human coronaviruses. *Trends Immunol.* **41**, 355–359 (2020).
2. F. Krammer, SARS-CoV-2 vaccines in development. *Nature* **586**, 516–527 (2020).
3. Y. Dong *et al.*, A systematic review of SARS-CoV-2 vaccine candidates. *Signal Transduct. Target. Ther.* **5**, 237 (2020).
4. E. Gavor, Y. K. Choong, S. Y. Er, H. Sivaraman, J. Sivaraman, Structural basis of SARS-CoV-2 and SARS-CoV antibody interactions. *Trends Immunol.* **41**, 1006–1022 (2020).
5. Z. Ke *et al.*, Structures and distributions of SARS-CoV-2 spike proteins on intact virions. *Nature* **588**, 498–502 (2020).
6. A. C. Walls *et al.*, Structure, function, and antigenicity of the SARS-CoV-2 spike glycoprotein. *Cell* **181**, 281–292.e6 (2020).
7. T. M. Clausen *et al.*, SARS-CoV-2 infection depends on cellular heparan sulfate and ACE2. *Cell* **183**, 1043–1057.e15 (2020).
8. T. F. Rogers *et al.*, Isolation of potent SARS-CoV-2 neutralizing antibodies and protection from disease in a small animal model. *Science* **369**, 956–963 (2020).
9. Q. Wang *et al.*, Structural and functional basis of SARS-CoV-2 entry by using human ACE2. *Cell* **181**, 894–904.e9 (2020).
10. J. Lan *et al.*, Structure of the SARS-CoV-2 spike receptor-binding domain bound to the ACE2 receptor. *Nature* **581**, 215–220 (2020).
11. COG-UK, "COG-UK update on SARS-CoV-2 Spike mutations of special interest" (Rep. 1, COG-UK, 2020).
12. H. Tegally *et al.*, Emergence and rapid spread of a new severe acute respiratory syndrome-related coronavirus 2 (SARS-CoV-2) lineage with multiple spike mutations in South Africa. *medRxiv* [Preprint] (2020). https://doi.org/10.1101/2020.12.21.20248640 (Accessed 22 December 2020).
13. E. C. Sabino *et al.*, Resurgence of COVID-19 in Manaus, Brazil, despite high seroprevalence. *Lancet* **397**, 452–455 (2021).
14. S. Elbe, G. Buckland-Merrett, Data, disease and diplomacy: GISAID's innovative contribution to global health. *Glob. Chall.* **1**, 33–46 (2017).
15. Y. Shu, J. McCauley, GISAID: Global initiative on sharing all influenza data—From vision to reality. *Eurosurveillance* **22**, 30494 (2017).
16. L. A. Jackson *et al.*, An mRNA vaccine against SARS-CoV-2—Preliminary report. *N. Engl. J. Med.* **383**, 1920–1931 (2020).
17. A. Manenti *et al.*, Evaluation of SARS-CoV-2 neutralizing antibodies using a CPE-based colorimetric live virus micro-neutralization assay in human serum samples. *J. Med. Virol.* **92**, 2096–2104 (2020).
18. P. M. Folegatti *et al.*, Safety and immunogenicity of the ChAdOx1 nCoV-19 vaccine against SARS-CoV-2: A preliminary report of a phase 1/2, single-blind, randomised controlled trial. *Lancet* **396**, 467–478 (2020).
19. S. J. Zost *et al.*, Potently neutralizing and protective human antibodies against SARS-CoV-2. *Nature* **584**, 443–449 (2020).

20. E. Andreano *et al*., Extremely potent human monoclonal antibodies from COVID-19 convalescent patients. *Cell* **184**, 1821–1835.e1816 (2021).
21. X. Chi *et al*., A neutralizing human antibody binds to the N-terminal domain of the Spike protein of SARS-CoV-2. *Science* **369**, 650–655 (2020).
22. A. Baum *et al*., Antibody cocktail to SARS-CoV-2 spike protein prevents rapid mutational escape seen with individual antibodies. *Science* **369**, 1014–1018 (2020).
23. Y. Bar-On *et al*., Safety and antiviral activity of combination HIV-1 broadly neutralizing antibodies in viremic individuals. *Nat. Med.* **24**, 1701–1707 (2018).
24. S. Nakagawa, T. Miyazawa, Genome evolution of SARS-CoV-2 and its virological characteristics. *Inflamm. Regen.* **40**, 17 (2020).
25. F. Robson *et al*., Coronavirus RNA proofreading: Molecular basis and therapeutic targeting. *Mol. Cell* **79**, 710–727 (2020).
26. B. Choi *et al*., Persistence and evolution of SARS-CoV-2 in an immunocompromised host. *N. Engl. J. Med.* **383**, 2291–2293 (2020).
27. A. J. Greaney *et al*., Complete mapping of mutations to the SARS-CoV-2 spike receptor-binding domain that escape antibody recognition. *Cell Host Microbe* **29**, 44–57 (2021).
28. F. Fagiani, M. Catanzaro, C. Lanni, Molecular features of IGHV3-53-encoded antibodies elicited by SARS-CoV-2. *Signal Transduct. Target. Ther.* **5**, 170 (2020).
29. Z. Wang *et al*., mRNA vaccine-elicited antibodies to SARS-CoV-2 and circulating variants. *Nature* **592**, 616–622 (2021).
30. P. Wang *et al*., Increased resistance of SARS-CoV-2 variants B.1.351 and B.1.1.7 to antibody neutralization. *bioRxiv* [Preprint] (2021). https://doi.org/10.1101/2021.01.25.428137 (Accessed 12 February 2021).
31. R. L. Gottlieb *et al*., Effect of bamlanivimab as monotherapy or in combination with etesevimab on viral load in patients with mild to moderate COVID-19: A randomized clinical trial. *JAMA* **325**, 632–644 (2021).
32. M. O. Altman *et al*., Human Influenza A virus hemagglutinin glycan evolution follows a temporal pattern to a glycan limit. *mBio* **10**, e00204–e00219 (2019).
33. M. Zhang *et al*., Tracking global patterns of N-linked glycosylation site variation in highly variable viral glycoproteins: HIV, SIV, and HCV envelopes and influenza hemagglutinin. *Glycobiology* **14**, 1229–1246 (2004).
34. W. Wang *et al*., A systematic study of the N-glycosylation sites of HIV-1 envelope protein on infectivity and antibody-mediated neutralization. *Retrovirology* **10**, 14 (2013).
35. Wang W, *et al*. (2015) N463 glycosylation site on V5 loop of a mutant gp120 regulates the sensitivity of HIV-1 to neutralizing monoclonal antibodies VRC01/03. *J. Acquired Immune Defic. Syndr. (1999)* **69**, 270–277.
36. S. Crotty, Hybrid immunity. *Science* **372**, 1392–1393 (2021).
37. E. Andreano, R. Rappuoli, SARS-CoV-2 escaped natural immunity, raising questions about vaccines and therapies. *Nat. Med.* **27**, 759–761 (2021).
38. C.-L. Hsieh *et al*. Structure-based design of prefusion-stabilized SARS-CoV-2 spikes. *Science* **369**, 1501–1505 (2020).
39. T. Grant, A. Rohou, N. Grigorieff, *cis*TEM, user-friendly software for single-particle image processing. *eLife* **7**, 7 (2018).
40. A. Punjani, J. L. Rubinstein, D. J. Fleet, M. A. Brubaker, cryoSPARC: Algorithms for rapid unsupervised cryo-EM structure determination. *Nat. Methods* **14**, 290–296 (2017).
41. S. Bangaru *et al*., Structural analysis of full-length SARS-CoV-2 spike protein from an advanced vaccine candidate. *Science* **370**, 1089–1094 (2020).
42. R. Yan *et al*. Structural basis for the recognition of SARS-CoV-2 by full-length human ACE2. *Science* **367**, 1444–1448 (2020).
43. W. Humphrey, A. Dalke, K. Schulten, VMD: Visual molecular dynamics. *J. Mol. Graph.* **14**, 27–38 (1996).

Since January 2020 Elsevier has created a COVID-19 resource centre with free information in English and Mandarin on the novel coronavirus COVID-19. The COVID-19 resource centre is hosted on Elsevier Connect, the company's public news and information website.

Elsevier hereby grants permission to make all its COVID-19-related research that is available on the COVID-19 resource centre - including this research content - immediately available in PubMed Central and other publicly funded repositories, such as the WHO COVID database with rights for unrestricted research re-use and analyses in any form or by any means with acknowledgement of the original source. These permissions are granted for free by Elsevier for as long as the COVID-19 resource centre remains active.

Cell

Article

Extremely potent human monoclonal antibodies from COVID-19 convalescent patients

Graphical abstract

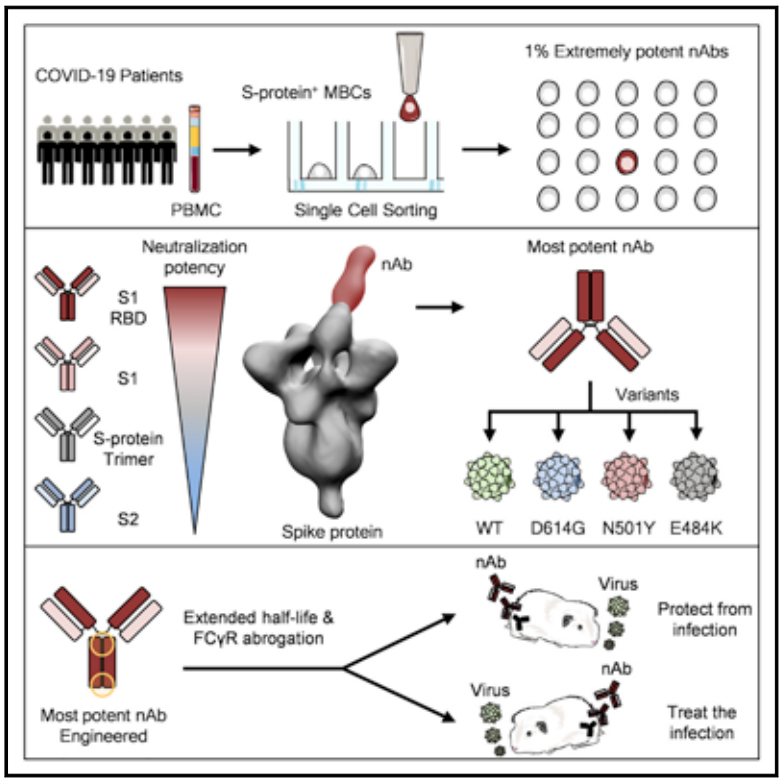

Highlights

- Human memory B cells encoding extremely potent neutralizing antibodies are rare
- Most potent antibodies recognize the tip of the spike receptor-binding domain
- Selected neutralizing antibody neutralizes SARS-CoV-2 emerging variants
- Potent antibody prevents and treats hamster infection without Fc-functions

Authors

Emanuele Andreano, Emanuele Nicastri, Ida Paciello, ..., Claudia Sala, Giuseppe Ippolito, Rino Rappuoli

Correspondence

rino.r.rappuoli@gsk.com

In brief

Extremely potent neutralizing human monoclonal antibodies, though rare, are isolated from COVID-19 convalescent patients and suitable for prophylactic and therapeutic interventions of wild-type SARS-CoV-2 as well as emerging variants.

Andreano et al., 2021, Cell *184*, 1821–1835
April 1, 2021
https://doi.org/10.1016/j.cell.2021.02.035

CellPress

Cell

CellPress

Article

Extremely potent human monoclonal antibodies from COVID-19 convalescent patients

Emanuele Andreano,[1,17] Emanuele Nicastri,[4,17] Ida Paciello,[1] Piero Pileri,[1] Noemi Manganaro,[1] Giulia Piccini,[2] Alessandro Manenti,[2,3] Elisa Pantano,[1] Anna Kabanova,[1,11] Marco Troisi,[1,9] Fabiola Vacca,[1,9] Dario Cardamone,[1,10] Concetta De Santi,[1] Jonathan L. Torres,[16] Gabriel Ozorowski,[16] Linda Benincasa,[3] Hyesun Jang,[13] Cecilia Di Genova,[15] Lorenzo Depau,[12] Jlenia Brunetti,[12] Chiara Agrati,[4] Maria Rosaria Capobianchi,[4] Concetta Castilletti,[4] Arianna Emiliozzi,[5,6] Massimiliano Fabbiani,[6] Francesca Montagnani,[5,6] Luisa Bracci,[12] Giuseppe Sautto,[13] Ted M. Ross,[13,14] Emanuele Montomoli,[2,3,7] Nigel Temperton,[15] Andrew B. Ward,[16] Claudia Sala,[1] Giuseppe Ippolito,[4] and Rino Rappuoli[1,8,18,*]

[1]Monoclonal Antibody Discovery (MAD) Lab, Fondazione Toscana Life Sciences, Siena, Italy
[2]VisMederi S.r.l, Siena, Italy
[3]VisMederi Research S.r.l., Siena, Italy
[4]National Institute for Infectious Diseases Lazzaro Spallanzani, IRCCS, Rome, Italy
[5]Department of Medical Biotechnologies, University of Siena, Siena, Italy
[6]Department of Medical Sciences, Infectious and Tropical Diseases Unit, University Hospital of Siena, Siena, Italy
[7]Department of Molecular and Developmental Medicine, University of Siena, Siena, Italy
[8]Faculty of Medicine, Imperial College, London, UK
[9]Department of Biotechnology, Chemistry and Pharmacy, University of Siena, Siena, Italy
[10]University of Turin, Turin, Italy
[11]Tumour Immunology Unit, Fondazione Toscana Life Sciences, Siena, Italy
[12]MedBiotech Hub and Competence Center, Department of Medical Biotechnologies, University of Siena, Siena, Italy
[13]Center for Vaccines and Immunology, University of Georgia, Athens, GA 30602, USA
[14]Department of Infectious Diseases, University of Georgia, Athens, GA 30602, USA
[15]Viral Pseudotype Unit, Medway School of Pharmacy, University of Kent, Chatham, UK
[16]Department of Integrative Structural and Computational Biology, The Scripps Research Institute, La Jolla, CA 92037, USA
[17]These authors contributed equally
[18]Lead contact
*Correspondence: rino.r.rappuoli@gsk.com
https://doi.org/10.1016/j.cell.2021.02.035

SUMMARY

Human monoclonal antibodies are safe, preventive, and therapeutic tools that can be rapidly developed to help restore the massive health and economic disruption caused by the coronavirus disease 2019 (COVID-19) pandemic. By single-cell sorting 4,277 SARS-CoV-2 spike protein-specific memory B cells from 14 COVID-19 survivors, 453 neutralizing antibodies were identified. The most potent neutralizing antibodies recognized the spike protein receptor-binding domain, followed in potency by antibodies that recognize the S1 domain, the spike protein trimer, and the S2 subunit. Only 1.4% of them neutralized the authentic virus with a potency of 1–10 ng/mL. The most potent monoclonal antibody, engineered to reduce the risk of antibody-dependent enhancement and prolong half-life, neutralized the authentic wild-type virus and emerging variants containing D614G, E484K, and N501Y substitutions. Prophylactic and therapeutic efficacy in the hamster model was observed at 0.25 and 4 mg/kg respectively in absence of Fc functions.

INTRODUCTION

The impact of the severe acute respiratory syndrome coronavirus 2 (SARS-CoV-2) pandemic, with more than 100 million cases, over 2 million deaths, an estimated cost of 16 trillion US dollars to the USA economy (Cutler and Summers, 2020), and 45 million people filing unemployment in the United States alone, is unprecedented (Aratani, 2020).

Vaccines and drugs against SARS-CoV-2 have recently received emergency use authorization (EUA) by the Food and Drug Administration (FDA) for prevention and treatment of coronavirus disease 2019 (COVID-19) (FDA, 2021, 2020).

In spite of this, it is predictable that waves of infection will continue to spread globally, and it is likely to be followed by additional waves over the next few years. This is supported by the emergence of new SARS-CoV-2 variants in the United Kingdom, South Africa, Brazil, and Japan (CDC, 2021).

It is therefore imperative to quickly develop, in parallel to vaccines, therapeutic tools against SARS-CoV-2 and its variants. Among the many therapeutic options available, human

monoclonal antibodies (mAbs) can be developed in the shortest time frame. In fact, the extensive clinical experience with the safety of more than 50 commercially available mAbs approved to treat cancer, inflammatory, and autoimmune disorders provides high confidence of their safety (Wellcome and IAVI, 2020). These advantages, combined with the urgency of the SARS-CoV-2 pandemic, support and justify an accelerated regulatory pathway. In addition, the long industrial experience in developing and manufacturing mAbs decreases risks usually associated with technical development of investigational products. Finally, the incredible technical progress in this field allows shortening of conventional timelines and enables a path from discovery to proof-of-concept trials within 5–6 months (Kelley, 2020). A key example is the Ebola case, where mAbs were developed faster than vaccines or other drugs (Kupferschmidt, 2019), becoming the first therapeutic intervention recommended by the World Health Organization (WHO) and approved by the FDA (Mullard, 2020).

During the first months of this pandemic, many groups have been active in isolating and characterizing human monoclonal antibodies from COVID-19 convalescent patients or from humanized mice, and some of them have been progressing quickly to clinical trials for the prevention and cure of SARS-CoV-2 infection (Shi et al., 2020; Hansen et al., 2020; Hsieh et al., 2020; Pinto et al., 2020; Zost et al., 2020a, 2020b; Rogers et al., 2020, Alsoussi et al., 2020). Few of them are already in phase III clinical trials and reported promising preliminary results. Two of them received the EUA from the FDA (Lilly, 2020; Regeneron, 2020).

All these antibodies neutralize SARS-CoV-2 infection by binding to the spike glycoprotein (S protein), a trimeric class I viral fusion protein that mediates virus entry into host cells by engaging with the human angiotensin-converting enzyme 2 (hACE2) and cellular heparan sulfate as receptors (Clausen et al., 2020). The S protein exists in a metastable pre-fusion conformation and in a stable post-fusion form (Wang et al., 2020; Walls et al., 2020; Schäfer et al., 2020). Each S protein monomer is composed of two distinct regions, the S1 and S2 subunits. The S1 subunit contains the receptor-binding domain (RBD), which is responsible for the interaction with hACE2 and heparan sulfate on host cell membranes triggering the destabilization of the prefusion state of the S protein and consequent transition into the post-fusion conformation. This event results in the entry of the virus particle into the host cell and the onset of infection (Wrapp et al., 2020; Walls et al., 2020; Tay et al., 2020; Zou et al., 2020).

As for other mAbs in the field of infectious diseases (Hooft van Huijsduijnen et al., 2020; Sparrow et al., 2017), the dose of mAbs so far used in clinical trials against SARS-CoV-2 is high, ranging from 500 to 8,000 mgs (NCT04411628; NCT04427501; NCT04441918; NCT04425629; NCT04426695; NCT04452318). The high dose poses two important limits to the application of mAbs in the infectious diseases field. First, the high dosage has cost-associated implications, and it only allows for intravenous delivery, making this therapeutic intervention extremely costly and therefore available almost exclusively in high-income countries. Indeed, the high price of this intervention has been a barrier to the global access of mAbs and their use to other fields such as infectious diseases. A solution would be the development of extremely potent mAbs that can be used at lower dosages leading to cost reductions and that can be delivered via intramuscular or subcutaneous injections. A first example is the respiratory syncytial virus (RSV) case, where a potent mAb has recently shown its therapeutic effect in premature infants after only one intramuscular injection of 50 mg (Griffin et al., 2020).

The second limit of mAbs in the field of infectious diseases is the risk of antibody-dependent enhancement (ADE) of disease, which is usually mediated by the binding of the fragment crystallizable (Fc) region portion of the antibody to Fc gamma receptors (FcγRs) expressed by immune cells (Lee et al., 2020). ADE has been clearly demonstrated in the case of SARS-CoV, RSV, and dengue viruses, and the theoretical risk has been raised in the case of SARS-CoV-2 (Lee et al., 2020; Katzelnick et al., 2017; Arvin et al., 2020).

In this work, we pushed the limits of mAb application to fight infectious diseases by selecting extremely potent antibodies with the aim of using them at low dosage to make them affordable and conveniently delivered by intramuscular injection. In addition, we mitigated the risk of ADE by engineering their Fc region. Despite complete lack of Fc-receptor-binding and Fc-mediated cellular activities, engineered mAbs were able to prevent and treat SARS-CoV-2 infection in golden Syrian hamster at a concentration of 0.25 and 4 mg/kg respectively. These antibodies have the potential to globally extend the access and affordability of this important medical tool.

RESULTS

Isolation and characterization of S protein-specific antibodies from SARS-CoV-2 convalescent patients

To retrieve mAbs specific for SARS-CoV-2 S protein, peripheral blood mononuclear cells (PBMCs) from fourteen COVID-19 convalescent patients enrolled in this study were collected and stained with fluorescently labeled S protein trimer to identify antigen-specific memory B cells (MBCs). Figure 1 summarizes the overall experimental strategy. The gating strategy described in Figure S1A was used to single-cell sort, into 384-well plates, IgG^+ and IgA^+ MBCs binding to the SARS-CoV-2 S protein trimer in its prefusion conformation. The sorting strategy aimed to specifically identify class-switched MBCs ($CD19^+CD27^+IgD^-IgM^-$) to identify only memory B lymphocytes that underwent maturation processes. A total of 4,277 S protein-binding MBCs were successfully retrieved with frequencies ranging from 0.17% to 1.41% (Table S1). Following the sorting procedure, S $protein^+$ MBCs were incubated over a layer of 3T3-CD40L feeder cells in the presence of IL-2 and IL-21 stimuli for 2 weeks to allow natural production of immunoglobulins (Huang et al., 2013). Subsequently, MBC supernatants containing IgG or IgA were tested for their ability to bind either the SARS-CoV-2 S protein trimer in its prefusion conformation or the S protein S1 + S2 subunits (Figure 2A; Figure S2B) by enzyme linked immunosorbent assay (ELISA). A panel of 1,731 mAbs specific for the SARS-CoV-2 S protein were identified showing a broad range of signal intensities (Figure 2A; Table S1).

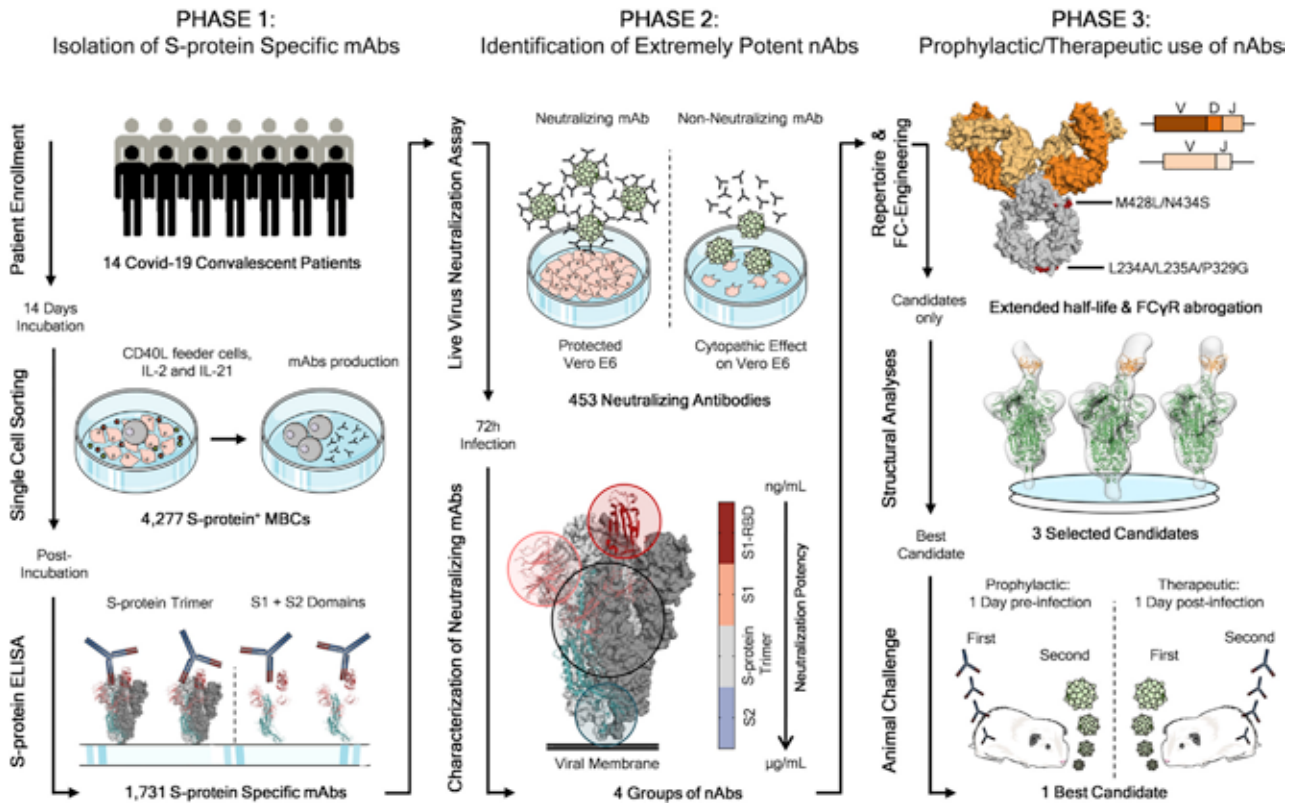

Figure 1. Workflow and timeline for SARS-CoV-2 neutralizing antibodies identification

The overall scheme shows three different phases for the identification of SARS-CoV-2 neutralizing antibodies (nAbs). Phase 1 consisted in the enrolment of COVID-19 patients (n = 14) from which PBMCs were isolated. Memory B cells were single-cell sorted (n = 4,277), and after 2 weeks of incubation, antibodies were screened for their binding specificity against the S protein trimer and S1/S2 domains. Once S protein-specific monoclonal antibodies (mAbs) were identified (n = 1,731) phase 2 started. All specific mAbs were tested *in vitro* to evaluate their neutralization activity against the authentic SARS-CoV-2 virus, and 453 nAbs were identified. nAbs showing different binding profiles on the S protein surface were selected for further functional characterization and to identify different neutralizing regions on the antigen. Phase 3 starts with the characterization of the heavy and light chain sequences of selected mAbs (n = 14) and the engineering of the Fc portion of three most promising candidates. The latter were also selected for structural analyses that allowed the identification of the neutralizing epitopes on the S protein. Finally, the most potent antibody was tested for its prophylactic and therapeutic effect in a golden Syrian hamster model of SARS-CoV-2 infection.

Identification of S protein-specific mAbs able to neutralize SARS-CoV-2

The 1,731 supernatants containing S protein-specific mAbs, were screened *in vitro* for their ability to block the binding of the streptavidin-labeled S protein to Vero E6 cell receptors and for their ability to neutralize authentic SARS-CoV-2 virus by *in vitro* microneutralization assay. In the neutralization of binding (NoB) assay, 339 of the 1,731 tested (19.6%) S protein-specific mAbs were able to neutralize the antigen/receptor binding, showing a broad array of neutralization potency ranging from 50% to 100% (Figure S2C; Table S1).

As for the authentic virus neutralization assay, supernatants containing naturally produced IgG or IgA were tested for their ability to protect the layer of Vero E6 cells from the cytopathic effect triggered by SARS-CoV-2 infection. To increase the throughput of our approach, supernatants were tested at a single-point dilution, and to increase the sensitivity of our first screening, a viral titer of 25 50% tissue culture infectious dose ($TCID_{50}$) was used. For this screening, mAbs were classified as neutralizing, partially neutralizing, and non-neutralizing based on their complete, partial, or absent ability to prevent the infection of Vero E6 cells, respectively. Out of 1,731 mAbs tested in this study, a panel of 453 (26.2%) mAbs neutralized the authentic virus and prevented infection of Vero E6 cells (Table S1). The percentage of partially neutralizing antibodies and neutralizing antibodies (nAbs) identified in each donor was extremely variable ranging from 2.6%–29.7% and 2.8%–26.4% respectively (Figure 2B; Table S2). The majority of nAbs were able to specifically recognize the S protein S1 domain (57.5%; n = 244), while 7.3% (n = 53) of nAbs were specific for the S2 domain, and 35.2% (n = 156) did not recognize single domains but only the S protein in its trimeric conformation (Figure S2A; Table S3). From the panel of 453 nAbs, we recovered the heavy chain (HC) and light chain (LC) variable regions of 220 nAbs, which were expressed as full-length immunoglobulin G1 (IgG1) using the transcriptionally active PCR (TAP) approach to characterize their neutralization potency against the live virus at 100 $TCID_{50}$. The vast majority of nAbs identified (65.9%; n = 145) had a low neutralizing potency and required more than 500 ng/mL to achieve 100% inhibitory concentration (IC_{100}). A smaller fraction of the antibodies had an intermediate neutralizing potency (23.6%; n = 52)

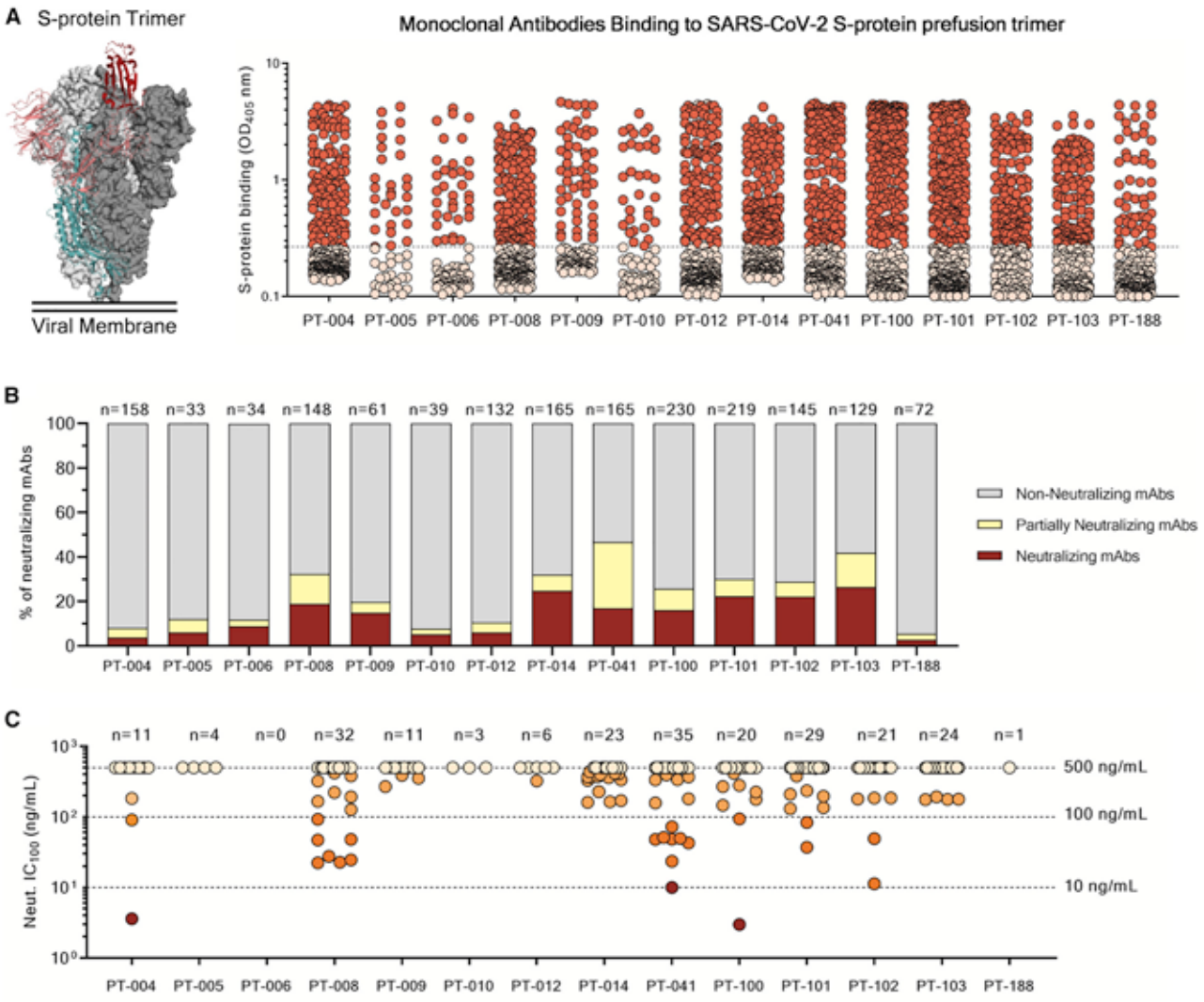

Figure 2. Identification of SARS-CoV-2 S protein-specific nAbs

(A) The graph shows supernatants tested for binding to the SARS-CoV-2 S-protein stabilized in its prefusion conformation. Threshold of positivity has been set as two times the value of the blank (dotted line). Red dots represent mAbs that bind to the S protein, while pink dots represent mAbs that do not bind.

(B) The bar graph shows the percentage of non-neutralizing (gray), partially neutralizing (pale yellow), and neutralizing antibodies (dark red) identified per each donor. The total number (n) of antibodies tested per individual is shown on top of each bar.

(C) The graph shows the neutralization potency of each nAb tested once expressed as recombinant full-length IgG1. Dashed lines show different ranges of neutralization potency (500, 100, and 10 ng/mL). Dots were colored based on their neutralization potency and were classified as weakly neutralizing (>500 ng/mL; pale orange), medium neutralizing (100–500 ng/mL; orange), highly neutralizing (10–100 ng/mL; dark orange), and extremely neutralizing (1–10 ng/mL; dark red). The total number (n) of antibodies tested per individual is shown on top of each graph. A COVID-19 convalescent plasma and an unrelated plasma were used as positive and negative control, respectively, in all the assays.

requiring between 100 and 500 ng/mL to achieve the IC_{100}, while 9.1% (n = 20) required between 10 and 100 ng/mL. Finally, only 1.4% (n = 3) of the expressed nAbs were classified as extremely potent nAbs, showing an IC_{100} lower than 10 ng/mL (Figure 2C; Figure S2B; Table S4).

SARS-CoV-2 neutralizing antibodies can be classified into four groups

Based on the first round of screening, 14 nAbs were selected for further characterization. All nAbs were able to bind the SARS-CoV-2 S protein in its trimeric conformation (Figure 3A). The mAbs named J08, I14, F05, G12, C14, B07, I21, J13, and D14 were also able to specifically bind the S1 domain (Figure 3B). The nAbs named H20, I15, F10, and F20 were not able to bind single S1 or S2 domains but only the Sprotein in its trimeric state, while the nAb L19 bound only the S2 subunit (Figures 3B and 3C). Among the group of S1-specific nAbs, only J08, I14, F05, G12, C14, and B07 were able to bind the S1 RBD and to strongly inhibit the interaction between the S protein and Vero E6 receptors, showing a half maximal effective concentration (EC_{50}) at the

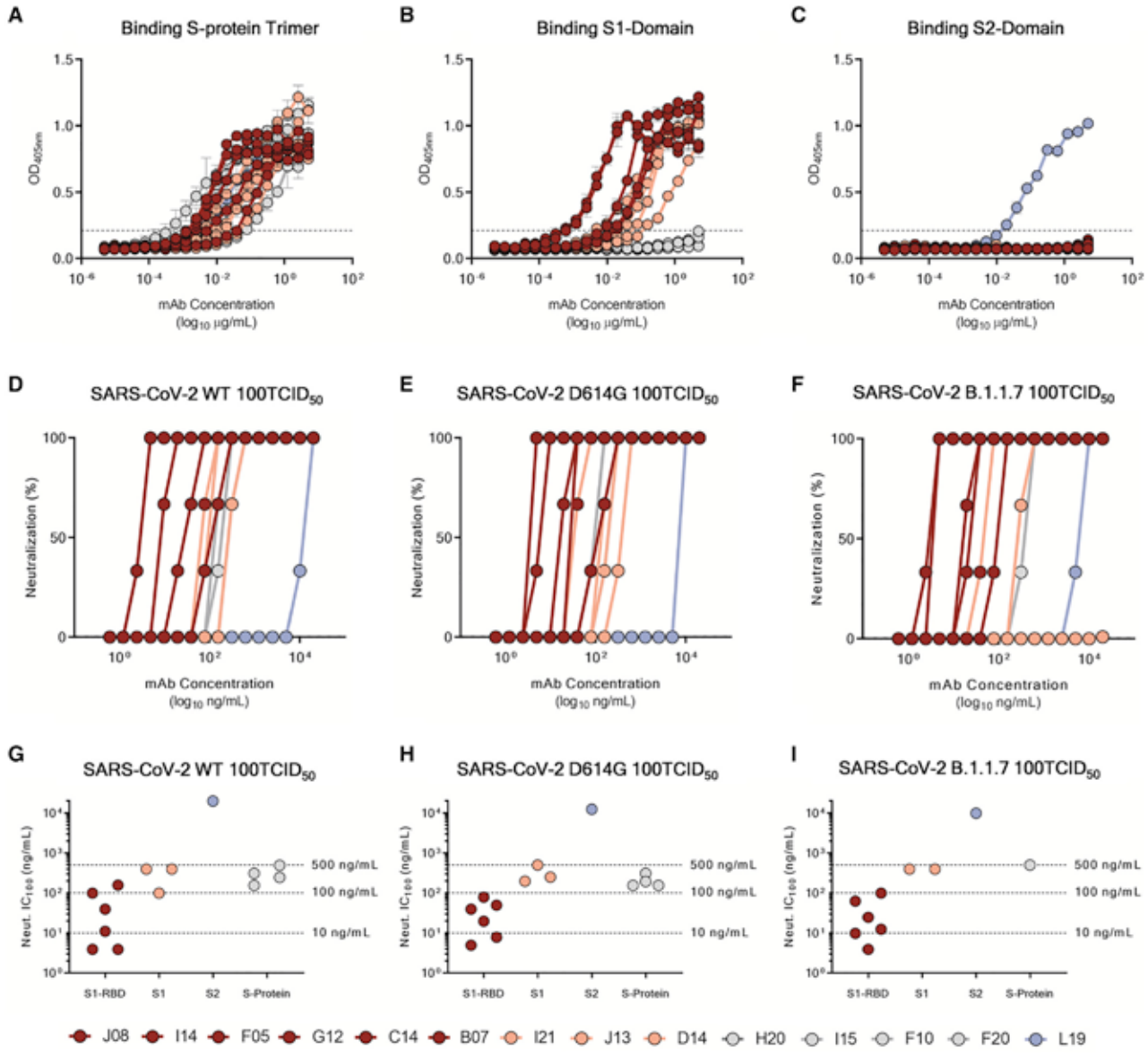

Figure 3. Functional characterization of potent SARS-CoV-2 S protein-specific nAbs

(A–C) Graphs show binding curves to the S protein in its trimeric conformation, S1 domain, and S2 domain. Mean ± SD of technical triplicates are shown. Dashed lines represent the threshold of positivity.

(D–F) Neutralization curves for selected antibodies were shown as percentage of viral neutralization against the authentic SARS-CoV-2 wild type (D), D614G variant (E), and the emerging variant B.1.1.7 (F). Data are representative of technical triplicates. A neutralizing COVID-19 convalescent plasma and an unrelated plasma were used as positive and negative control, respectively.

(G–I) Neutralization potency of 14 selected antibodies against the authentic SARS-CoV-2 wild type (G), D614G variant (H), and the emerging variant B.1.1.7 (I). Dashed lines show different ranges of neutralization potency (500, 100, and 10 ng/mL). In all graphs, selected antibodies are shown in dark red, pink, gray, and light blue based on their ability to recognize the SARS-CoV-2 S1 RBD, S1 domain, S protein trimer only, and S2 domain, respectively.

NoB assay of 78.6, 15.6, and 68.5 ng/mL for J08-MUT, I14-MUT, and F05-MUT, respectively (Figures S3A and S3B). On the other hand, I21, J13, and D14, despite showing S1 binding specificity, did not show any binding to the RBD and NoB activity (Figure S3A). Based on this description, four different groups of nAbs against SARS-CoV-2 were identified. The first group (Group I) is composed of S1 RBD-specific nAbs (J08, I14, F05, G12, C14, and B07), which showed neutralization potency against the authentic wild type (WT), the D614G variant, and the emerging variant recently isolated in the UK B.1.1.7. S1 RBD-specific nAbs showing a neutralizing potency ranging from 3.9 to 157.5 ng/mL (Figures 3D–3I; Table S5) and picomolar affinity to the S protein with an equilibrium dissociation constant (KD) ranging from 0.2 to 4.6 E^{-10}M (Figure S4). In addition to the

D614G and the B.1.1.7 variants, the S1 RBD-specific nAb J08 showed also to neutralize SARS-CoV-2 variants containing the E484K mutation (Andreano et al., 2020). The second group (Group II) included S1-specific nAbs that did not bind the RBD (I21, J13, and D14). These antibodies also showed good neutralization potency ranging from 99.2 to 500.0 ng/mL (Figures 3D–3I; Table S5) but inferior to that of S1 RBD-directed nAbs. One antibody from this group was not able to neutralize the B.1.1.7 variant (I21). The third group (Group III) is composed of antibodies able to bind the S-protein only in its whole trimeric conformation (H20, I15, F10, and F20). Antibodies belonging to this group showed lower affinity to the S protein trimer (KD 64.0 E^{-10}M–757.0 E^{-10}M) compared to Group I nAbs and medium neutralization potencies ranging from 155.0 to 492.2 ng/mL against the authentic WT and D614G (Figures 3D–3I; Figure S4; Table S5). On the other hand, only one S protein-specific nAb (D21) showed moderate neutralization activity against the B.1.1.7 with an IC_{100} of 500.0 ng/mL. Three S protein-specific nAbs (I15, F10, and F20) did not show any functional activity against this latter variant (Figures 3D–3I; Table S5). The fourth and final group (Group IV) is composed of antibodies that exclusively recognized the S2 domain. Different antibodies with similar properties were identified for Group IV, but only the nAb L19 is shown. The Group IV nAb L19 shows the lowest neutralization potency with 19.8 μg/mL for the authentic WT, 12.5 μg/mL against the D614G, and 9.9 μg/mL against the B.1.1.7 variant (Figures 3D–3I; Table S5).

All the antibodies described above were also tested for their ability to cross-neutralize other human coronavirus strains. nAbs were tested against lentiviral pseudotypes expressing the SARS-CoV-2, SARS-CoV-2 D614G, SARS-CoV, and Middle East respiratory syndrome (MERS)-CoV S protein on their viral membrane surface. Neutralization activity was shown against SARS-CoV-2 and D614G pseudotypes, therefore confirming previous data. None of the antibodies reported here were able to cross-neutralize other coronavirus species (Figure S5).

Different pathogen vulnerability regions identified on the S protein

The fourteen selected nAbs were further characterized by a competition assay that allowed speculation on the S protein regions recognized by these antibodies. Briefly, beads were coated with SARS-CoV-2 trimeric S protein and incubated with a primary unlabeled antibody in order to saturate the binding site on the antigen surface. Following the first incubation step, a secondary Alexa-647-labeled antibody was incubated with the antigen/unlabeled-mAb complex. If the secondary labeled antibody did not recognize the same epitope as the primary unlabeled mAb, a fluorescent signal would be detected when tested by flow cytometry. Through this assay, we observed that all Group I nAbs competed among themselves for binding to the S protein RBD, indicating that these antibodies possibly clash against each other and recognize a similar epitope region. All Group II nAbs showed different competition profiles and competed with Group II and Group III nAbs. These results confirmed that Group III antibodies can recognize various regions on the S protein surface as they compete with themselves as well as with antibodies belonging to Group II. Interestingly, nAbs belonging to Group II also competed with the B07 RBD-directed antibody, thereby suggesting that this latter nAb may have a different binding orientation compared to other nAbs included in the Group I. Finally, the Group IV nAb L19 did not compete with any of the other groups identified in this study, suggesting that this class of nAbs recognizes a distant epitope region as compared to Group I, II, and III nAbs (Figures 4A and 4B)

Genetic characterization of SARS-CoV-2 nAbs

The genes encoding the HCs and LCs of the 14 selected nAbs were sequenced, and their IGHV and IGKV genes were compared with publicly available SARS-CoV-2 neutralizing antibody sequences (Figures 5A and 5B). Four nAbs used one of the most predominant HC V genes for SARS-CoV-2 nAbs (IGHV1-69), while three nAbs used one of the least representative HCV genes (IGHV1-24). Two other nAbs employed the most common germline observed for SARS-CoV-2 nAbs, which is IGHV3-53 (Figure 5A) (Yuan et al., 2020). Interestingly, while IGHV1-69 and IGHV1-24 accommodate IGHJ diversity, nAbs belonging to the IGHV3-53 gene family only showed recombination with the IGHJ6 gene (Table S6). The HC V genes somatic hypermutation level and complementary determining region 3 (H-CDR3) length were also evaluated. Our selected nAbs displayed a low level of somatic mutations when compared to the inferred germlines with sequence identities ranging from 95.6% to 99.3% (Figure 5C left panel; Table S6), confirming what was observed in previous publications (Pinto et al., 2020; Zost et al., 2020b; Rogers et al., 2020; Griffin et al., 2020). The H-CDR3 length spanned from 7 to 21 amino acids (aa) with the majority of the antibodies (n = 6; 42.0%) having a length of 14 to 16 aa that is slightly bigger than previously observed (Figure 5C right panel; Table S6). All of our nAbs used the κ chain, and the majority of them used the common genes IGKV1-9 and IGKV3-11 (n = 6; 42.0%) (Figure 5B; Table S6). The level of IGKV somatic hypermutation was extremely low for LCs showing a percentage of sequence identities ranging from 94.3% to 98.9% (Figure 5D left panel; Table S6). The LC CDR3 (L-CDR3) lengths were ranging from 5 to 10 aa, which is in line with what was previously observed for SARS-CoV-2 nAbs (Figure 5D right panel; Table S6). When paired HC and LC gene analysis was performed, IGHV1-69-derived nAbs were found to rearrange exclusively with IGKV3 gene family, whereas IGHV1-24-derived nAbs accommodate LC diversity (Table S6). Of note, some of our candidates showed unique HC and LC pairing when compared to the public SARS-CoV-2 nAb repertoire. Particularly, five different HC and LC rearrangements not previously described for nAbs against SARS-CoV-2 were identified. These included the IGHV1-24;IGKV1-9, IGHV1-24;IGKV3-15, IGHV1-46;IGKV1-16, IGHV3-30;IGKV1-9, and IGHV3-53;IGKV1-17 (Figure 5E).

Fc engineering of candidate nAbs to abrogate Fc receptor binding and extend half-life

ADE of disease is a potential clinical risk following coronavirus infection (Lee et al., 2020). Therefore, to optimize the suitability for clinical development and reduce the risk of ADE, five different point mutations were introduced in the constant region (Fc) of the three most potent nAbs (J08, I14, and F05), which were renamed

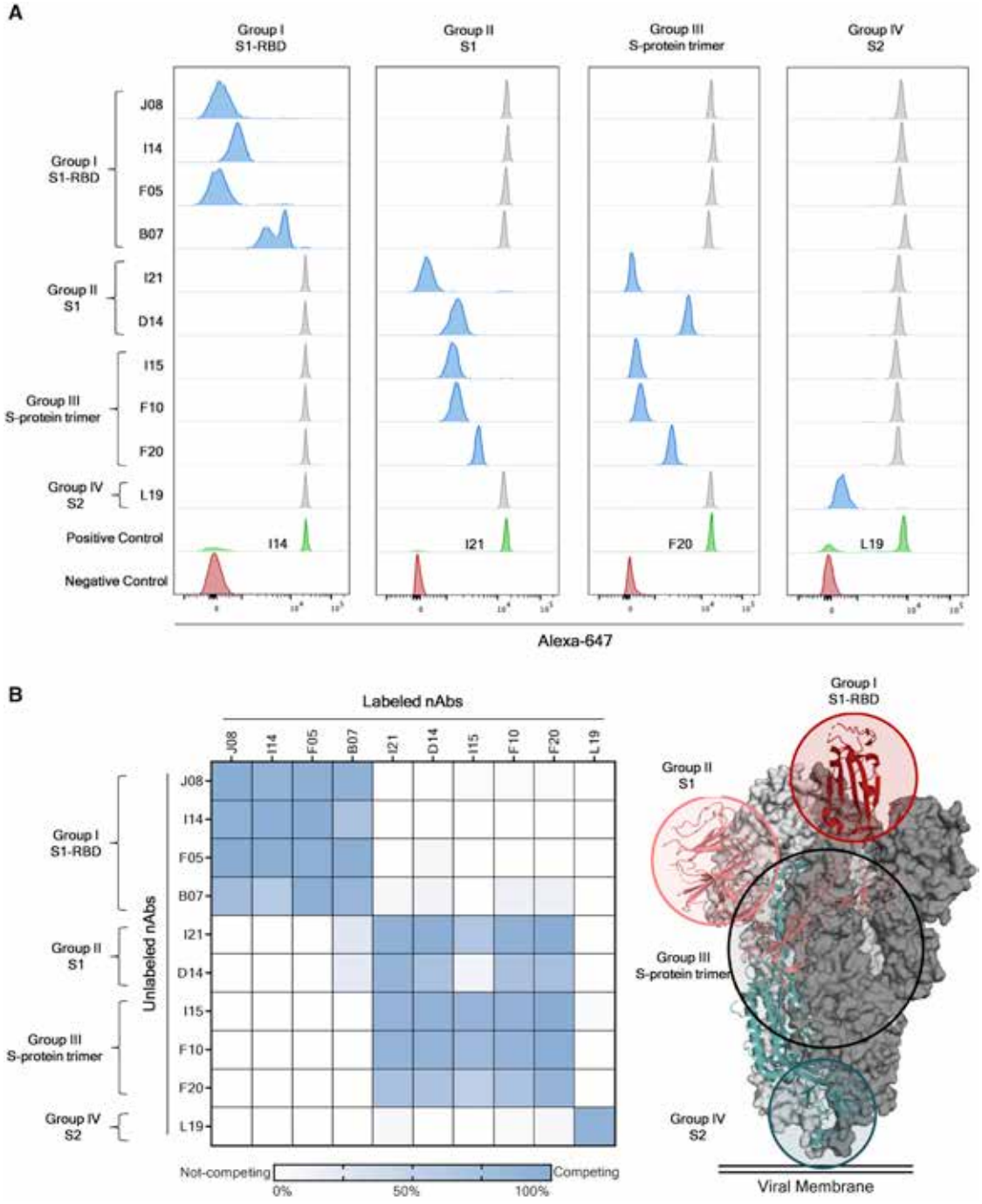

Figure 4. Identification of four different sites of pathogen vulnerability on the S protein surface

(A) Representative cytometer peaks per each of the four antibody groups are shown. Positive (beads conjugated with only primary labeled antibody) and negative (un-conjugated beads) controls are shown as green and red peaks, respectively. Competing and not-competing nAbs are shown in blue and gray peaks, respectively.

(B) The heatmap shows the competition matrix observed among the 14 nAbs tested. Threshold of competition was set at 50% of fluorescent signal reduction. A speculative representation of the vulnerability sites is shown on the S protein surface.

J08-MUT, I14-MUT, and F05-MUT. The first two point mutations (M428L and N434S) were introduced to enhance antibody half-life and to increase tissue distribution and persistence (Zalevsky et al., 2010; Gaudinski et al., 2018; Pegu et al., 2017). The remaining three point mutations (L234A, L235A, and P329G) were introduced to reduce antibody dependent

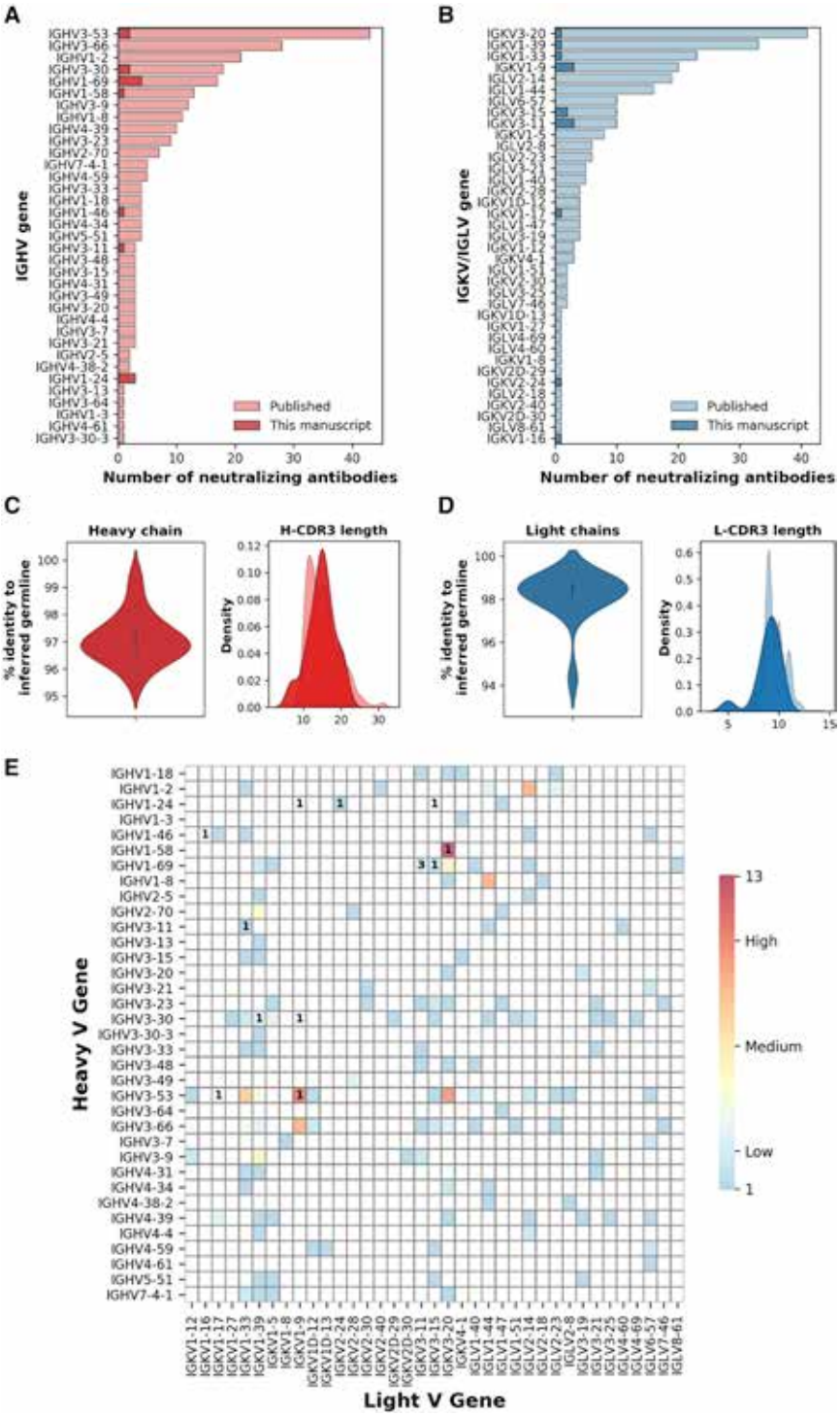

Figure 5. Heavy and light chain analyses of selected nAbs

(A and B) Bar graphs show the heavy and light chains usage for neutralizing antibodies against SARS-CoV-2 in the public repertoire compared to the antibodies identified in this study. Our and public antibodies are shown in dark and light colors, respectively.

(C and D) The heavy and light chain percentage of identity to the inferred germline and amino acidic CDR3 length are shown as violin and distribution plot, respectively.

(E) The heatmap shows the frequency of heavy and light chain pairing for SARS-CoV-2 neutralizing human mAbs already published. The number within the heatmap cells represent the amount of nAbs described in this manuscript showing already published (colored cells) or novel heavy and light chain rearrangements (blank cells).

functions such as binding to FcγRs and cell-based activities (Schlothauer et al., 2016).

To confirm the lack of FcγR binding as well as the extended half-life, a beads-based Luminex assay was performed. Briefly the beads were coated with SARS-CoV-2 S protein RBD. Antibodies were tested at eight-point dilutions, and the binding was detected with FcγR2A and neonatal Fc receptor (FcRn) at pH6.2 and 7.4. The FcγR2A was selected as it is predominantly expressed on the surface of phagocytic cells (such as monocytes, macrophages, and neutrophils) and is associated with phagocytosis of immune complexes and antibody-opsonized targets (Ackerman et al., 2013). On the other hand, FcRn, which is highly expressed on endothelial cells and circulating monocytes, was selected as it is responsible for the recycling and serum half-life of IgG in the circulation (Mackness et al., 2019). This latter receptor was shown to possess a tighter binding at lower pH (e.g., pH 6.2) compared to a physiological pH (e.g., pH 7.4) (Booth et al., 2018). Results shown in Figure S6 demonstrate that binding to the FcγR2A was completely abrogated for the mutated version of candidate nAbs (J08-MUT, I14-MUT, and F05-MUT) compared to their respective WT versions (J08, I14, and F05) and controls (CR3022 and unrelated protein) (Figure S6A). Furthermore, Fc-engineered antibodies showed increased binding activity to the FcRn at both pH 6.2 and 7.4 compared to their WT counterpart (Figures S6B and S6C). Finally, to evaluate the lack of Fc-mediated cellular activities by our three candidate nAbs, the antibody-dependent neutrophil phagocytosis (ADNP) and antibody-dependent natural killer (ADNK) cell activations were evaluated (Butler et al., 2019; Ackerman et al., 2016; Karsten et al., 2019; Boudreau et al., 2020). For the ADNP assay, primary human neutrophils were used to detect antibody binding to SARS-CoV-2 S protein RBD-coated beads, while ADNK

activity was evaluated by using primary human NK cells and detecting the release of the proinflammatory cytokine interferon gamma (IFN-γ). Complete abrogation of both ADNP and ADNK was observed for all three Fc-engineered candidate nAbs compared to their WT versions and control antibody (CR3022), thus confirming the lack of Fc-mediated cellular activities (Figures S6D and S6E).

Potency and autoreactivity evaluation of Fc-engineered candidates

The three engineered antibodies were tested to confirm their binding specificity and neutralization potency against both the WT, the widespread SARS-CoV-2 D614G mutant and the emerging variant B.1.1.7 (Korber et al., 2020, CDC, 2021) to evaluate their cross-neutralization ability. The three engineered nAbs maintained their S1 domain binding specificity and extremely high neutralization potency with J08-MUT and F05-MUT being able to neutralize both the WT and the D614G variant with an IC_{100} lower than 10 ng/mL (both at 3.9 ng/mL for the WT and the D614G strains) (Figure S6F – K; Table S5). The antibody J08-MUT also showed extreme neutralization potency against emerging variants as it was able to neutralize the B.1.1.7 with an identical IC_{100} compared to the WT virus (Figure S6K; Table S5) and has also showed to neutralize variants that include the E484K mutation (Andreano et al., 2020).

Since it has been reported that SARS-CoV-2 elicited antibodies that can cross-react with human tissues, cytokines, phospholipids, and phospholipid-binding proteins (Zuo et al., 2020; Bastard et al., 2020; Kreer et al., 2020), the three candidate mAbs in both their WT and MUT versions were tested through an indirect immunofluorescent assay against human epithelial type 2 (HEp-2) cells, which expose clinically relevant proteins to detect autoantibody activities (Figure S7A). As reported in Figure S7B, the positive control presents a different range of detectable signals based on the initial dilution steps (from bright green at 1:1 to very dim green at 1:100). Among all samples tested, only F05 showed moderate level of autoreactivity to human cells, while no signal could be measured for the other antibodies (Figure S7B).

Structural analyses of candidate nAbs

Single-particle negative-stain electron microscopy (nsEM) was used to visualize a stabilized SARS-2-CoV-6P-Mut7 S protein in complex with three separate Fabs: J08, I14, and F05. This recombinant, soluble S protein primarily exhibits 3 RBD's "down" but can switch to RBD "up" conformation with antibody bound. Inspection of the 2D class averages revealed a mixed stoichiometry of unbound S protein, one Fab bound, and two Fab bound classes, which allowed for 3D refinements of each (Figure 6A). The three different Fabs bind to the RBD in the "up" conformation, although at different angles and rotations, likely due to the flexibility of the RBD. Model docking of PDB 7BYR (one RBD "up" bound to antibody) shows that the fabs overlap with the receptor-binding motif (RBM) and therefore are positioned to sterically block receptor hACE2 engagement (Figure 6B). To determine the epitope, HC and LC sequences of Fabs J08, I14, and F05 were used to create synthetic models for docking into the nsEM maps. Based on the docking, we predicted that a loop containing residues 477 to 489 (STPCNGVEGFNCY) appeared to be involved in the binding specifically with residue F486 extending into a cavity that is in the middle of the HC and LC of each antibody.

J08-MUT prevents SARS-CoV-2 infection in the golden Syrian hamster

The golden Syrian hamster model has been widely used to assess monoclonal antibody prophylactic and therapeutic activities against SARS-CoV-2 infection. This model has shown to manifest severe forms of SARS-CoV-2 infection mimicking more closely the clinical disease observed in humans (Baum et al., 2020; Imai et al., 2020; Rogers et al., 2020; Sia et al., 2020). We designed a prophylactic study in golden Syrian hamster to evaluate the efficacy of J08-MUT in preventing SARS-CoV-2 infection. For this study, 30 hamsters were divided into five arms (six animals each), which received, J08-MUT at 4, 1, and 0.25 mg/kg via intraperitoneal injection. Placebo and IgG1 isotype control groups were included in the study, which received a saline solution and an anti-influenza antibody at the concentration of 4 mg/kg, respectively. The J08-MUT at 4 mg/kg group and the 1 and 0.25 mg/kg groups were tested in two independent experiments. The IgG1 isotype control group was tested in parallel with the J08-MUT 4 mg/kg group, whereas the placebo is an average of the two experiments. Animals were challenged with 100 μL of SARS-CoV-2 solution (5×10^5 plaque-forming units [PFU]) via intranasal distillation 24 h post-administration of the antibody. Three hamsters per group were sacrificed at 3 days post infection, while the remaining animals were culled at day 8 (Figure 7A). Body weight change was evaluated daily and considered as a proxy for disease severity. Animals in the control group and those that received the IgG1 isotype antibody lost more than 5% of their original body weight from day 1 to day 6 and then stabilized. These data are in line with previously published data of SARS-CoV-2 infection in a golden Syrian hamster model (Kreye et al., 2020; Liu et al., 2020). In marked contrast, in the prophylactic study, all animals that received J08-MUT were significantly protected from weight loss. Protection was present at all J08-MUT concentrations and was dose dependent (Figure 7B). When J08-MUT was administered at 4 mg/kg, we observed protection from SARS-CoV-2 infection and only a minimal weight loss (average −1.8% of body weight) was noticed 1 day post viral challenge. A higher body weight loss was observed 1 day post infection in hamsters that received J08-MUT at 1 mg/kg (from −1.8% to −3.3%) and 0.25 mg/kg (from −1.8% to −4.7%). In the J08-MUT 4 mg/kg group, all animals quickly recovered and reached their initial weight by day 3. From day 4 on all hamsters gained weight increasing up to 5% from their initial body weight. Hamsters that received the 1 and 0.25 mg/kg dosages completely recovered their initial body weight at day 6 and 8, respectively. Hamsters in the control groups did not recover their initial body weight and at day 8, still showed around 5% of weight loss (Figure 7B). The prophylactic activity of J08-MUT was also reflected in the complete absence of viral titer in the lung tissue at 3 days post infection in all hamsters that received J08-MUT at 4 and 1 mg/kg and also in two out of three hamsters that received J08-MUT at 0.25 mg/kg. On the other hand, hamsters that

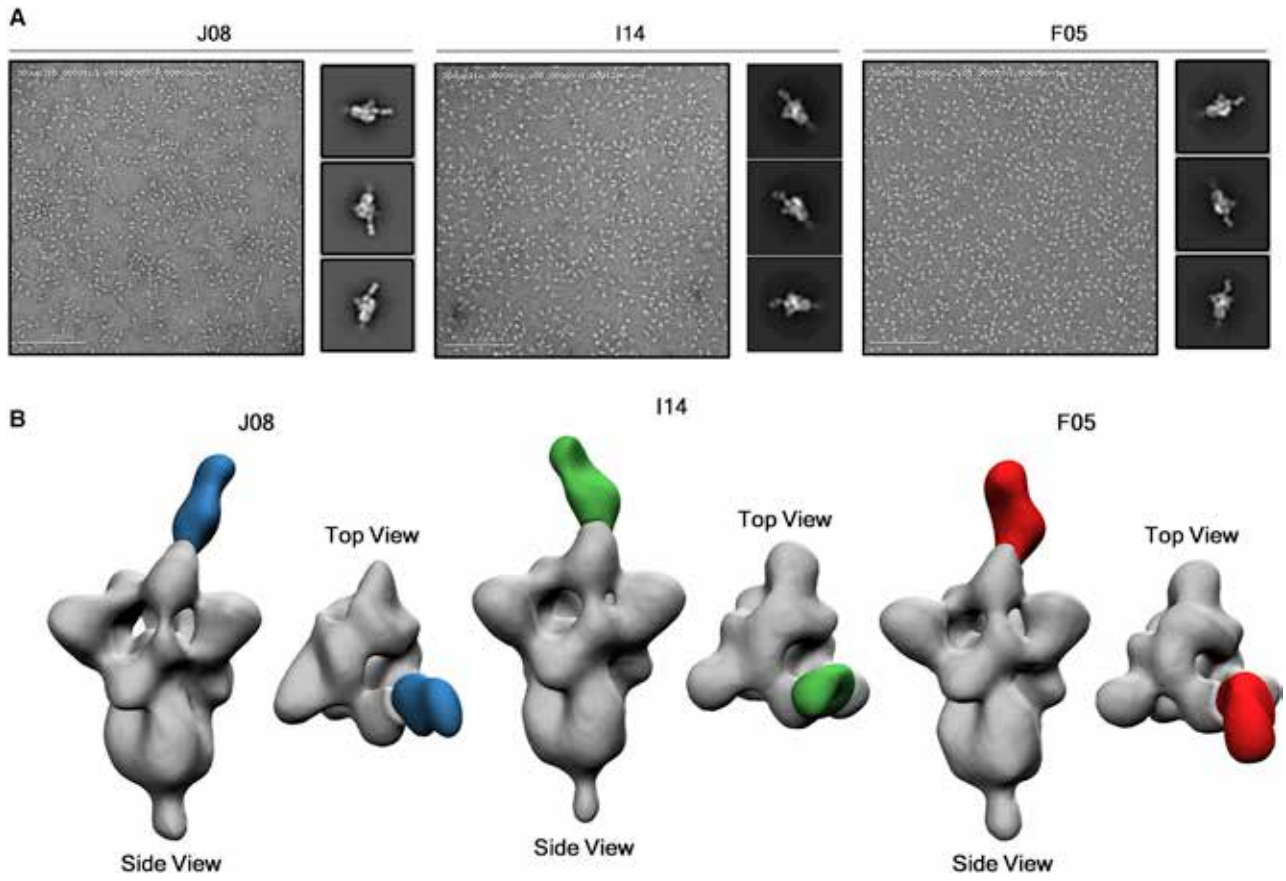

Figure 6. EM epitope mapping of RBD mAbs

(A) Negative stain for J08, I14, and F05 in complex with the S protein. 200 nm scale bar is shown.

(B) Figures show the binding of J08 (blue), I14 (green), and F05 (red) to the SARS-CoV-2 S protein RBD.

received the IgG1 isotype control or in the placebo group showed a significantly higher viral titer (Figure 7D).

Finally, we performed an ELISA assay to detect the presence of human IgG in hamster sera. All samples that received J08-MUT or the IgG1 isotype control showed detectable human IgGs in the sera in a dose-dependent fashion, while no human IgGs were detected in the placebo group (Figures 7E and 7F). Human IgGs were detected at 3 and up to 7 days post infection (Figures 7E and 7F).

J08-MUT therapy of SARS-CoV-2 infection in the golden Syrian hamster

For the therapeutic study, three groups of six animals each were used to evaluate the ability of J08-MUT to treat SARS-CoV-2 infection in the golden Syrian hamster model. One group received J08-MUT via intraperitoneal injection at 4 mg/kg, and the other two groups received placebo and 4mg/kg IgG1 isotype control, respectively. The experiment was performed in parallel with the initial prophylactic study where J08-MUT was administered at 4 mg/kg and the two control groups. Animals were challenged with 100 μL of SARS-CoV-2 solution (5×10^5 PFU) via intranasal distillation 24 h prior to the administration of the antibody. Three hamsters per group were sacrificed at 3 days post infection while the remaining animals were culled at day 12 (Figure 7A). Despite J08-MUT and control groups showed a similar trend in weight loss in the first 4 days post infection, the treatment group showed a significantly quicker weight recovery (Figure 7C). At day 12, only hamsters that received J08-MUT recovered the initial body weight (Figure 7C). When we analyzed the viral titer in lung tissues, we observed complete absence of the virus at day 3 in all the hamsters treated with J08-MUT at 4 mg/kg, while animals that received the IgG1 isotype control or in the placebo group showed a significantly higher viral titer (Figure 7G). To evaluate the presence of human antibodies in hamster sera, we performed an ELISA assay. All samples that received J08-MUT or the IgG1 isotype control showed detectable human IgGs in the sera in a dose-dependent fashion, while no human IgGs were detected in the placebo group (Figures 7H and 7I). Human IgGs were detected at 3 and up to 11 days post infection (Figures 7H and 7I).

DISCUSSION

This work describes a systematic screening of memory B cells from SARS-CoV-2 convalescent patients to identify extremely potent mAbs against SARS-CoV-2 and their engineering to

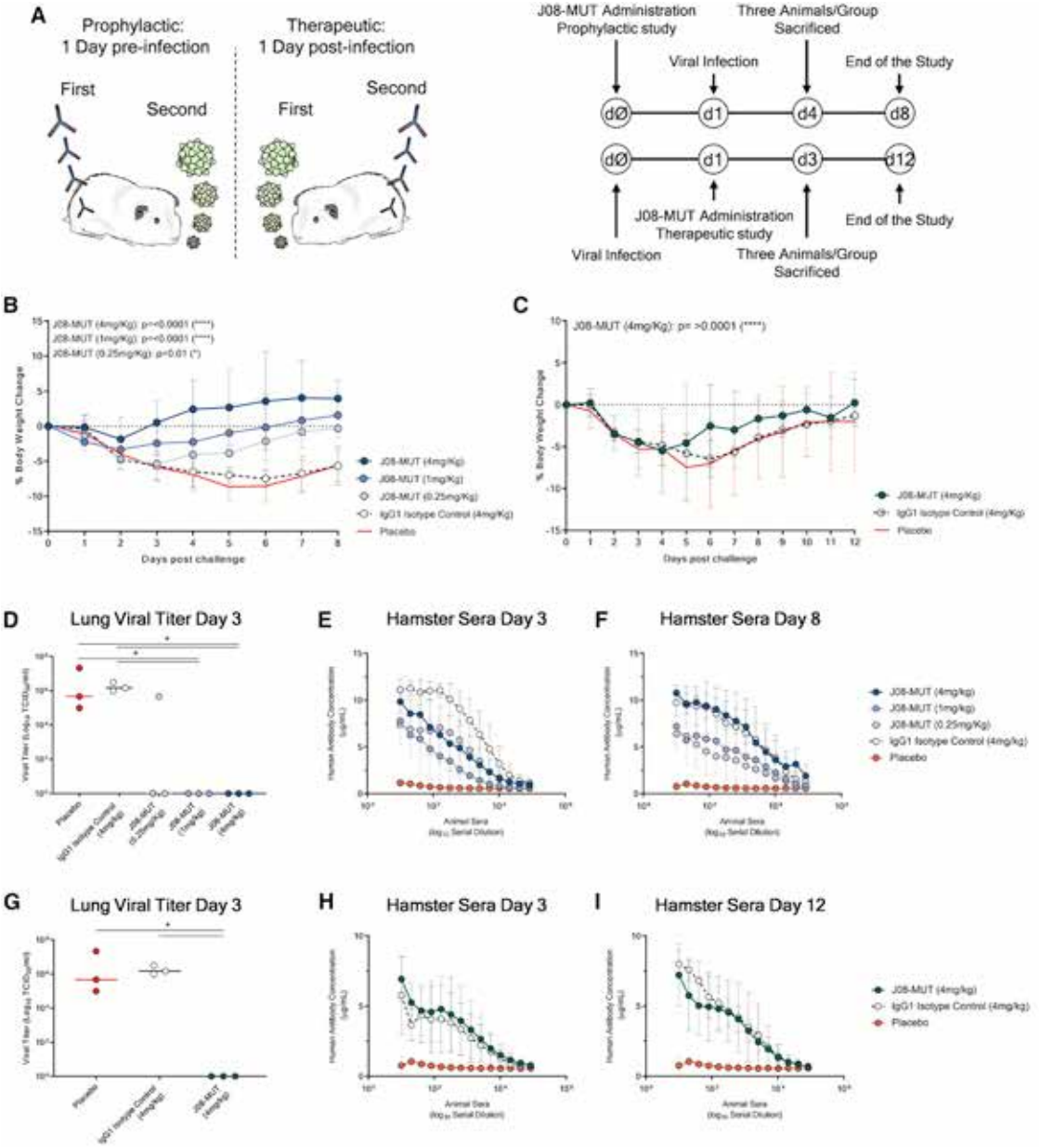

Figure 7. Prophylactic and therapeutic efficacy of J08-MUT in the golden Syrian hamster model of SARS-CoV-2 infection

(A) Schematic representation and timelines of prophylactic and therapeutic studies performed in golden Syrian hamster.

(B and C) The figure shows the prophylactic impact of J08-MUT at three different concentrations (4, 1, and 0.25 mg/kg) (B) on body weight loss change (C). The figure shows the therapeutic impact of J08-MUT at 4 mg/kg on body weight loss change. Mean ± SD are denoted in the graphs.

(D–F) The figures show the lung viral titer at day 3 (D) and the detection of human antibodies in hamster sera at day 3 (E) and day 8 (F) in the prophylactic study. Mean ± SD of technical triplicates are shown.

(G–I) The figures show the lung viral titer at day 3 (G) and the detection of human antibodies in hamster sera at day 3 (H) and day 12 (I) in the therapeutic study. Mean ± SD of technical triplicates are shown. Statistical differences were calculated with two-way analysis of variance (ANOVA) for body weight change and with a nonparametric Mann–Whitney t test for the lung viral titer. Significances are shown as *$p < 0.05$, **$p < 0.01$, ***$p < 0.001$, and ****$p < 0.0001$.

extend half-life and eliminate the potential risk of ADE. The best antibody neutralized the authentic WT virus and emerging variants at pico molar concentration *in vitro* and showed prophylactic and therapeutic efficacy in a SARS-CoV-2 hamsters model of infection when used at 0.25 and 4 mg/kg, respectively. The antibody described is a promising candidate for the development of a broadly affordable tool for prevention and therapy of COVID-19.

In the search for potent antibodies, we found that approximately 10% of the total B cells against the S protein isolated

produce neutralizing antibodies, and these can be divided into four different groups recognizing the S1 RBD, S1 domain, S2 domain, and the S protein trimer. Most potently neutralizing antibodies are extremely rare and recognize the RBD, followed in potency by antibodies recognizing the S1 domain, the trimeric structure and the S2 subunit. From these data we can conclude that in COVID-19 convalescent patients, most of the observed neutralization titers are likely mediated by antibodies with medium-high neutralizing potency. Indeed, the extremely potent antibodies and the antibodies against the S2 subunit are unlikely to contribute to the overall neutralizing titers because they are respectively too rare and too poor neutralizers to be able to make a difference. We and others found that the antibody repertoire of convalescent patients is mostly germline-like. This may be a consequence of the loss of Bcl-6-expressing follicular helper T cells and the loss of germinal centers in COVID-19 patients, which may limit and constrain the B cell affinity maturation (Kaneko et al., 2020). It will be therefore important to perform similar studies following vaccination as it is likely that the repertoire of neutralizing antibodies induced by vaccination may be different from the one described here.

Out of the 453 neutralizing antibodies that were tested and characterized, one antibody (J08) showed extremely high neutralization potency against both the WT SARS-CoV-2 virus isolated in Wuhan and emerging variants containing the D614G, E484K, and N501Y variants. During the last few months, several groups reported the identification, 3D structure and passive protection in animal models of neutralizing antibodies against SARS-CoV-2. Most of these studies, with few exceptions, reported antibodies that require from 20 to several hundred ng/mL to neutralize 50% of the virus *in vitro*. While these antibodies are potentially good for therapy, they will require a high dosage, which is associated with elevated cost of goods, low production capacity, and delivery by intravenous infusion.

The extremely potent mAb described in our study is likely to allow the use of lower quantities of antibodies to reach prophylactic and therapeutic efficacy and as a consequence, decrease the cost of goods and enable sustainable development and manufacturability. This solution may increase the number of doses produced annually and therefore increase antibodies availability in high-income countries as well as low-and middle-income countries. Therefore, our antibodies have the potential to meet the expectations of the call to action to expand access to mAb-based products, recently published by the Wellcome Trust and supported by the WHO and the Coalition for Epidemic Preparedness Innovations (Wellcome and IAVI, 2020).

A potential issue associated with the use of human mAbs against viral pathogens is the potential selection of escape mutants. This is usually addressed by using a combination of antibodies directed against non-overlapping epitopes. While this is an ultimate clear solution, it increases the complexity of development, costs of production, drug availability, and affordability. In our case, we believe that selection of escape mutants upon treatment with a single mAb may be quite difficult as the SARS-CoV-2 RNA-dependent polymerase possesses a proofreading machinery (Romano et al., 2020), and the epitope recognized by the antibodies herein described overlaps with the region necessary to bind the hACE2 receptor. In this regard, it took more than 70 days of continuous co-culture of the virus in presence of the antibodies before we were able to detect the first emergence of escape mutants of the WT SARS-CoV-2 (data not shown).

Finally, a peculiar part of our approach consisted in depleting possible antibody Fc-mediated functions of the antibodies to avoid the risk of ADE. While there is no evidence of ADE in SARS-CoV-2, and most vaccines and mAbs tested so far seem to be safe, it is too early to make definitive conclusions. In addition, two recently published reports suggested that we need to continue to monitor the potential risk of ADE. The first report showed that severe SARS-CoV-2 patients are characterized by an increased proinflammatory signature mediated by the Fcγ receptors triggered by afucosylated IgG1 antibodies (Chakraborty et al., 2020). The second report described that one antibody was associated with worse clinical outcomes when administered to hospitalized patients requiring high-flow oxygen or mechanical ventilation (Lilly, 2020). Therefore, we believe it is important to develop and test antibodies where Fc-mediated functions have been eliminated in the clinical practice. Since the Fc portion contributes significantly to the *in vivo* potency of the antibodies (Schäfer et al., 2020), removing Fc functions may be a problem for mAbs with low neutralization potency because they may no longer be effective when tested in clinical settings, as already described in other contexts (DiLillo et al., 2014). The extremely high potency shown by our antibodies allowed us to remove Fc functions while maintaining *in vivo* potency at minimal dosage.

Limitations of the study

While we believe that our antibodies are extremely potent when compared to most of those described in literature, we acknowledge that in most cases, direct comparison was not performed, and we rely on published data.

The second limitation of the study is that *in vitro* neutralization and *in vivo* protection in the SARS-CoV-2 hamster model of infection cannot be fully predictive of the behavior of the same antibody in humans, and therefore the real benefit of described antibodies can only be assessed in clinical studies.

STAR★METHODS

Detailed methods are provided in the online version of this paper and include the following:

- KEY RESOURCES TABLE
- RESOURCE AVAILABILITY
  - Lead contact
  - Materials availability
  - Data and code availability
- EXPERIMENTAL MODEL AND SUBJECT DETAILS
  - Enrollment of SARS-COV-2 convalescent donors and human sample collection
- METHOD DETAILS
  - Single cell sorting of SARS-CoV-2 S-protein$^+$ memory B cells from COVID-19 convalescent donors
  - Expression and purification of SARS-CoV-2 S-protein prefusion trimer and receptor binding domain

- ELISA assay with S1 and S2 subunits of SARS-CoV-2 S-protein
- ELISA assay with SARS-CoV-2 S-protein prefusion trimer and S1 – S2 subunits
- SARS-CoV-2 virus and cell infection
- Neutralization of Binding (NoB) Assay
- Single cell RT-PCR and Ig gene amplification
- Cloning of variable region genes and recombinant antibody expression in transcriptionally active PCR
- Flask expression and purification of human monoclonal antibodies
- Viral propagation and titration
- SARS-CoV-2 authentic virus neutralization assay
- Production and titration of SARS-CoV-2 pseudotyped lentiviral reporter particles
- SARS-CoV-2 pseudotyped lentivirus neutralization assay
- Characterization of SARS-CoV-2 RBD-Antibodies binding by Flow cytometry
- Flow Cytometry-Based S-protein Competition assay
- Antigen-specific FcγR binding
- Antibody-dependent neutrophil phagocytosis
- Antibody-dependent NK cell activation
- Affinity evaluation of SARS-CoV-2 neutralizing antibodies
- Autoreactivity screening test on HEp-2 Cells
- Genetic Analyses of SARS-CoV-2 S-protein specific nAbs
- Negative-stain electron microscopy
- Prophylactic and therapeutic passive transfer studies in golden Syrian hamsters
- Determination of viral load by $TCID_{50}$ assay
- Human IgG detection in hamster sera

SUPPLEMENTAL INFORMATION

Supplemental Information can be found online at https://doi.org/10.1016/j.cell.2021.02.035.

ACKNOWLEDGMENTS

We wish to thank Fondazione Toscana Life Sciences in the persons of Dr. Fabrizio Landi and Dr. Andrea Paolini and the whole Administration for their help and support. In particular, we would like to thank Mr. Francesco Senatore, Mrs. Laura Canavacci, and Mrs. Cinzia Giordano for their support in preparing all the documents needed for the ethical approval of the clinical studies carried out within this project. We wish to thank the National Institute for Infectious Diseases, IRCCS, Lazzaro Spallanzani Rome (IT), and the Azienda Ospedaliera Universitaria Senese, Siena (IT) for providing blood samples from COVID-19 convalescent donors under studies approved by local ethic committees. We also wish to thank all the nursing staff who chose to cooperate for blood withdrawal and all the donors who decided to participate in this study. We would like to thank the whole GSK Vaccines Pre-clinical Evidence Generation and Assay – Immunolgy function led by Dr. Oretta Finco for their availability and support as well as Mrs. Simona Tavarini, Mrs. Chiara Sammicheli, Dr. Monia Bardelli, Dr. Michela Brazzoli, Dr. Elisabetta Frigimelica, Dr. Erica Borgogni, and Dr. Elisa Faenzi for sharing their expertise, extreme availability, and technical support. We would also like to thank Dr. Mariagrazia Pizza and Dr. Simone Pecetta for initial insightful advice and discussions on this project. We would like to thank Dr. Jason McLellan and his team for generously providing the SARS-CoV-2 S protein stabilized in its prefusion conformation used in this study. Furthermore, we would like to thank Dr. Daniel Wrapp and Dr. Nianshuang Wang for the precious information and suggestions. The authors wish to thank Seromyx for their support in assessing the functionality of the antibodies Fc portion. The authors would like to thank the University of Georgia Animal Resource staff, technicians, and veterinarians for animal care as well as the staff of the University of Georgia AHRC BSL-3 facility for providing biosafety and animal care. The following reagent was deposited by the Centers for Disease Control and Prevention and obtained through BEI Resources, NIAID, NIH: SARS-Related Coronavirus 2 Isolate USA-WA1/2020, NR-52281. This work was funded by the European Research Council (ERC) advanced grant agreement no. 787552 (vAMRes). The Laboratory is also supported by the Wellcome Trust. This publication was supported by funds from the "Centro Regionale Medicina di Precisione" and by all the people who answered the call to fight with us the battle against SARS-CoV-2 with their kind donations on the platform ForFunding (https://www.forfunding.intesasanpaolo.com/DonationPlatform-ISP/nav/progetto/id/3380). This publication was supported by the European Virus Archive goes Global (EVAg) project, which has received funding from the European Union's Horizon 2020 research and innovation program under grant agreement no. 653316. This publication was supported by the COVID-2020-12371817 project, which has received funding from the Italian Ministry of Health. This work was funded, in part, by the University of Georgia (UGA) (UGA-001) and a contract by Fondazione Toscana Life Sciences. In addition, T.M.R. is supported by the Georgia Research Alliance as an Eminent Scholar. We wish to thank AchilleS Vaccines and the EU Malaria Fund for funding and managing the development of the human monoclonal antibody for clinical studies.

AUTHOR CONTRIBUTIONS

E.A., I.P., P.P., N.M., E.P., G.P., A.M., L. Benincasa, M.T., F.V., A.K., J.B., L.D., C.D.G., H.J., G.S., J.L.T., G.O., C.D.S., and D.C. conceived, performed experiments, and analyzed data. E.N., C.A., C.C., F.M., A.E., and M.F. enrolled patients and isolated PBMCs. R.R. and E.A. wrote the manuscript. A.B.W., E.M., N.T., T.M.R., M.R.C., G.I., L. Bracci, C.S., and R.R. coordinated the project.

DECLARATION OF INTERESTS

R.R. is an employee of GSK group of companies. E.A., A.K., D.C., C.D.S, I.P., N.M., E.P., P.P., C.S., M.T., F.V., and R.R. are listed as inventors of full-length human monoclonal antibodies described in Italian patent applications no. 102020000015754 filed on June 30, 2020 and no. 102020000018955 filed on August 3, 2020.

Received: November 24, 2020
Revised: January 25, 2021
Accepted: February 16, 2021
Published: February 23, 2021

REFERENCES

Ackerman, M.E., Dugast, A.-S., McAndrew, E.G., Tsoukas, S., Licht, A.F., Irvine, D.J., and Alter, G. (2013). Enhanced phagocytic activity of HIV-specific antibodies correlates with natural production of immunoglobulins with skewed affinity for FcγR2a and FcγR2b. J. Virol. *87*, 5468–5476.

Ackerman, M.E., Mikhailova, A., Brown, E.P., Dowell, K.G., Walker, B.D., Bailey-Kellogg, C., Suscovich, T.J., and Alter, G. (2016). Polyfunctional HIV-Specific Antibody Responses Are Associated with Spontaneous HIV Control. PLoS Pathog. *12*, e1005315.

Alsoussi, W.B., Turner, J.S., Case, J.B., Zhao, H., Schmitz, A.J., Zhou, J.Q., Chen, R.E., Lei, T., Rizk, A.A., McIntire, K.M., et al. (2020). A Potently Neutralizing Antibody Protects Mice against SARS-CoV-2 Infection. J. Immunol. *205*, 915–922.

Andreano, E., Piccini, G., Licastro, D., Casalino, L., Johnson, N.V., Paciello, I., Monego, S.D., Pantano, E., Manganaro, N., Manenti, A., et al. (2020). SARS-CoV-2 escape in vitrofrom a highly neutralizing COVID-19 convalescent plasma. bioRxiv. https://doi.org/10.1101/2020.12.28.424451.

Aratani, L. (2020). Jobless America: the coronavirus unemployment crisis in figures. The Guardian, May 28, 2020. https://www.theguardian.com/business/2020/may/28/jobless-america-unemployment-coronavirus-in-figures.

Arvin, A.M., Fink, K., Schmid, M.A., Cathcart, A., Spreafico, R., Havenar-Daughton, C., Lanzavecchia, A., Corti, D., and Virgin, H.W. (2020). A perspective on potential antibody-dependent enhancement of SARS-CoV-2. Nature *584*, 353–363.

Bastard, P., Rosen, L.B., Zhang, Q., Michailidis, E., Hoffmann, H.H., Zhang, Y., Dorgham, K., Philippot, Q., Rosain, J., Béziat, V., et al. (2020). Autoantibodies against type I IFNs in patients with life-threatening COVID-19. Science *370*, eabd4585.

Baum, A., Ajithdoss, D., Copin, R., Zhou, A., Lanza, K., Negron, N., Ni, M., Wei, Y., Mohammadi, K., Musser, B., et al. (2020). REGN-COV2 antibodies prevent and treat SARS-CoV-2 infection in rhesus macaques and hamsters. Science *370*, 1110–1115.

Booth, B.J., Ramakrishnan, B., Narayan, K., Wollacott, A.M., Babcock, G.J., Shriver, Z., and Viswanathan, K. (2018). Extending human IgG half-life using structure-guided design. MAbs *10*, 1098–1110.

Boudreau, C.M., Yu, W.-H., Suscovich, T.J., Talbot, H.K., Edwards, K.M., and Alter, G. (2020). Selective induction of antibody effector functional responses using MF59-adjuvanted vaccination. J. Clin. Invest. *130*, 662–672.

Butler, A.L., Fallon, J.K., and Alter, G. (2019). A Sample-Sparing Multiplexed ADCP Assay. Front. Immunol. *10*, 1851.

Carnell, G.W., Ferrara, F., Grehan, K., Thompson, C.P., and Temperton, N.J. (2015). Pseudotype-based neutralization assays for influenza: a systematic analysis. Front. Immunol. *6*, 161.

Carnell, G.W., Grehan, K., Ferrara, F., Molesti, E., and Temperton, N. (2017). An Optimized Method for the Production Using PEI, Titration and Neutralization of SARS-CoV Spike Luciferase Pseudotypes. Bio Protoc. *7*, e2514.

CDC (2021). Emerging SARS-CoV-2 Variants. https://www.cdc.gov/coronavirus/2019-ncov/more/science-and-research/scientific-brief-emerging-variants.html.

Chakraborty, S., Gonzalez, J., Edwards, K., Mallajosyula, V., Buzzanco, A.S., Sherwood, R., Buffone, C., Kathale, N., Providenza, S., Xie, M.M., et al. (2020). Proinflammatory IgG Fc structures in patients with severe COVID-19. Nat. Immunol. *22*, 67–73.

Clausen, T.M., Sandoval, D.R., Spliid, C.B., Pihl, J., Perrett, H.R., Painter, C.D., Narayanan, A., Majowicz, S.A., Kwong, E.A., McVicar, R.N., et al. (2020). SARS-CoV-2 Infection Depends on Cellular Heparan Sulfate and ACE2. Cell *183*, 1043–1057.e15.

Cutler, D.M., and Summers, L.H. (2020). The COVID-19 Pandemic and the $16 Trillion Virus. JAMA *324*, 1495–1496.

DiLillo, D.J., Tan, G.S., Palese, P., and Ravetch, J.V. (2014). Broadly neutralizing hemagglutinin stalk-specific antibodies require FcγR interactions for protection against influenza virus in vivo. Nat. Med. *20*, 143–151.

FDA (2020). Coronavirus (COVID-19) Update: FDA Authorizes Monoclonal Antibodies for Treatment of COVID-19. https://www.fda.gov/news-events/press-announcements/coronavirus-covid-19-update-fda-authorizes-monoclonal-antibodies-treatment-covid-19.

FDA (2021). COVID-19 Vaccines. https://www.fda.gov/emergency-preparedness-and-response/coronavirus-disease-2019-covid-19/covid-19-vaccines.

Gaudinski, M.R., Coates, E.E., Houser, K.V., Chen, G.L., Yamshchikov, G., Saunders, J.G., Holman, L.A., Gordon, I., Plummer, S., Hendel, C.S., et al.; VRC 606 Study Team (2018). Safety and pharmacokinetics of the Fc-modified HIV-1 human monoclonal antibody VRC01LS: A Phase 1 open-label clinical trial in healthy adults. PLoS Med. *15*, e1002493.

Grehan, K., Ferrara, F., and Temperton, N. (2015). An optimised method for the production of MERS-CoV spike expressing viral pseudotypes. MethodsX *2*, 379–384.

Griffin, M.P., Yuan, Y., Takas, T., Domachowske, J.B., Madhi, S.A., Manzoni, P., Simões, E.A.F., Esser, M.T., Khan, A.A., Dubovsky, F., et al.; Nirsevimab Study Group (2020). Single-Dose Nirsevimab for Prevention of RSV in Preterm Infants. N. Engl. J. Med. *383*, 415–425.

Hansen, J., Baum, A., Pascal, K.E., Russo, V., Giordano, S., Wloga, E., Fulton, B.O., Yan, Y., Koon, K., Patel, K., et al. (2020). Studies in humanized mice and convalescent humans yield a SARS-CoV-2 antibody cocktail. Science *369*, 1010–1014.

Hooft van Huijsduijnen, R., Kojima, S., Carter, D., Okabe, H., Sato, A., Akahata, W., Wells, T.N.C., and Katsuno, K. (2020). Reassessing therapeutic antibodies for neglected and tropical diseases. PLoS Negl. Trop. Dis. *14*, e0007860.

Hsieh, C.L., Goldsmith, J.A., Schaub, J.M., DiVenere, A.M., Kuo, H.C., Javanmardi, K., Le, K.C., Wrapp, D., Lee, A.G., Liu, Y., et al. (2020). Structure-based design of prefusion-stabilized SARS-CoV-2 spikes. Science *369*, 1501–1505.

Huang, J., Doria-Rose, N.A., Longo, N.S., Laub, L., Lin, C.L., Turk, E., Kang, B.H., Migueles, S.A., Bailer, R.T., Mascola, J.R., and Connors, M. (2013). Isolation of human monoclonal antibodies from peripheral blood B cells. Nat. Protoc. *8*, 1907–1915.

Imai, M., Iwatsuki-Horimoto, K., Hatta, M., Loeber, S., Halfmann, P.J., Nakajima, N., Watanabe, T., Ujie, M., Takahashi, K., Ito, M., et al. (2020). Syrian hamsters as a small animal model for SARS-CoV-2 infection and countermeasure development. Proc Natl Acad Sci U S A *117*, 16587–16595.

Jang, H., and Ross, T.M. (2020). Dried SARS-CoV-2 virus maintains infectivity to Vero E6 cells for up to 48 h. Vet. Microbiol. *251*, 108907.

Kaneko, N., Kuo, H.-H., Boucau, J., Farmer, J.R., Allard-Chamard, H., Mahajan, V.S., Piechocka-Trocha, A., Lefteri, K., Osborn, M., Bals, J., et al.; Massachusetts Consortium on Pathogen Readiness Specimen Working Group (2020). Loss of Bcl-6-Expressing T Follicular Helper Cells and Germinal Centers in COVID-19. Cell *183*, 143–157.e13.

Karsten, C.B., Mehta, N., Shin, S.A., Diefenbach, T.J., Slein, M.D., Karpinski, W., Irvine, E.B., Broge, T., Suscovich, T.J., and Alter, G. (2019). A versatile high-throughput assay to characterize antibody-mediated neutrophil phagocytosis. J. Immunol. Methods *471*, 46–56.

Katzelnick, L.C., Gresh, L., Halloran, M.E., Mercado, J.C., Kuan, G., Gordon, A., Balmaseda, A., and Harris, E. (2017). Antibody-dependent enhancement of severe dengue disease in humans. Science *358*, 929–932.

Kelley, B. (2020). Developing therapeutic monoclonal antibodies at pandemic pace. Nat. Biotechnol. *38*, 540–545.

Korber, B., Fischer, W.M., Gnanakaran, S., Yoon, H., Theiler, J., Abfalterer, W., Hengartner, N., Giorgi, E.E., Bhattacharya, T., Foley, B., et al. (2020). Tracking Changes in SARS-CoV-2 Spike: Evidence that D614G Increases Infectivity of the COVID-19 Virus. Cell *182*, 812–827.e19.

Kreer, C., Zehner, M., Weber, T., Ercanoglu, M.S., Gieselmann, L., Rohde, C., Halwe, S., Korenkov, M., Schommers, P., Vanshylla, K., et al. (2020). Longitudinal Isolation of Potent Near-Germline SARS-CoV-2-Neutralizing Antibodies from COVID-19 Patients. Cell *182*, 843–854.e12.

Kreye, J., Reincke, S.M., Kornau, H.-C., Sánchez-Sendin, E., Corman, V.M., Liu, H., Yuan, M., Wu, N.C., Zhu, X., Lee, C.D., et al. (2020). A Therapeutic Non-self-reactive SARS-CoV-2 Antibody Protects from Lung Pathology in a COVID-19 Hamster Model. Cell *183*, 1058–1069.e19.

Kundi, M. (1999). One-hit models for virus inactivation studies. Antiviral Res. *41*, 145–152.

Kupferschmidt, K. (2019). Successful Ebola treatments promise to tame outbreak. Science *365*, 628–629.

Lander, G.C., Stagg, S.M., Voss, N.R., Cheng, A., Fellmann, D., Pulokas, J., Yoshioka, C., Irving, C., Mulder, A., Lau, P.-W., et al. (2009). Appion: an integrated, database-driven pipeline to facilitate EM image processing. J. Struct. Biol. *166*, 95–102.

Lee, W.S., Wheatley, A.K., Kent, S.J., and DeKosky, B.J. (2020). Antibody-dependent enhancement and SARS-CoV-2 vaccines and therapies. Nat. Microbiol. *5*, 1185–1191.

Lilly (2020). Lilly's neutralizing antibody bamlanivimab (LY-CoV555) receives FDA emergency use authorization for the treatment of recently diagnosed COVID-19. https://investor.lilly.com/news-releases/news-release-details/lillys-neutralizing-antibody-bamlanivimab-ly-cov555-receives-fda.

Liu, L., Wang, P., Nair, M.S., Yu, J., Rapp, M., Wang, Q., Luo, Y., Chan, J.F.W., Sahi, V., Figueroa, A., et al. (2020). Potent neutralizing antibodies against multiple epitopes on SARS-CoV-2 spike. Nature *584*, 450–456.

Mackness, B.C., Jaworski, J.A., Boudanova, E., Park, A., Valente, D., Mauriac, C., Pasquier, O., Schmidt, T., Kabiri, M., Kandira, A., et al. (2019). Antibody Fc engineering for enhanced neonatal Fc receptor binding and prolonged circulation half-life. MAbs *11*, 1276–1288.

Manenti, A., Maggetti, M., Casa, E., Martinuzzi, D., Torelli, A., Trombetta, C.M., Marchi, S., and Montomoli, E. (2020). Evaluation of SARS-CoV-2 neutralizing antibodies using a CPE-based colorimetric live virus micro-neutralization assay in human serum samples. J. Med. Virol. *92*, 2096–2104.

Mullard, A. (2020). FDA approves antibody cocktail for Ebola virus. Nat. Rev. Drug Discov. *19*, 827.

Pegu, A., Hessell, A.J., Mascola, J.R., and Haigwood, N.L. (2017). Use of broadly neutralizing antibodies for HIV-1 prevention. Immunol. Rev. *275*, 296–312.

Pettersen, E.F., Goddard, T.D., Huang, C.C., Couch, G.S., Greenblatt, D.M., Meng, E.C., and Ferrin, T.E. (2004). UCSF Chimera–a visualization system for exploratory research and analysis. J. Comput. Chem. *25*, 1605–1612.

Pinto, D., Park, Y.J., Beltramello, M., Walls, A.C., Tortorici, M.A., Bianchi, S., Jaconi, S., Culap, K., Zatta, F., De Marco, A., et al. (2020). Cross-neutralization of SARS-CoV-2 by a human monoclonal SARS-CoV antibody. Nature *583*, 290–295.

Regeneron (2020). Regeneron's casirivimab and imdevimab antibody cocktail for COVID-19 is first combination therapy to receive FDA emergency use authorization. https://investor.regeneron.com/news-releases/news-release-details/regenerons-regen-cov2-first-antibody-cocktail-covid-19-receive.

Rogers, T.F., Zhao, F., Huang, D., Beutler, N., Burns, A., He, W.-T., Limbo, O., Smith, C., Song, G., Woehl, J., et al. (2020). Isolation of potent SARS-CoV-2 neutralizing antibodies and protection from disease in a small animal model. Science *369*, 956–963.

Romano, M., Ruggiero, A., Squeglia, F., Maga, G., and Berisio, R. (2020). A Structural View of SARS-CoV-2 RNA Replication Machinery: RNA Synthesis, Proofreading and Final Capping. Cells *9*, 1267.

Schäfer, A., Muecksch, F., Lorenzi, J.C.C., Leist, S.R., Cipolla, M., Bournazos, S., Schmidt, F., Maison, R.M., Gazumyan, A., Martinez, D.R., et al. (2020). Antibody potency, effector function, and combinations in protection and therapy for SARS-CoV-2 infection *in vivo*. J. Exp. Med. *218*, e20201993.

Scheres, S.H. (2012). RELION: implementation of a Bayesian approach to cryo-EM structure determination. J. Struct. Biol. *180*, 519–530.

Schlothauer, T., Herter, S., Koller, C.F., Grau-Richards, S., Steinhart, V., Spick, C., Kubbies, M., Klein, C., Umaña, P., and Mössner, E. (2016). Novel human IgG1 and IgG4 Fc-engineered antibodies with completely abolished immune effector functions. Protein Eng. Des. Sel. *29*, 457–466.

Shi, R., Shan, C., Duan, X., Chen, Z., Liu, P., Song, J., Song, T., Bi, X., Han, C., Wu, L., et al. (2020). A human neutralizing antibody targets the receptor-binding site of SARS-CoV-2. Nature *584*, 120–124.

Sia, S.F., Yan, L.M., Chin, A.W.H., Fung, K., Choy, K.T., Wong, A.Y.L., Kaewpreedee, P., Perera, R.A.P.M., Poon, L.L.M., Nicholls, J.M., et al. (2020). Pathogenesis and transmission of SARS-CoV-2 in golden hamsters. Nature *583*, 834–838.

Sparrow, E., Friede, M., Sheikh, M., and Torvaldsen, S. (2017). Therapeutic antibodies for infectious diseases. Bull. World Health Organ. *95*, 235–237.

Suloway, C., Pulokas, J., Fellmann, D., Cheng, A., Guerra, F., Quispe, J., Stagg, S., Potter, C.S., and Carragher, B. (2005). Automated molecular microscopy: the new Leginon system. J. Struct. Biol. *151*, 41–60.

Tay, M.Z., Poh, C.M., Renia, L., Macary, P.A., and Ng, L.F.P. (2020). The trinity of COVID-19: immunity, inflammation and intervention. Nat. Rev. Immunol. *20*, 363–374.

Tiller, T., Meffre, E., Yurasov, S., Tsuiji, M., Nussenzweig, M.C., and Wardemann, H. (2008). Efficient generation of monoclonal antibodies from single human B cells by single cell RT-PCR and expression vector cloning. J. Immunol. Methods *329*, 112–124.

Voss, N.R., Yoshioka, C.K., Radermacher, M., Potter, C.S., and Carragher, B. (2009). DoG Picker and TiltPicker: software tools to facilitate particle selection in single particle electron microscopy. J. Struct. Biol. *166*, 205–213.

Walls, A.C., Park, Y.J., Tortorici, M.A., Wall, A., McGuire, A.T., and Veesler, D. (2020). Structure, Function, and Antigenicity of the SARS-CoV-2 Spike Glycoprotein. Cell *181*, 281–292.e6.

Wang, Q., Zhang, Y., Wu, L., Niu, S., Song, C., Zhang, Z., Lu, G., Qiao, C., Hu, Y., Yuen, K.Y., et al. (2020). Structural and Functional Basis of SARS-CoV-2 Entry by Using Human ACE2. Cell *181*, 894–904.e9.

Wardemann, H., and Busse, C.E. (2019). Expression Cloning of Antibodies from Single Human B Cells. Methods Mol. Biol. *1956*, 105–125.

Wellcome and IAVI (2020). Expanding access to monoclonal antibody-based products: a global call to action. https://www.iavi.org/news-resources/expanding-access-to-monoclonal-antibody-based-products-a-global-call-to-action.

Wrapp, D., Wang, N., Corbett, K.S., Goldsmith, J.A., Hsieh, C.L., Abiona, O., Graham, B.S., and McLellan, J.S. (2020). Cryo-EM structure of the 2019-nCoV spike in the prefusion conformation. Science *367*, 1260–1263.

Yuan, M., Liu, H., Wu, N.C., Lee, C.-C.D., Zhu, X., Zhao, F., Huang, D., Yu, W., Hua, Y., Tien, H., et al. (2020). Structural basis of a shared antibody response to SARS-CoV-2. Science *369*, 1119–1123.

Zalevsky, J., Chamberlain, A.K., Horton, H.M., Karki, S., Leung, I.W.L., Sproule, T.J., Lazar, G.A., Roopenian, D.C., and Desjarlais, J.R. (2010). Enhanced antibody half-life improves in vivo activity. Nat. Biotechnol. *28*, 157–159.

Zost, S.J., Gilchuk, P., Case, J.B., Binshtein, E., Chen, R.E., Nkolola, J.P., Schäfer, A., Reidy, J.X., Trivette, A., Nargi, R.S., et al. (2020a). Potently neutralizing and protective human antibodies against SARS-CoV-2. Nature *584*, 443–449.

Zost, S.J., Gilchuk, P., Chen, R.E., Case, J.B., Reidy, J.X., Trivette, A., Nargi, R.S., Sutton, R.E., Suryadevara, N., Chen, E.C., et al. (2020b). Rapid isolation and profiling of a diverse panel of human monoclonal antibodies targeting the SARS-CoV-2 spike protein. Nat. Med. *26*, 1422–1427.

Zou, X., Chen, K., Zou, J., Han, P., Hao, J., and Han, Z. (2020). Single-cell RNA-seq data analysis on the receptor ACE2 expression reveals the potential risk of different human organs vulnerable to 2019-nCoV infection. Front. Med. *14*, 185–192.

Zuo, Y., Estes, S.K., Ali, R.A., Gandhi, A.A., Yalavarthi, S., Shi, H., Sule, G., Gockman, K., Madison, J.A., Zuo, M., et al. (2020). Prothrombotic autoantibodies in serum from patients hospitalized with COVID-19. Sci. Transl. Med. *12*, eabd3876.

STAR★METHODS

KEY RESOURCES TABLE

REAGENT or RESOURCE	SOURCE	IDENTIFIER
Antibodies and fluorophores		
CD19 V421	BD Biosciences	Cat# 562440; RRID:AB_11153299
IgM PerCP-Cy5.5	BD Biosciences	Cat# 561285; RRID:AB_10611998
CD27 PE	BD Biosciences	Cat# 340425; RRID:AB_400032
IgD-A700	BD Biosciences	Cat# 561302; RRID:AB_10646035
CD3 PE-Cy7	BioLegend	Cat# 300420; RRID:AB_439781
CD14 PE-Cy7	BioLegend	Cat# 301814; RRID:AB_389353
Streptavidin-PE	Thermo Fisher	Cat#12-4317-87
Goat Anti-Human IgA-UNLB	Southern Biotech	Cat# 2050-01; RRID:AB_2795701
Goat Anti-Human IgA-Alkaline Phosphatase	Southern Biotech	Cat# 2050-04; RRID:AB_2795704
Goat Anti-Human IgG-UNLB	Southern Biotech	Cat# 2040-01; RRID:AB_2795640
Bacterial and virus strains		
SARS-CoV-2 wild type	EVAg	GenBank: MT066156.1
SARS-CoV-2 D614G	EVAg	GenBank: MT527178.1
SARS-CoV-2 B.1.1.7	INMI	GISAID accession number: EPI_ISL_736997
Biological samples		
PBMCs and IgGs of donor PT-004	This paper	N/A
PBMCs and IgGs of donor PT-005	This paper	N/A
PBMCs and IgGs of donor PT-006	This paper	N/A
PBMCs and IgGs of donor PT-008	This paper	N/A
PBMCs and IgGs of donor PT-009	This paper	N/A
PBMCs and IgGs of donor PT-010	This paper	N/A
PBMCs and IgGs of donor PT-012	This paper	N/A
PBMCs and IgGs of donor PT-014	This paper	N/A
PBMCs and IgGs of donor PT-041	This paper	N/A
PBMCs and IgGs of donor PT-100	This paper	N/A
PBMCs and IgGs of donor PT-101	This paper	N/A
PBMCs and IgGs of donor PT-102	This paper	N/A
PBMCs and IgGs of donor PT-103	This paper	N/A
PBMCs and IgGs of donor PT-188	This paper	N/A
Chemicals, peptides, and recombinant proteins		
Fetal Bovine Serum (FBS) Hyclone	Sigma-Aldrich	Cat#D2650
DMSO	Sigma-Aldrich	Cat#D2650
RNaseOUT Recombinant Ribonuclease Inhibitor	Thermo Fisher	Cat#10777-019
SuperScript IV Reverse Transcriptase	Thermo Fisher	Cat#18091200
DEPC-Treated water	Thermo Fisher	Cat#AM9916
dNTP Set (100 mM)	Thermo Fisher	Cat#10297018
MgCl2 Magnesium Chloride 25mM	Thermo Fisher	Cat#AB0359
Kapa Long Range Polymerase	Sigma-Aldrich	Cat#KK3005
NEBuilder® HiFi DNA Assembly Master Mix	New England BioLabs	Cat#E2621X
Q5® High-Fidelity DNA Polymerases	New England BioLabs	Cat#M0491L
Expi293™ Expression Medium	Thermo Fisher	Cat#A1435101

(*Continued on next page*)

Continued

REAGENT or RESOURCE	SOURCE	IDENTIFIER
ExpiFectamine™ 293 Transfection Kit	Thermo Fisher	Cat#A14524
Ultra Pure Bovine serum albumin (BSA)	Thermo Fisher	Cat#AM2618
DMEM high Glucose	Thermo Fisher	Cat#11965092
Ficoll-Paque™ PREMIUM	Sigma-Aldrich	Cat#GE17-5442-03
MycoZap Plus-PR	Lonza	Cat#VZA2022
IMDM with GlutaMAX	Thermo Fisher	Cat# 31980048
Benzonase Nuclease	Sigma-Aldrich	Cat#70664-3
IL-2 Recombinant Human Protein	Thermo Fisher	Cat#PHC0023
IL-21 Recombinant Human Protein	Thermo Fisher	Cat#PHC0211
Strep-Tactin DY488	IBA lifesciences	Cat#2-1562-050
Slide-A-Lyzer™ Dialysis Cassettes	Thermo Fisher	Cat#66003
HiTrap Protein G HP column	Cytiva	Cat#17040503
HisTrap FF Crude column	Cytiva	Cat#17528601
SARS Coronavirus Spike Glycoprotein (S1)	The Native Antigen Company	Cat#REC31809
SARS Coronavirus Spike Glycoprotein (S2)	The Native Antigen Company	Cat#REC31807
Tween-20	VWR	Cat#A4974.0250
SARS Coronavirus Spike Glycoprotein (S1)	The Native Antigen Company	Cat#REC31806-500
SARS Coronavirus Spike Glycoprotein (S2)	The Native Antigen Company	Cat#REC31807-500
Alkaline Phosphatase Yellow (pNPP) Liquid Substrate System	Sigma-Aldrich	Cat#P7998
Goat Anti-Human IgG-UNLB	SouthernBiotech	Cat#2040-01
Critical commercial assays		
NOVA Lite Hep-2 ANA Kit	Inova Diagnostics / Werfen	Cat#066708100
ELISA Starter Accessory Kit	Bethyl Laboratories	Cat#E101
APEX Alexa Fluor 647 Antibody Labeling Kit	Thermo Fisher	Cat#A10475
Pierce BCA Protein Assay Kit	Thermo Fisher	Cat#23227
Deposited data		
Cloned and tested SARS-CoV-2-neutralizing antibodies	This paper	Patent Application
Experimental models: cell lines		
VERO E6 cell line	ATCC	Cat#CRL-1586
Expi293F™ cells	Thermo Fisher	Cat#A14527
3T3-msCD40L Cells	NIH AIDS Reagent Program	Cat#12535
Oligonucleotides		
Single cell PCR Primer	This paper	N/A
Random Hexamer Primer	Thermo Fisher	Cat#SO142
TAP forward primer (TTAGGCACCCCAGGCTTTAC)	This paper	N/A
TAP forward primer (AGATGGTTCTTTCCGCCTCA)	This paper	N/A
Recombinant DNA		
Human antibody expression vectors (IgG1, Igl, Igk)	(Tiller et al., 2008)	N/A
Plasmid encoding SARS-CoV-2 S ectodomain (amino acids 1-1208 of SARS-CoV-2 S; GenBank: MN908947)	(Wrapp et al., 2020)	N/A
Plasmid encoding SARS-CoV-2 RBD (amino acids 319 - 591 of SARS-CoV-2 S; GenBank: MN908947)	Jason McLellan Lab	N/A
pCDNA3.1+-SARS-CoV-2 Spike from Wuhan-Hu-1 isolate (GenBank MN908947.3) codon optimized	This paper	pCDNA-S2

(*Continued on next page*)

Continued

REAGENT or RESOURCE	SOURCE	IDENTIFIER
pCAGGS-SARS-CoV-2 Spike from Wuhan-Hu-1 isolate (GenBank MN908947.3) encoding D614G mutation and codon optimized	This paper	pCAGGS-S2 D614G
pCAGGS-SARS1 Spike protein codon optimized	(Carnell et al., 2017)	pCAGGS-S1
pCAGGS-MERS Spike protein codon optimized	(Grehan et al., 2015)	pCAGGS-MERS
pCSFLW Firefly luciferase encoding plasmid	(Carnell et al., 2015)	pCSFLW
p8.91 HIV Gag/Pol-encoding plasmid	(Carnell et al., 2015)	p8.91
Software and algorithms		
Prism 8	GraphPad	https://www.graphpad.com/
FlowJo 10.5.3	FlowJo, LLC	https://www.flowjo.com
FastQC	Babraham Institute	https://www.bioinformatics.babraham.ac.uk/projects/fastqc/
MultiQC 1.9	MultiQC	https://multiqc.info/
Trimmomatic 0.39	USADELLAB	http://www.usadellab.org/cms/?page=trimmomatic
MiXCR	MI Lanoratory	https://mixcr.readthedocs.io/en/master/index.html
NumPy	NumPy	https://numpy.org/
Python 3.7.4	Python Software Foundation	https://www.python.org/
Other		
BD FACS Aria III Cell Sorter	BD Biosciences	https://www.bdbiosciences.com
BD FACS Canto II	BD Biosciences	https://www.bdbiosciences.com
Leica DMI-microscope	Leica Biosystem	https://www.leica-microsystems.com
LUNA-II Automated Cell Counter	Logo Biosystems	https://logosbio.com
Qubit Fluorometric Quantification	Thermo Fisher	https://www.thermofisher.com
ÄKTA go	Cytiva Lifesciences	https://www.cytivalifesciences.com
GloMax Luminometer	Promega	https://ita.promega.com
Varioskan LUX multimode microplate reader	Thermo Fisher	https://www.thermofisher.com

RESOURCE AVAILABILITY

Lead contact

Further information and requests for resources and reagents should be directed to and will be fulfilled by the Lead Contact, Rino Rappuoli (rino.r.rappuoli@gsk.com).

Materials availability

Reasonable amounts of antibodies will be made available by the Lead Contact upon request under a Material Transfer Agreement (MTA) for non-commercial usage.

Data and code availability

Nucleotide and amino acidic sequences of all SARS-CoV-2-neutralizing antibodies were deposited in the Italian patent applications n. 102020000015754 filed on June 30th 2020 and 102020000018955 filed on August 3rd 2020. The accession number for the nucleotide sequences of all SARS-CoV-2-neutralizing antibodies reported in this paper is GenBank: MW_598287 - MW_598314.

EXPERIMENTAL MODEL AND SUBJECT DETAILS

Enrollment of SARS-COV-2 convalescent donors and human sample collection

This work results from a collaboration with the National Institute for Infectious Diseases, IRCCS – Lazzaro Spallanzani Rome (IT) and Azienda Ospedaliera Universitaria Senese, Siena (IT) that provided samples from SARS-CoV-2 convalescent donors, of both sexes, who gave their written consent. The study was approved by local ethics committees (Parere 18_2020 in Rome and Parere 17065 in Siena) and conducted according to good clinical practice in accordance with the declaration of Helsinki (European Council 2001, US Code of Federal Regulations, ICH 1997). This study was unblinded and not randomized.

METHOD DETAILS

Single cell sorting of SARS-CoV-2 S-protein$^+$ memory B cells from COVID-19 convalescent donors

Blood samples were screened for SARS-CoV-2 RNA and for antibodies against HIV, HBV and HCV. Peripheral blood mononuclear cells (PBMCs) were isolated from heparin-treated whole blood by density gradient centrifugation (Ficoll-Paque PREMIUM, Sigma-Aldrich). After separation, PBMC were stained with Live/Dead Fixable Aqua (Invitrogen; Thermo Scientific) in 100 μL final volume diluted 1:500 at room temperature RT. After 20 min incubation cells were washed with PBS and unspecific bindings were saturated with 50 μL of 20% normal rabbit serum (Life technologies) in PBS . Following 20 min incubation at 4°C cells were washed with PBS and stained with SARS-CoV-2 S-protein labeled with Strep-Tactin®XT DY-488 (iba-lifesciences cat# 2-1562-050) for 30 min at 4°C. After incubation the following staining mix was used CD19 V421 (BD cat# 562440), IgM PerCP-Cy5.5 (BD cat# 561285), CD27 PE (BD cat# 340425), IgD-A700 (BD cat# 561302), CD3 PE-Cy7 (BioLegend cat# 300420), CD14 PE-Cy7 (BioLegend cat# 301814), CD56 PE-Cy7 (BioLegend cat# 318318) and cells were incubated at 4°C for additional 30 min. Stained MBCs were single cell-sorted with a BD FACS Aria III (BD Biosciences) into 384-well plates containing 3T3-CD40L feeder cells and were incubated with IL-2 and IL-21 for 14 days as previously described (Huang et al., 2013).

Expression and purification of SARS-CoV-2 S-protein prefusion trimer and receptor binding domain

Plasmid encoding SARS-CoV-2 S-2P construct (Wrapp et al., 2020) and S-protein RBD (generously provided by Jason S. McLellan) were transiently transfected at 1 μg/mL culture into Expi293F cells (Thermo Fisher) using ExpiFectamine 293 Reagent. Cells were grown for six days at 37°C with 8% CO_2 shaking 125 rpm according to the manufacturer's protocol (Thermo Fisher); ExpiFectamine 293 Transfection Enhancers 1 and 2 were added 16 to 18 h post-transfection to boost transfection, cell viability, and protein expression. Cell cultures were harvested three and six days after transfection. Cells were separated from the medium by centrifugation (1,100 g for 10 min at 24°C). Collected supernatants were then pooled and clarified by centrifugation (3,000 g for 15 min at 4°C) followed by filtration through a 0.45 μm filter. Chromatography was conducted at room temperature using the ÄKTA go purification system from GE Healthcare Life Sciences. Expressed proteins were purified by using an immobilized metal affinity chromatography (FF Crude) followed by dialysis into final buffer. Specifically, the filtrated culture supernatant was purified with a 5 mL HisTrap FF Crude column (GE Healthcare Life Sciences) previously equilibrated in Buffer A (20 mM NaH_2PO_4, 500 mM NaCl + 30 mM imidazol pH 7.4).

The flow rate for all steps of the HisTrap FF Crude column was 5 mL/min. The culture supernatant of spike and RBD cell culture was applied to a single 5 mL HisTrap FF Crude column. The column was washed in Buffer A for 4 column volumes (CV) with the all 4 CV collected as the column wash. Recombinant proteins were eluted from the column applying a first step elution of 4 CV of 50% Buffer B (20 mM NaH2PO4, 500 mM NaCl + 500 mM imidazol pH 7.4) and a second step elution of 2 CV of 100% Buffer B. Elution steps were collected in 1 fractions of 1 mL each. Eluted fractions were analyzed by SDS-PAGE and appropriate fractions containing recombinant proteins were pooled. Final pools were dialyzed against phosphate buffered saline (PBS) pH 7.4 using Slide-A-Lyzer G2 Dialysis Cassette 3.5K (Thermo Scientific) overnight at 4°C. The dialysis buffer used was at least 200 times the volume of the sample.

The final protein concentration was determined by measuring the A520 using the Pierce BCA protein assay kit (Thermo Scientific). Final protein was dispensed in aliquots of 0.5 mL each and stored at −80°C.

ELISA assay with S1 and S2 subunits of SARS-CoV-2 S-protein

The presence of S1- and S2-binding antibodies in culture supernatants of monoclonal S-protein-specific memory B cells was assessed by means of an ELISA implemented with the use of a commercial kit (ELISA Starter Accessory Kit, Catalogue No. E101; Bethyl Laboratories). Briefly, 384-well flat-bottom microtiter plates (384 well plates, Microplate Clear, Greiner Bio-one) were coated with 25 μL/well of antigen (1:1 mix of S1 and S2 subunits, 1 μg/mL each; The Native Antigen Company, Oxford, United Kingdom) diluted in coating buffer (0.05 M carbonate-bicarbonate solution, pH 9.6), and incubated overnight at 4°C. The plates were then washed three times with 100 μL/well washing buffer (50 mM Tris Buffered Saline (TBS) pH 8.0, 0.05% Tween-20) and saturated with 50 μL/well blocking buffer containing Bovine Serum Albumin (BSA) (50 mM TBS pH 8.0, 1% BSA, 0.05% Tween-20) for 1 h (h) at 37°C. After further washing, samples diluted 1:5 in blocking buffer were added to the plate. Blocking buffer was used as a blank. After an incubation of 1 h at 37°C, plates were washed and incubated with 25 μL/well secondary antibody (horseradish peroxidase (HRP)-conjugated goat anti-human IgG-Fc Fragment polyclonal antibody, diluted 1:10,000 in blocking buffer, Catalogue No. A80-104P; (Bethyl Laboratories) for 1 h at 37°C. After three washes, 25 μL/well TMB One Component HRP Microwell Substrate (Bethyl Laboratories) was added and incubated 10–15 min at RT in the dark. Color development was terminated by addition of 25 μL/well 0.2 M H_2SO_4. Absorbance was measured at 450 nm in a Varioskan Lux microplate reader (Thermo Fisher Scientific). Plasma from COVID-19 convalescent donors (Andreano et al., 2020) and unrelated plasma were used as positive and negative control respectively. The threshold for sample positivity was set at twice the optical density (OD) of the blank.

ELISA assay with SARS-CoV-2 S-protein prefusion trimer and S1 – S2 subunits

ELISA assay was used to detect SARS-CoV-2 S-protein specific mAbs and to screen plasma from SARS-CoV-2 convalescent donors. 384-well plates (384 well plates, microplate clear; Greiner Bio-one) were coated with 3 μg/mL of streptavidin (Thermo Fisher) diluted in coating buffer (0.05 M carbonate-bicarbonate solution, pH 9.6) and incubated at RT overnight. Plates were then coated with SARS-CoV-2 S-protein, S1 or S2 domains at 3 μg/mL and incubated for 1 h at RT. 50 μL/well of saturation buffer (PBS/BSA 1%) was

used to saturate unspecific binding and plates were incubated at 37°C for 1 h without CO_2. For the first round of screening, supernatants were diluted 1:5 in PBS/BSA 1%/Tween20 0.05% in 25 μL/well final volume and incubated for 1 h at 37°C without CO_2. For purified antibodies, and to assess EC_{50}, mAbs were tested at a starting concentration of 5 μg/mL and diluted step 1:2 in PBS/BSA 1%/Tween20 0.05% in 25 μL/well final volume for 1 h at 37°C without CO_2. 25 μL/well of alkaline phosphatase-conjugated goat anti-human IgG (Sigma-Aldrich) and IgA (Southern Biotech) were used as secondary antibodies. Wells were washed three times between each step with PBS/BSA 1%/Tween20 0.05%. pNPP (p-nitrophenyl phosphate) (Sigma-Aldrich) was used as soluble substrate to detect SARS-CoV-2 S-protein, S1 or S2 specific mAbs and the final reaction was measured by using the Varioskan Lux Reader (Thermo Fisher Scientific) at a wavelength of 405 nm. Plasma from COVID-19 convalescent donors (Andreano et al., 2020) and unrelated plasma were used as positive and negative control respectively. Samples were considered as positive if OD at 405 nm (OD_{405}) was twice the blank.

SARS-CoV-2 virus and cell infection

African green monkey kidney cell line Vero E6 cells (American Type Culture Collection [ATCC] #CRL-1586) were cultured in Dulbecco's Modified Eagle's Medium (DMEM) - high glucose (Euroclone, Pero, Italy) supplemented with 2 mM L- Glutamine (Lonza, Milano, Italy), penicillin (100 U/mL) - streptomycin (100 μg/mL) mixture (Lonza, Milano, Italy) and 10% Foetal Bovine Serum (FBS) (Euroclone, Pero, Italy). Cells were maintained at 37°C, in a 5% CO_2 humidified environment and passaged every 3-4 days.

Wild type SARS-CoV-2 (SARS-CoV-2/INMI1-Isolate/2020/Italy: MT066156), D614G (SARS-CoV-2/human/ITA/INMI4/2020, clade GR, D614G (S): MT527178) and B.1.1.7 (INMI-118 GISAID accession number EPI_ISL_736997) viruses were purchased from the European Virus Archive goes Global (EVAg, Spallanzani Institute, Rome)or received from the Spallanzani Institute, Rome. For virus propagation, sub-confluent Vero E6 cell monolayers were prepared in T175 flasks (Sarstedt) containing supplemented D-MEM high glucose medium. For titration and neutralization tests of SARS-CoV-2, Vero E6 were seeded in 96-well plates (Sarstedt) at a density of 1.5×10^4 cells/well the day before the assay.

Neutralization of Binding (NoB) Assay

To study the binding of the SARS-CoV-2 S-protein to cell-surface receptor(s) we developed an assay to assess recombinant S-protein specific binding to target cells and neutralization thereof. To this aim the stabilized S-protein was coupled to Streptavidin-PE (eBioscience # 12-4317-87, Thermo Fisher) for 1 h at RT and then incubated with Vero E6 cells. Binding was assessed by flow cytometry. The stabilized S-protein bound Vero E6 cells with high affinity (data not shown). To assess the content of neutralizing antibodies in sera or in B cell culture supernatants, two microliters of SARS-CoV-2 Spike-Streptavidin-PE at 5 - 10 μg/mL in PBS-5%FCS were mixed with two microliters of various dilutions of sera or B cell culture supernatants in U bottom 96-well plates. After incubation at 37°C for 1 h, 30×10^3 Vero E6 cells suspended in two microliters of PBS 5% FCS were added and incubated for additional 45 min at 4°C. Non-bound protein and antibodies were removed and cell-bound PE-fluorescence was analyzed with a FACS Canto II flow cytometer (Becton Dickinson). Data were analyzed using the FlowJo data analysis software package (TreeStar, USA). The specific neutralization was calculated as follows: NoB (%) = 1 – (Sample MFI value – background MFI value) / (Negative Control MFI value – background MFI value). Plasma from COVID-19 convalescent donors (Andreano et al., 2020) and unrelated plasma were used as positive and negative control respectively.

Single cell RT-PCR and Ig gene amplification

From the original 384-well sorting plate, 5 μL of cell lysate was used to perform RT-PCR. Total RNA from single cells was reverse transcribed in 25 μL of reaction volume composed by 1 μL of random hexamer primers (50 ng/μL), 1 μL of dNTP-Mix (10 mM), 2 μL 0.1 M DTT, 40 U/μL RNase OUT, $MgCl_2$ (25 mM), 5x FS buffer and Superscript IV reverse transcriptase (Invitrogen). Final volume was reached by adding nuclease-free water (DEPC). Reverse transcription (RT) reaction was performed at 42°C/10', 25°C/10', 50°C/60' and 94°/5¿. Heavy (VH) and light (VL) chain amplicons were obtained via two rounds of PCR. All PCR reactions were performed in a nuclease-free water (DEPC) in a total volume of 25 μL/well. Briefly, 4 μL of cDNA were used for the first round of PCR (PCRI). PCRI-master mix contained 10 μM of VH and 10 μM VL primer-mix, 10mM dNTP mix, 0.125 μL of Kapa Long Range Polymerase (Sigma), 1.5 μL MgCl2 and 5 μL of 5x Kapa Long Range Buffer. PCRI reaction was performed at 95°/3¿, 5 cycles at 95°C/30'', 57°C/30'', 72°C/30'' and 30 cycles at 95°C/30'', 60°C/30'', 72°C/30'' and a final extension of 72°/2'. All nested PCR reactions (PCRII) were performed using 3.5 μL of unpurified PCRI product using the same cycle conditions. PCRII products were then purified by Millipore MultiScreen® PCRμ96 plate according to manufacture instructions. Samples were eluted with 30 μL nuclease-free water (DEPC) into 96-well plates and quantify by.

Cloning of variable region genes and recombinant antibody expression in transcriptionally active PCR

Vector digestions were carried out with the respective restriction enzymes AgeI, SalI and XhoI as previously described (Tiller et al., 2008, Wardemann and Busse, 2019). Briefly, 75 ng of IgH, Igλ and Igκ purified PCRII products were ligated by using the Gibson Assembly NEB into 25 ng of respective human Igγ1, Igκ and Igλ expression vectors. The reaction was performed into 5 μL of total volume. Ligation product was 10-fold diluted in nuclease-free water (DEPC) and used as template for transcriptionally active PCR (TAP) reaction which allowed the direct use of linear DNA fragments for *in vitro* expression. The entire process consists of one PCR amplification step, using primers to attach functional promoter (human CMV) and terminator sequences (SV40) onto the

fragment PCRII products. TAP reaction was performed in a total volume of 25 μL using 5 μL of Q5 polymerase (NEB), 5 μL of GC Enhancer (NEB), 5 μL of 5X buffer,10 mM dNTPs, 0.125 μL of forward/reverse primers and 3 μL of ligation product. TAP reaction was performed by using the following cycles: 98°/2', 35 cycles 98°/10'', 61°/20'', 72°/1' and 72°/5¿ as final extention step. TAP products were purified under the same PCRII conditions, quantified by Qubit Fluorometric Quantitation assay (Invitrogen) and used for transient transfection in Expi293F cell line using manufacturing instructions.

Flask expression and purification of human monoclonal antibodies

Expi293F cells (Thermo Fisher) were transiently transfected with plasmids carrying the antibody heavy chain and the light chains with a 1:2 ratio. Cells were grown for six days at 37°C with 8% CO_2 shaking at 125 rpm according to the manufacturer's protocol (Thermo Fisher); ExpiFectamine 293 transfection enhancers 1 and 2 were added 16 to 18 h post-transfection to boost cell viability and protein expression. Cell cultures were harvested three and six days after transfection. Cells were separated from the medium by centrifugation (1,100 g for 10 min at 24°C). Supernatants collected were then pooled and clarified by centrifugation (3000 g for 15 min, 4°C) followed by filtration through a 0.45 μm filter. Chromatography was conducted at room temperature using the ÄKTA go purification system from GE Healthcare Life Sciences. Affinity chromatography was used to purify expressed monoclonal antibodies using an immobilized protein G column able to bind to Fc region. Specifically, filtrated culture supernatants were purified with a 1 mL HiTrap Protein G HP column (GE Healthcare Life Sciences) previously equilibrated in Buffer A (0.02 M NaH_2PO_4 pH 7). The flow rate for all steps of the HiTrap Protein G HP column was 1 mL/min. The culture supernatant for every monoclonal antibody cell culture was applied to a single 1 mL HiTrap Protein G HP column. The column was equilibrated in Buffer A for at least 6 column volumes (CV) which was collected as column wash. Each monoclonal antibody was eluted from the column applying a step elution of 6 CV of Buffer B (0.1 M glycine-HCl, pH 2.7). Elution steps were collected in 1 fractions of 1 mL each. Eluted fractions were analyzed by non-reducing SDS-PAGE and fractions showing the presence of IgG were pooled together. Final pools was dialyzed in PBS buffer pH 7.4 using Slide-A-Lyzer G2 Dialysis Cassette 3.5K (Thermo Scientific) overnight at 4°C. The dialysis buffer used was at least 200 times the volume of the sample. For each antibody purified the concentration was determined by measuring the A520 using Pierce BCA Protein Assay Kit (Thermo Scientific). All the purified antibodies were aliquoted and stored at −80°C.

Viral propagation and titration

The SARS-CoV-2 virus was propagated in Vero E6 cells cultured in DMEM high Glucose supplemented with 2% FBS, 100 U/mL penicillin, 100 μg/mL streptomycin. Cells were seeded at a density of $1x10^6$ cells/mL in T175 flasks and incubated at 37°C, 5% CO_2 for 18 - 20 h. The sub-confluent cell monolayer was then washed twice with sterile Dulbecco's PBS (DPBS). Cells were inoculated with 3,5 mL of the virus properly diluted in DMEM 2% FBS at a multiplicity of infection (MOI) of 0.001, and incubated for 1 h at 37°C in a humidified environment with 5% CO_2. At the end of the incubation, 50 mL of DMEM 2% FBS were added to the flasks. The infected cultures were incubated at 37°C, 5% CO_2 and monitored daily until approximately 80%–90% of the cells exhibited cytopathic effect (CPE). Culture supernatants were then collected, centrifuged at 4°C at 1,600 rpm for 8 min to allow removal of cell debris, aliquoted and stored at −80°C as the harvested viral stock. Viral titers were determined in confluent monolayers of Vero E6 cells seeded in 96-well plates using a 50% tissue culture infectious dose assay ($TCID_{50}$). Cells were infected with serial 1:10 dilutions (from 10^{-1} to 10^{-11}) of the virus and incubated at 37°C, in a humidified atmosphere with 5% CO_2. Plates were monitored daily for the presence of SARS-CoV-2 induced CPE for 4 days using an inverted optical microscope. The virus titer was estimated according to Spearman-Karber formula (Kundi, 1999) and defined as the reciprocal of the highest viral dilution leading to at least 50% CPE in inoculated wells.

SARS-CoV-2 authentic virus neutralization assay

All SARS-CoV-2 authentic virus neutralization assays were performed in the biosafety level 3 (BSL3) laboratories at Toscana Life Sciences in Siena (Italy) and Vismederi Srl, Siena (Italy). BSL3 laboratories are approved by a Certified Biosafety Professional and are inspected every year by local authorities. The neutralization activity of culture supernatants from monoclonal was evaluated using a CPE-based assay as previously described (Manenti et al., 2020). S-protein-specific memory B cells produced antibodies were initially evaluated by means of a qualitative live-virus based neutralization assay against a one-point dilution of the samples. Supernatants were mixed in a 1:3 ratio with a SARS-CoV-2 viral solution containing 25 $TCID_{50}$ of virus (final volume: 30 μL). After 1 h incubation at 37°C, 5% CO_2, 25 μL of each virus-supernatant mixture was added to the wells of a 96-well plate containing a sub-confluent Vero E6 cell monolayer. Following a 2 h incubation at 37°C, the virus-serum mixture was removed and 100 μl of DMEM 2% FBS were added to each well. Plates were incubated for 3 days at 37°C in a humidified environment with 5% CO_2, then examined for CPE by means of an inverted optical microscope. Absence or presence of CPE was defined by comparison of each well with the positive control (plasma sample showing high neutralizing activity of SARS-CoV-2 in infected Vero E6 cells (Andreano et al., 2020) and negative control (human serum sample negative for SARS-CoV-2 in ELISA and neutralization assays). Following expression as full-length IgG1 recombinant antibodies were quantitatively tested for their neutralization potency against both the wild type, D614G variant and the B.1.1.7 emerging variants. The assay was performed as previously described but using a viral titer of 100 $TCID_{50}$. Antibodies were prepared at a starting concentration of 20 μg/mL and diluted step 1:2. Technical triplicates were performed for each experiment.

Production and titration of SARS-CoV-2 pseudotyped lentiviral reporter particles

Pseudotype stocks were prepared by FuGENE-HD (Promega) co-transfection of HEK293T/17 with SARS-CoV-2 spike pcDNA3.1 + expression plasmid, HIV gag-pol p8.91 plasmid and firefly luciferase expressing plasmid pCSFLW in a 1:0.8:1.2 ratio. 2 × 10^6 cells/cm^2 were plated 24 h prior to transfection in 10cm cell culture dishes. 48 and 72 h post transfection, pseudotype-containing culture medium was harvested and filtered thought a 0.45um syringe filter to clear cell debris. Aliquots were stored at −80°C. Titration assays were performed by transduction of HEK293T/17 cells pre-transfected with ACE2 and TMPRRS2 plasmids to calculate the viral titer and infectious dose (PV input) for neutralization assays. SARS-CoV-2 D614G pseudotype was produced using the same procedure as described above. SARS-1 pseudotype was produced in a 1:0.5:0.8 ratio. MERS-pseudotype was produced as previously described (Grehan et al., 2015).

SARS-CoV-2 pseudotyped lentivirus neutralization assay

The potency of the neutralizing mAbs was assessed using lentiviral particles expressing SARS-CoV-2 spike protein on their surface and containing firefly luciferase as marker gene for detection of infection. Briefly, 2 × 10^6 HEK293T cells were pre-transfected in a 10 cm dish the day before the neutralization assay with ACE2 and TMPRSS2 plasmids in order to be used as optimal target cells for SARS-CoV-2 PV entry. In a 96-well plate mAbs were 2-fold serially diluted in duplicate in culture medium (DMEM supplemented with 10% fetal bovine serum and 1% penicillin/streptomycin) starting at 20 μg/mL in a total volume of 100 μL. 1x10^6 RLU of SARS-CoV-2 pseudotyped lentiviral particles were added to each well and incubated at 37°C for 1 h. Each plate included PV plus cell only (virus control) and cells only (background control). 1 × 10^4 pre-transfected HEK293T cells suspended in 50 μL complete media were added per well and incubated for 48 h at 37°C and 5% CO2. Firefly luciferase activity (luminescence) was measured using the Bright-Glo assay system with a GloMax luminometer (Promega, UK). The raw Relative Luminescence Unit (RLU) data points were converted to a percentage neutralization value, whereby 100% neutralization equals the mean cell only RLU value control and 0% neutralization equals the mean PV only RLU value control. The normalized data was then plotted using Prism 8 (GraphPad) on a neutralization percentage scale and a NT50 value calculated, using the non-linear regression analysis. Plasma from COVID-19 convalescent donors showing neutralization activity against SARS-CoV-2 (Andreano et al., 2020) were also assessed in this assay.

Characterization of SARS-CoV-2 RBD-Antibodies binding by Flow cytometry

Flow cytometry analysis was performed to define antibodies interaction with S-protein-receptor-binding domain (RBD). Briefly, APEX Antibody Labeling Kits (Invitrogen) was used to conjugate 20 μg of selected antibodies to Alexa fluor 647, according to the manufacturer instructions. To assess the ability of each antibody to bind the RBD domain, 1 mg of magnetic beads (Dynabeads His-Tag, Invitrogen) were coated with 70 μg of histidine tagged RBD, and then 20 μg/mL of each labeled antibody were incubated with 40 μg/mL of beads-bound RBD for 1 h on ice. Then, samples were washed with 200 μL of Phosphate-buffered saline (PBS), resuspended in 150 μL of PBS and assessed with a FACS Canto II flow cytometer (Becton Dickinson). Results were analyzed by FlowJo (version 10).

Flow Cytometry-Based S-protein Competition assay

Antibodies specificity to bind SARS-CoV-2 S-protein and their possible competition was analyzed performing a Flow cytometer-based assay. To this aim, 200 μg of stabilized histidine tagged S-protein were coated with 1 mg of magnetic beads (Dynabeads His-Tag, Invitrogen). 20 μg of each antibody were labeled with Alexa fluor 647 working with the APEX Antibody Labeling Kits (Invitrogen). To test competitive binding profiles of the antibody panel selected, beads-bound S-protein (40 μg/mL) were pre-incubated with unlabeled antibodies (40 μg/mL) for 1 h on ice. Then, each set of the beads-antibody complexes were washed with PBS and separately incubated with each labeled antibody (20 μg/mL) for 1 h on ice. After incubation, the mix Beads-antibodies was washed, resuspended in 150 μL of PBS and analyzed using FACS Canto II flow cytometer (Becton Dickinson). Beads-bound and non-bound S-protein incubated with labeled antibodies were used as positive and negative control, respectively. Population gating and analysis was carried out using FlowJo (version 10).

Antigen-specific FcγR binding

Fluorescently coded microspheres were used to profile the ability of selected antibodies to interact with Fc receptors (Boudreau et al., 2020). The antigen of interest (SARS –CoV-2 S-protein RBD) was covalently coupled to different bead sets via primary amine conjugation. The beads were incubated with diluted antibody (diluted in PBS), allowing ''on bead'' affinity purification of antigen-specific antibodies. The bound antibodies were subsequently probed with tetramerized recombinant human FcγR2A and FcRN and analyzed using Luminex. The data is reported as the median fluorescence intensity of PE for a specific bead channel.

Antibody-dependent neutrophil phagocytosis

Antibody-dependent neutrophil phagocytosis (ADNP) assesses the ability of antibodies to induce the phagocytosis of antigen-coated targets by primary neutrophils. The assay was performed as previously described (Karsten et al., 2019, Boudreau et al., 2020). Briefly, fluorescent streptavidin-conjugated polystyrene beads were coupled to biotinylated SARS-CoV-2 Spike trimer. Diluted antibody (diluted in PBS) was added, and unbound antibodies were washed away. The antibody:bead complexes are added to primary neutrophils isolated from healthy blood donors using negative selection (StemCell EasySep Direct Human Neutrophil

Isolation Kit), and phagocytosis was allowed to proceed for 1 h. The cells were then washed and fixed, and the extent of phagocytosis was measured by flow cytometry. The data is reported as a phagocytic score, which considers the proportion of effector cells that phagocytosed and the degree of phagocytosis. Each sample is run in biological duplicate using neutrophils isolated from two distinct donors. The mAb were tested for ADNP activity at a range of 30 μg/mL to 137.17 ng/mL.

Antibody-dependent NK cell activation

Antibody-dependent NK cell activation (ADNKA) assesses antigen-specific antibody-mediated NK cell activation against protein-coated plates. This assay was performed as previously described (Boudreau et al., 2020). Stabilized SARS-CoV-2 Spike trimer was used to coat ELISA plates, which were then washed and blocked. Diluted antibody (diluted in PBS) was added to the antigen coated plates, and unbound antibodies were washed away. NK cells, purified from healthy blood donor leukopaks using commercially available negative selection kits (StemCell EasySep Human NK Cell Isolation Kit) were added, and the levels of IFN-γ was measured after 5 h using flow cytometry. The data is reported as the percent of cells positive for IFN-γ. Each sample is tested with at least two different NK cell donors, with all samples tested with each donor. The monoclonal antibodies were tested for ADNKA activity at a range of 20 μg/mL to 9.1449 ng/mL.

Affinity evaluation of SARS-CoV-2 neutralizing antibodies

Anti-Human IgG Polyclonal Antibody (Southern Biotech 2040-01) was immobilized via amine group on two flow cells of a CM5 sensor chip. For the immobilization, anti-human IgG Ab diluted in 10mM Na acetate pH 5.0 at the concentration of 25 μg/mL was injected for 360 s over the dextran matrix, which had been previously activated with a mixture of 0.1M 1-ethyl-3(3-dimethylaminopropyl)-carbodiimide (EDC) and 0.4 M N-hydroxyl succinimide (NHS) for 420 s. After injection of the antibody, Ethanolamine 1M was injected to neutralize activated group. 10 μL/min flow rate was used during the whole procedure. Anti-SPIKE protein human mAbs were diluted in HBS-EP+ (HEPES 10 mM, NaCl 150 mM, EDTA 3.4 mM, 0.05% p20, pH 7.4) and injected for 120 s at 10 μL/min flow rate over one of the two flow cells containing the immobilized Anti-Human IgG Antibody, while running buffer (HBS-EP+) was injected over the other flow cell to be taken as blank. Dilution of each mAb was adjusted in order to have comparable levels of RU for each capture mAb. Following the capture of each mAb by the immobilized anti-human IgG antibody, different concentrations of SPIKE protein (20 μg/mL, 10 μg/mL, 5 μg/mL, 2.5 μg/mL and 1 μg/mL in HBS-EP+) were injected over both the blank flow cell and the flow cell containing the captured mAb for 180 s at a flow rate of 80 μL/min. Dissociation was followed for 800 s, regeneration was achieved with a pulse (60 s) of Glycine pH 1.5. Kinetic rates and affinity constant of SPIKE protein binding to each mAb were calculated applying a 1:1 binding as fitting model using the Bia T200 evaluation software 3.1.

Autoreactivity screening test on HEp-2 Cells

The NOVA Lite HEp-2 ANA Kit (Inova Diagnostics) was used in accordance to the manufacturer's instructions to test antibodies the autoreactivity of selected antibodies which were tested at a concentration of 100 μg/mL. Kit positive and negative controls were used at three different dilutions (1:1, 1:10 and 1:100). Images were acquired using a DMI3000 B microscope (Leica) and an exposure time of 300 ms, channel intensity of 2000 and a gamma of 2.

Genetic Analyses of SARS-CoV-2 S-protein specific nAbs

A custom pipeline was developed for the analyses of antibody sequences and the characterization of the immunoglobulin genes. Raw sequences were stored as ab1 file and transformed into fastaq using Biopython. The reads were then quality checked using FastQC (https://www.bioinformatics.babraham.ac.uk/projects/fastqc/) and a report was generated using MultiQC (https://multiqc.info/). The antibody leader sequence and the terminal part of the constant region were removed by trimming using Trimmomatic (http://www.usadellab.org/cms/?page=trimmomatic). This latter program was also used to scan and remove low-quality reads using a sliding-window parameter. Once sequences were recovered, germline gene assignment and annotation were perfromed with MiXCR (https://mixcr.readthedocs.io/en/master/index.html), using the single-read alignment parameters, and a CSV-formatted output was generated. Finally, the sequences retrieved from the antibodies described in this manuscript were compared to published neutralizing antibodies against SARS-CoV-2. For this purpose, the Coronavirus Antibody Database, CoV-AbDab (http://opig.stats.ox.ac.uk/webapps/covabdab/) was downloaded and the antibodies with reported neutralization activity against SARS-CoV-2 were extracted. Comparison analysis were performed in Python using NumPy (https://numpy.org/) and, Pandas (https://pandas.pydata.org/) while figures were produced using the Matplotlib tool (https://matplotlib.org/) and Seaborn (https://seaborn.pydata.org/).

Negative-stain electron microscopy

Complexes were formed by incubating SARS-2 CoV-GSAS-6P-Mut7 and respective fabs at a 1:3 (trimer to fab) molar ratio for 30 min at room temperature. After diluting to 0.03 mg/mL in 1X TBS pH 7.4, the samples were deposited on plasma-cleaned copper mesh grids and stained with 2% uranyl formate for 55 s. Automated data collection was made possible through the Leginon software (Suloway et al., 2005) and a FEI Tecnai Spirit (120keV, 56,000x mag) paired with a FEI Eagle (4k by 4k) CCD camera. Other details include a defocus value of −1.5 μm, a pixel size of 2.06 Å per pixel, and a dose of 25 $e^{-}/Å^{2}$. Raw micrographs were stored in the Appion

database (Lander et al., 2009), particles were picked with DoGPicker (Voss et al., 2009), and 2D and 3D classification and refinements were performed in RELION 3.0 (Scheres, 2012). Map segmentation and model docking was done in UCSF Chimera (Pettersen et al., 2004).

Prophylactic and therapeutic passive transfer studies in golden Syrian hamsters

Six- to eight-month-old female Syrian hamsters were purchased from Charles River Laboratories and housed in microisolator units, allowed free access to food and water and cared for under U.S. Department of Agriculture (USDA) guidelines for laboratory animals. For the passive transfer prophylactic experiments, the day prior to SARS-CoV-2 infection six hamsters per group were intraperitoneally administered with 500 μL of a 4, 1 or 0.25 mg/kg dose of J08-MUT mAb. For the passive transfer therapeutic experiments, the day after SARS-CoV-2 infection six hamsters per group were intraperitoneally administered with 500 μL of a 4 mg/kg dose of J08-MUT mAb. Another two groups (n = 6/each) were administered with 500 μL of 4 mg/kg of the anti-influenza virus #1664 human mAb (manuscript in preparation) or PBS only to serve as human IgG1 isotype and mock control groups, respectively. The day after, hamsters were anesthetized using 5% isoflurane, and inoculated with 5×10^5 PFU of SARS-CoV-2 (2019-nCoV/USA-WA1/2020) via the intranasal route, in a final volume of 100 μL. Baseline body weights were measured before infection as well as monitored daily for 7 and 11 days post infection in the prophylactic and therapeutic studies respectively. All experiments with the hamsters were performed in accordance with the NRC Guide for Care and Use of Laboratory Animals, the Animal Welfare act, and the CDC/NIH Biosafety and Microbiological and Biomedical Laboratories as well as the guidelines set by the Institutional Animal Care and Use Committee (IACUC) of the University of Georgia who also approved the animal experimental protocol. All animal studies infection with SARS-CoV-2 were conducted in the Animal Health Research Center (AHRC) Biosafety Level 3 (BSL-3) laboratories of the University of Georgia.

Determination of viral load by $TCID_{50}$ assay

Lung tissues were homogenized in 1 mL of DMEM containing 1% fetal bovine serum (FBS) and 1% penicillin/streptomycin. The lung homogenate supernatant was diluted 10-fold (10° to 10^6) and used to determine median tissue culture infection dose ($TCID_{50}$) in Vero E6 cells as previously described (Jang and Ross, 2020).

Human IgG detection in hamster sera

ELISA assay was used to detect the human IgG J08-MUT in hamster sera. 384-well plates (384 well plates, Microplate Clear; Greiner Bio-one) were coated with 2 μg/mL of unlabled goat anti-human IgG (SouthernBiotech) diluted in sterile PBS and incubated at 4°C overnight. 50 μL/well of saturation buffer (PBS/BSA 1%) was used to saturate unspecific binding and plates were incubated at 37°C for 1 h without CO_2. Hamster sera were diluted in PBS/BSA 1%/Tween20 0.05% at a starting dilution of 1:10. Fourteen reciprocal dilutions were performed. Alkaline phosphatase-conjugated goat anti-human IgG (Sigma-Aldrich) was used as secondary antibody and pNPP (p-nitrophenyl phosphate) (Sigma-Aldrich) was used as soluble substrate. Wells were washed three times between each step with PBS/BSA 1%/Tween20 0.05%. The final reaction was measured by using the Varioskan Lux Reader (Thermo Fisher Scientific) at a wavelength of 405 nm. Samples were considered as positive if OD at 405 nm (OD_{405}) was twice the blank.

Cell
Article

CellPress

Supplemental figures

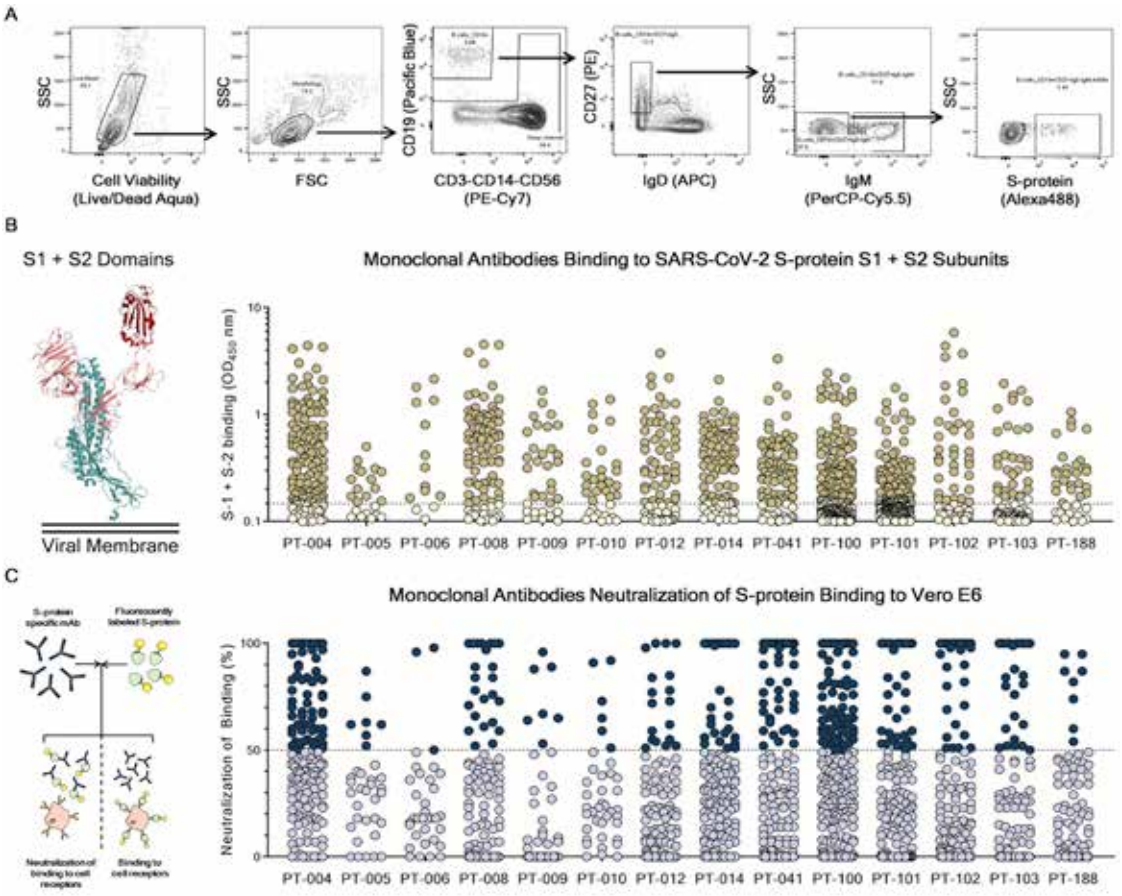

Figure S1. Gating strategy for single-cell sorting and monoclonal antibodies screening for S protein S1 + S2 subunits binding and neutralization of binding (NoB) activity, related to Figure 2

(A) Starting from top left to the right panel, the gating strategy shows: Live/Dead; Morphology; $CD19^+$ B cells; $CD19^+CD27^+IgD^-$; $CD19^+CD27^+IgD^-IgM^-$; $CD19^+CD27^+IgD^-IgM^-$S-protein$^+$ B cells.

(B) The graph shows supernatants tested for binding to the SARS-CoV-2 S-protein S1 + S2 subunits. Threshold of positivity has been set as two times the value of the blank (dotted line). Darker dots represent mAbs which bind to the S1 + S2 while light yellow dots represent mAbs which do not bind. (B) The graph shows supernatants tested by NoB assay. Threshold of positivity has been set as 50% of binding neutralization (dotted line). Dark blue dots represent mAbs able to neutralize the binding between SARS-CoV-2 and receptors on Vero E6 cells, while light blue dots represent non-neutralizing mAbs.

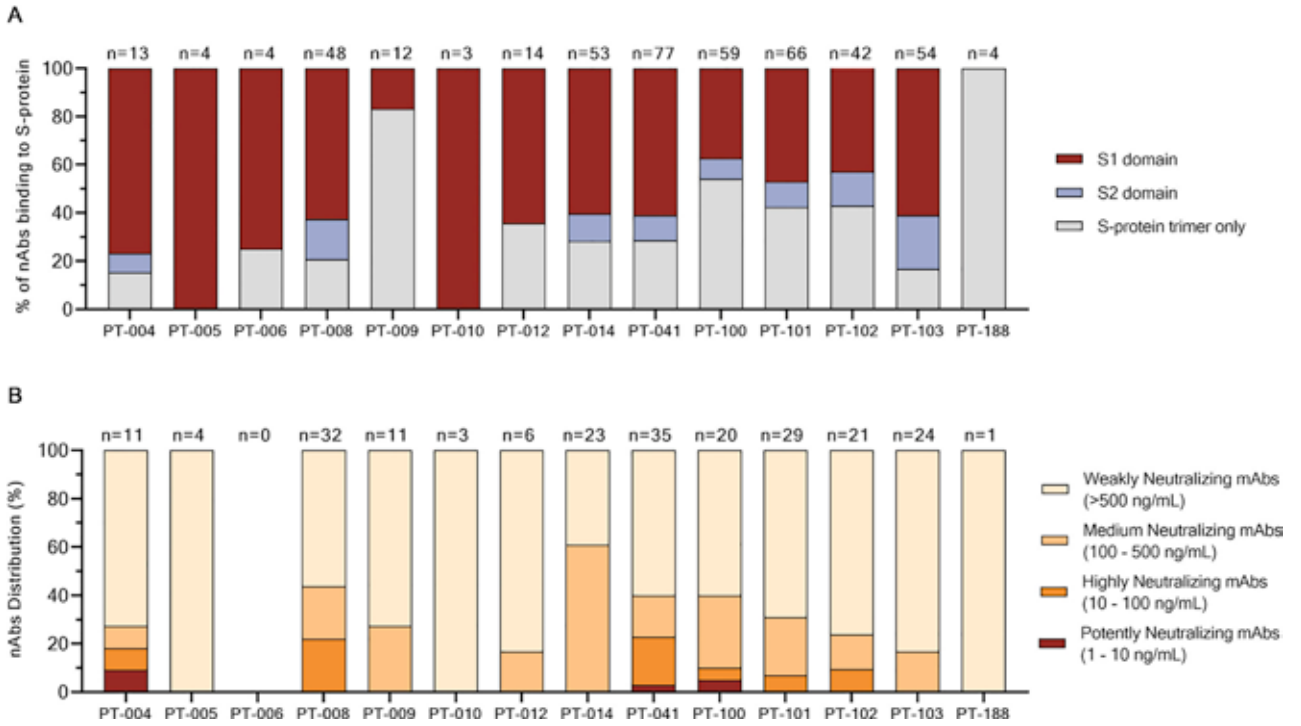

Figure S2. Characterization and distribution of SARS-CoV-2 S protein-specific nAbs, related to Figure 2

(A) The bar graph shows the distribution of nAbs binding to different S-protein domains. In dark red, light blue and gray are shown antibodies binding to the S1-domain, S2-domain and S-protein trimer respectively. The total number (n) of antibodies tested per individual is shown on top of each bar.

(B) The bar graph shows the distribution of nAbs with different neutralization potencies. nAbs were classified as weakly neutralizing (> 500 ng/mL; pale orange), medium neutralizing (100 – 500 ng/mL; orange), highly neutralizing (10 – 100 ng/mL; dark orange) and extremely neutralizing (1 – 10 ng/mL; dark red). The total number (n) of antibodies tested per individual is shown on top of each bar.

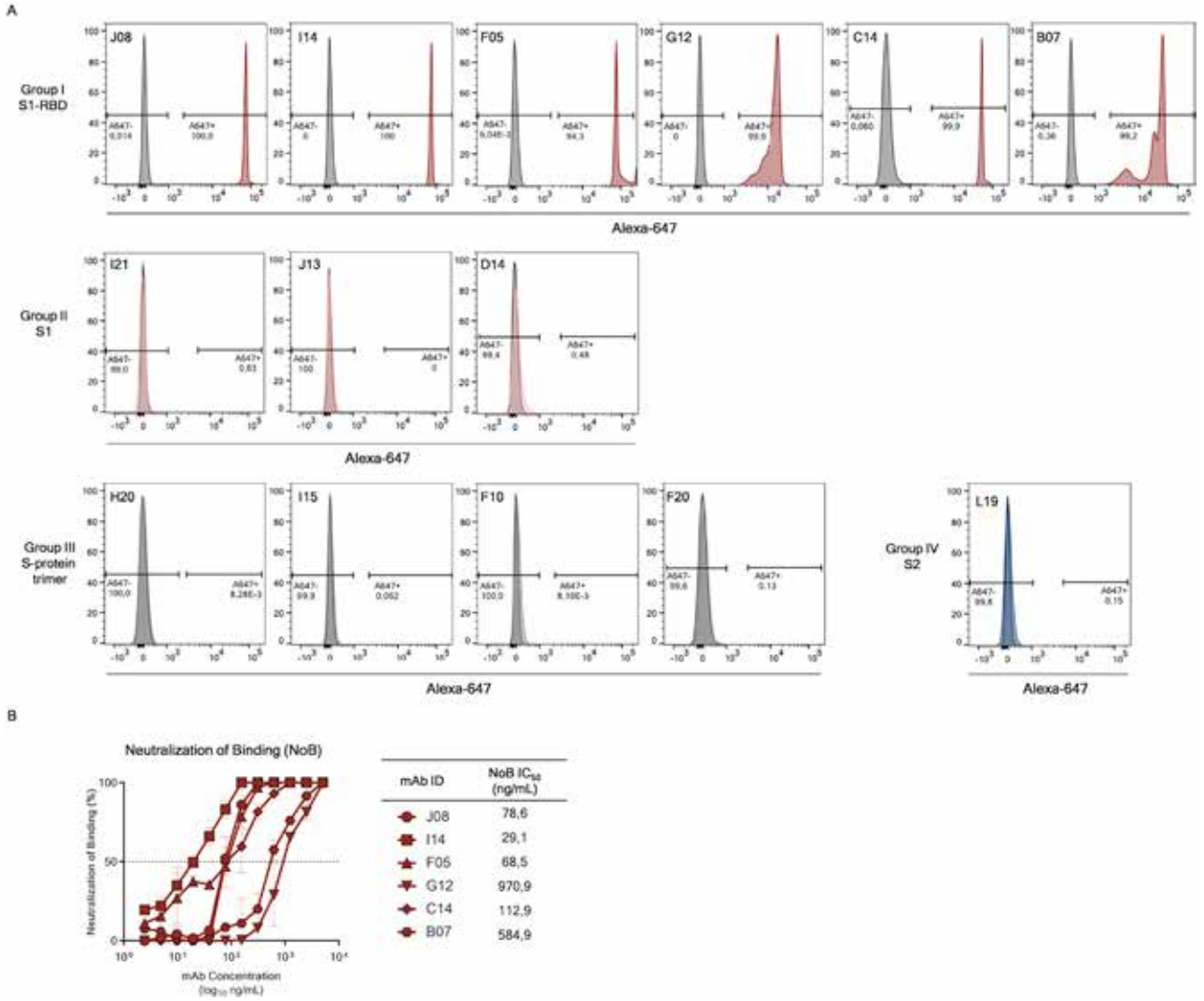

Figure S3. Binding to S protein receptor binding domain (RBD) and NoB activity of S1-RBD antibodies, related to Figure 3

(A) Histograms show the ability of selected antibodies to bind the S-protein RBD. Gray histograms represent the negative control while colored histograms show tested antibodies. Percentage of positive and negative populations are denoted on each graph.

(B) Neutralization of binding (NoB) curves for S1-RBD specific antibodies are shown as percentage of reduction of signal emitted by a fluorescently labled S-protein incubated with Vero E6 cells. Mean ± SD of technical duplicates are shown. Dashed lines represent the threshold of positivity; A neutralizing COVID-19 convalescent plasma and an unrelated plasma were used as positive and negative control, respectively.

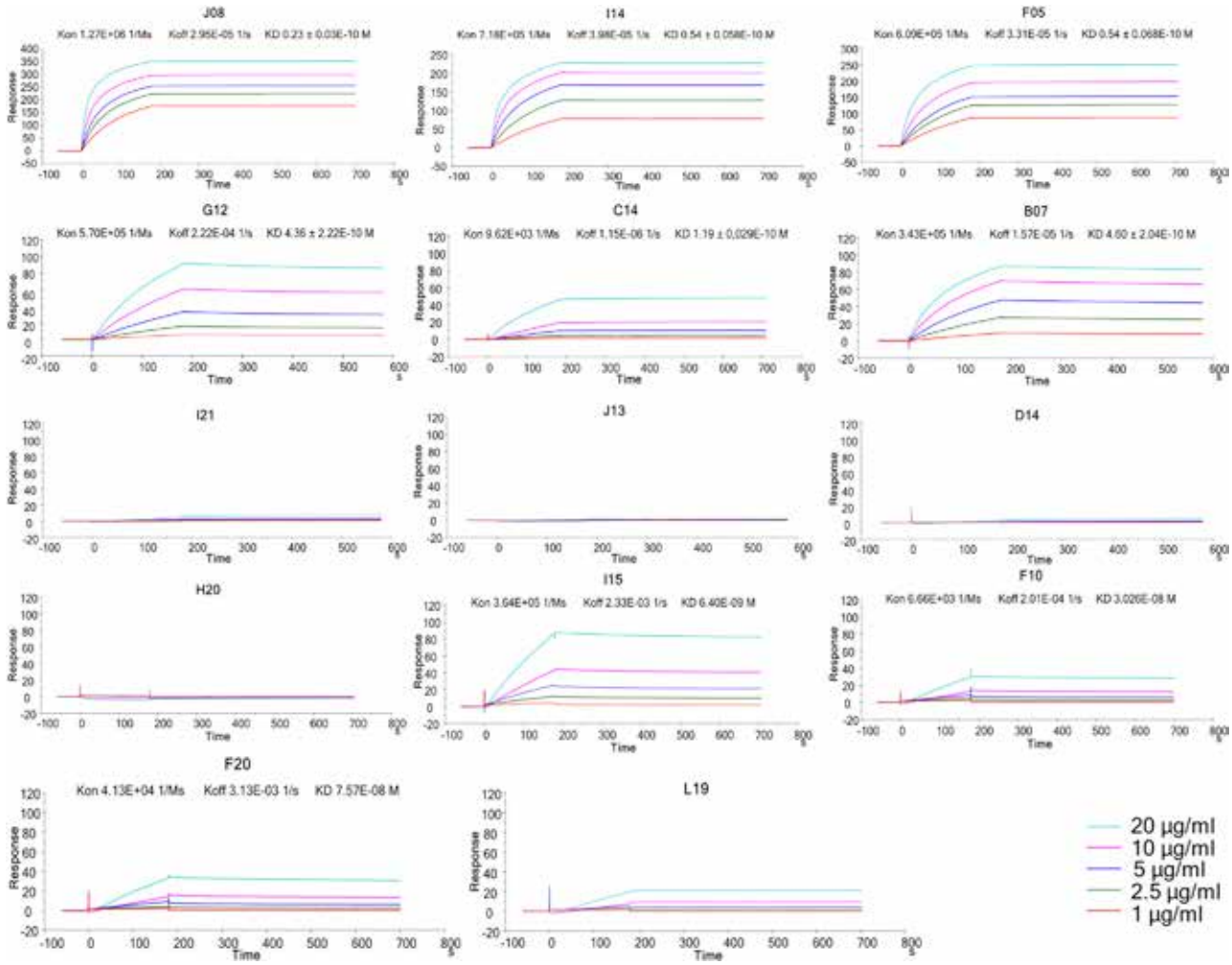

Figure S4. Binding kinetics of SARS-CoV-2 nAbs to the S protein antigen, related to Figure 3

Representative binding curves of selected antibodies to SARS-CoV-2 S-protein trimer. Different curve colors define the spike concentration used in the experiment. Kon, Koff and KD are denoted on each graph.

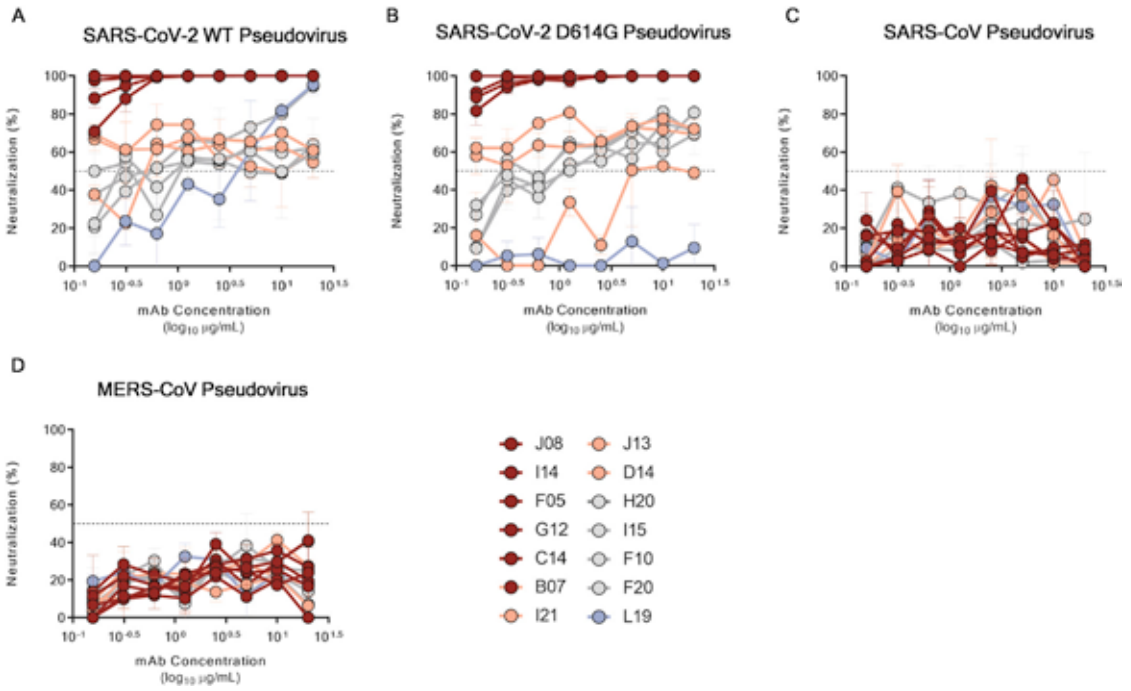

Figure S5. Neutralization activity of selected nAbs against SARS-CoV-2, SARS-CoV, and MERS-CoV pseudotypes, related to Figure 3

(A–D) Graphs show the neutralizing activities of 14 selected nAbs with different SARS-CoV-2 S-protein binding profiles against SARS-CoV-2, SARS-CoV-2 D614G, SARS-CoV and MERS-CoV pseudotypes respectively. Dashed lines represent the threshold of positivity. Mean ± SD of technical duplicates are shown. In all graphs selected antibodies are shown in dark red, pink, gray and light blue based on their ability to recognize the SARS-CoV-2 S1-RBD, S1-domain, S-protein trimer only and S2-domain respectively.

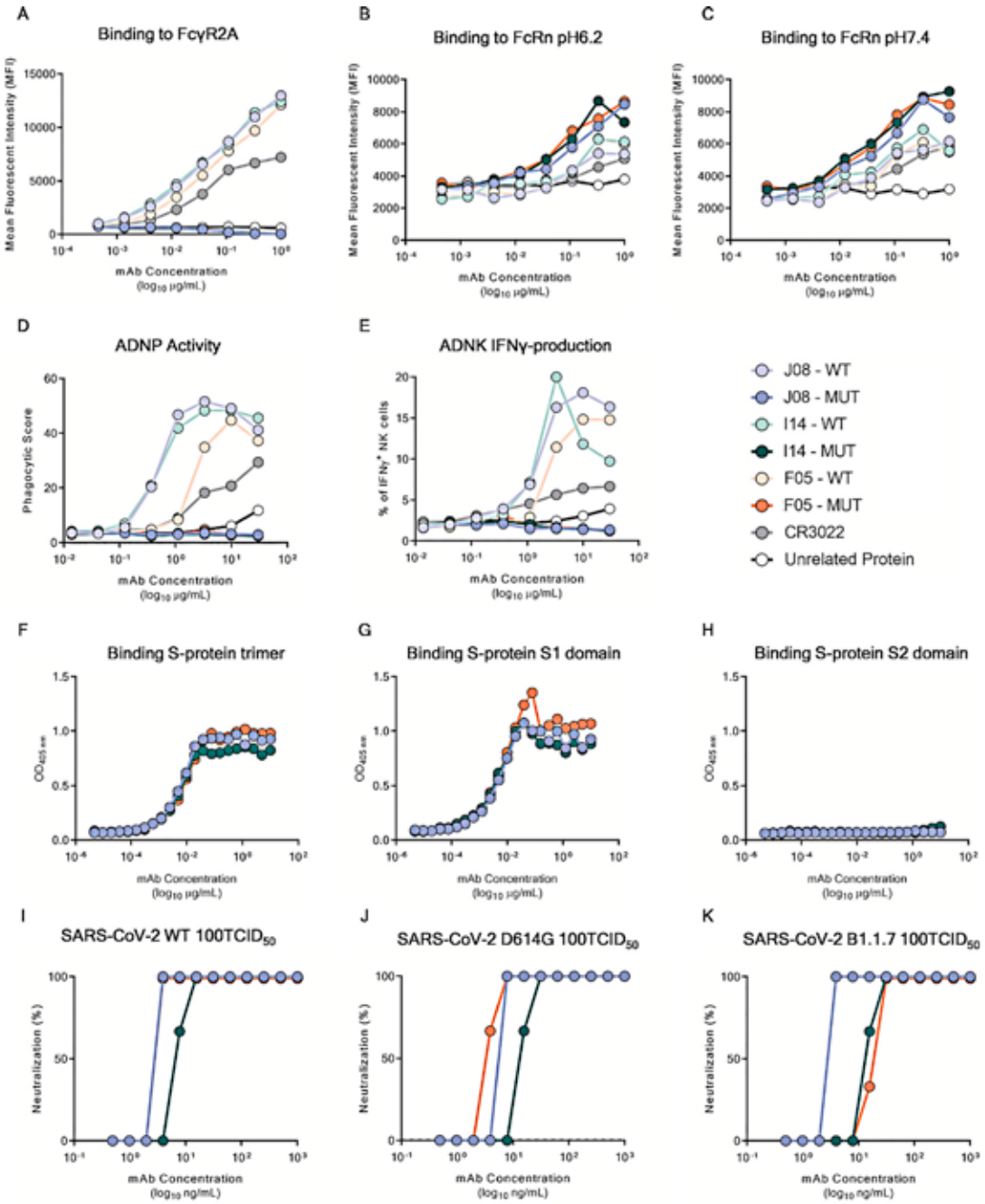

Figure S6. Characterization of Fc-engineered candidate nAbs, related to Figure 7

(A) the graph shows binding curves of J08, I14 and F05 MUT and WT to the FcγR2A.

(B and C) graphs show binding curves of J08, I14 and F05 MUT and WT to the FcRn at pH 6.2 (B) and 7.4 (C).

(D and E) Graphs show the ADNP and ADNK induced by J08, I14 and F05 MUT and WT versions; all the experiments were run as technical duplicates. In every experiment a control antibody (CR3022) and an unrelated protein were used as positive and negative control respectively.

(F–H) Graphs show binding curves to the S-protein in its trimeric conformation, S1-domain and S2-domain. Mean of technical triplicates are shown.

(I–K) Neutralization curves against the authentic SARS-CoV-2 wild type, the D614G variant and the B.1.1.7 emerging variant for J08-MUT, I14-MUT and F05-MUT shown in blue, green and red respectively. Data are representative of technical triplicates.

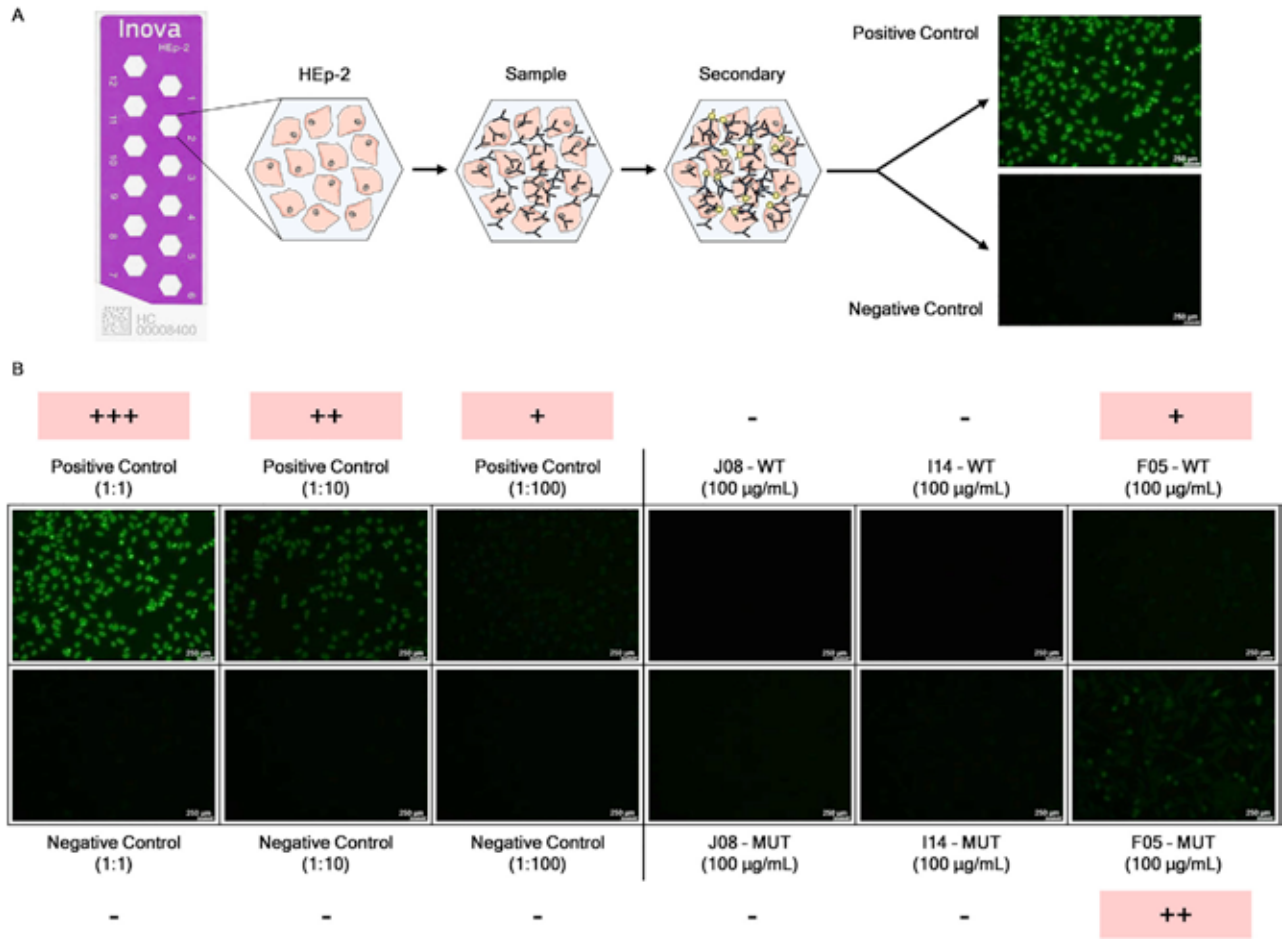

Figure S7. Autoreactivity assessment of selected SARS-CoV-2 candidate nAbs, related to Figure 7

(A) Schematic representation of the indirect immunofluorescent assay for the screening of autoreactive nAb.

(B) Single figures show the fluorescent signal detected per each sample tested in this assay. Positive and negative controls were used at three different dilutions (1:1, 1:10 and 1:100). Three candidate nAbs were incubated on HEp-2 cells at a concentration of 100 µg/mL. Representative pictures of the scoring system are shown. Autoreactive samples are highlighted in pink. 250 nm scale bar is shown.